UNIVERSIDADE FEDERAL DE SANTA CATARINA
CENTRO TECNOLÓGICO
PROGRAMA DE PÓS-GRADUAÇÃO EM ENGENHARIA MECÂNICA

Pedro Correa Jaeger Rocha

# METAL-CORED WIRE + ARC ADDITIVE MANUFACTURING OF THICK LAYERED STRUCTURES WITH GMAW PROCESS

Florianópolis
2020

Pedro Correa Jaeger Rocha

# METAL-CORED WIRE + ARC ADDITIVE MANUFACTURING OF THICK LAYERED STRUCTURES WITH GMAW PROCESS

Dissertação submetida ao Programa de Pós-Graduação em Engenharia Mecânica da Universidade Federal de Santa Catarina para a obtenção do Grau de Mestre em Engenharia Mecânica.
Orientador: Prof. Régis Henrique Gonçalves e Silva, Dr. Eng.

Florianópolis
2020

Ficha de identificação da obra elaborada pelo autor,
através do Programa de Geração Automática da Biblioteca Universitária da UFSC.

Rocha, Pedro Correa Jaeger
Metal-cored wire + arc additive manufacturing of thick layered structures with GMAW process / Pedro Correa Jaeger Rocha ; orientador, Régis Henrique Gonçalves e Silva, 2020.
110 p.

Dissertação (mestrado) - Universidade Federal de Santa Catarina, Centro Tecnológico, Programa de Pós-Graduação em Engenharia Mecânica, Florianópolis, 2020.

Inclui referências.

1. Engenharia Mecânica. 2. Soldagem. 3. Manufatura aditiva. 4. Arames tubulares. 5. Revestimento. I. Silva, Régis Henrique Gonçalves e . II. Universidade Federal de Santa Catarina. Programa de Pós-Graduação em Engenharia Mecânica. III. Título.

Pedro Correa Jaeger Rocha

**Metal-Cored Wire + Arc Additive Manufacturing of Thick Layered Structures with GMAW Process**

O presente trabalho em nível de mestrado foi avaliado e aprovado por banca examinadora composta pelos seguintes membros:

Prof. Américo Scotti, Ph.D.
University West, Suécia

Prof. Milton Pereira, Dr. Eng.
Universidade Federal de Santa Catarina

Dr. Cleber Marques
Universidade Federal de Santa Catarina

Certificamos que esta é a versão original e final do trabalho de conclusão que foi julgado adequado para obtenção do título de mestre em Engenharia Mecânica.

Documento assinado digitalmente
Paulo de Tarso Rocha de Mendonca
Data: 03/01/2021 08:00:04-0300
CPF: 149.822.691-49

Prof. Paulo de Tarso Rocha de Mendonça, Dr. Eng.
Coordenador do POSMEC UFSC

Documento assinado digitalmente
Regis Henrique Goncalves e Silva
Data: 02/01/2021 16:38:46-0300
CPF: 023.436.429-74

Prof. Régis Henrique Gonçalves e Silva, Dr. Eng.
Orientador

Florianópolis, 2020.

Aos meus pais, Sinval e Joice.

## AGRADECIMENTOS

Agradeço primeiramente à sociedade brasileira que financia o ensino superior público pela oportunidade e o desafio de me qualificar para poder ajudar no desenvolvimento de nosso amado Brasil.

À CAPES pela bolsa de ajuda de custo no valor de R$ 1200,00 durante 24 meses.

Agradeço ao presidente da empresa DURUM Verschleiss-Schutz, Herr Peter Knauf e ao diretor de P&D, Dr. Frank Schreiber, por toda a confiança depositada em mim desde a graduação até os dias de hoje.

Ao meu Orientador Prof. Dr. Regis Henrique Gonçalves e Silva pela orientação e incentivo neste dentre outros trabalhos conduzidos no LABSOLDA.

A todos os bolsistas de graduação e pós-graduação do LABSOLDA que contribuíram de alguma forma para consecução deste trabalho.

Aos meus amigos. Em especial ao Erick Gonzalez, Júlia Dornelles, Annette König e Regine König que estiveram ao meu lado nos momentos mais difíceis.

À minha família, em especial à minha mãe Joice, meu pai Sinval e minha irmã Vitória.

Danke Schön!

## RESUMO

Neste trabalho estuda-se a aplicação de materiais e equipamentos convencionas da indústria de revestimentos metálico por soldagem a arco na fabricação de componentes metálicos por manufatura aditiva. Ao utilizar-se estes processos convencionais e material de adição na forma de arame, denomina-se a técnica de manufatura como Wire + Arc Additive Manufacturing (WAAM), sobre a qual este trabalho disserta. Em contraste ao utilizado convencionalmente em WAAM, arames tubulares do tipo metal-cored são estudados neste trabalho. Foi escolhido um arame metal-cored de aço ao Manganês (0,4 % C, 15 % Mn) com 1,2 mm de diâmetro. Utilizou-se duas variantes do processo MIG/MAG com alimentação dinâmica e controle de corrente (CMT e CMT Pulse), ambas com velocidade de alimentação (3,5 m/min) e deslocamento (10 cm/min) constantes. Como metodologia de estudo, se propôs a deposição de corpos de prova em forma de paredes espessas (15 mm x 40 mm x 100 mm). Para atingir a geometria proposta, foram depositadas 20 camadas, com altura média de 2 mm, para cada corpo de prova. A estratégia de deposição consistiu em sobreposição de camadas com origem e incrementos de altura constantes. Ao final de cada camada se impôs a extinção do arco e um tempo de espera entre camadas constante. Analisou-se a dinâmica térmica da construção dos corpos de prova com uso da técnica de filmagem termográfica por infravermelho. Foram realizadas aquisições dos sinais elétricos do processo, filmagem em alta velocidade da deposição de material, análise do perfil de composição química e microdureza. Não foram observadas dificuldades na utilização de arames metal-cored em comparação a arames maciços convencionais. O arame metal-cored apresentou boa soldabilidade nas condições de soldagem e estratégia de deposição escolhidos, mesmo utilizando-se programa sinérgico não dedicado. Corpos de prova com dimensões similares ao objetivo foram alcançados para ambas variantes de processo. Como fase de validação, construiu-se corpos de prova em ambiente industrial, na empresa alemã DURUM Verschleiss Schutz. Os resultados demonstraram que, embora ajustes em movimentadores e bancadas de trabalho sejam necessários, há possibilidade de utilização dos equipamentos convencionais de uma empresa do ramo de revestimentos por soldagem para fabricação de peças por WAAM.



**Palavras-chave:** Manufatura Aditiva, Impressão 3D, FCAW, Arame Tubular, Aço Hadfield.

## RESUMO EXPANDIDO

### Introdução

As três primeiras revoluções industriais trouxeram produção em massa, linhas de montagem, eletricidade e tecnologia da informação, elevando a renda dos trabalhadores e fazendo da concorrência tecnológica o coração do desenvolvimento econômico. A quarta revolução industrial, que terá um impacto mais profundo e exponencial, é caracterizada por um conjunto de tecnologias que permitem a fusão do mundo físico, digital e biológico. Uma das tecnologias que cresce junto à essa revolução industrial é a manufatura aditiva (MA), popularmente conhecida como impressão em 3D. O princípio da manufatura aditiva é estabelecido no fato de que qualquer objeto pode ter seu desenho geométrico digital fatiado em camadas e reconstruído usando essas coordenadas bidimensionais como um caminho de deposição de material. Uma das variantes tecnológicas da MA para a construção de peças metálicas é chamada Directed Energy Deposition (DED). Esta categorização aglomera o conjunto de práticas em que uma fonte térmica é focada na fusão de um material de alimentação simultaneamente com sua deposição em um caminho previamente definido, formando camadas. Dentro desta categoria, o processo ainda pode ser classificado de acordo com a fonte de energia utilizada na fusão da matéria-prima. Quanto à forma da matéria-prima, duas formas principais podem ser observadas: a alimentação em pó e a alimentação em arame. Dentro da categoria DED encontra-se a variante que combina um arco elétrico como fonte térmica e o arame como matéria-prima, chamada Wire + Arc Additive Manufacturing (WAAM). Diferente de arames maciços usualmente utilizados, pode-se utilizar arames tubulares. Estes arames tubulares podem ser preenchidos com matéria prima em forma de pó, oferecendo novas possibilidades de processo. O emprego de arames tubulares para WAAM pode trazer benefícios como maiores taxas de deposição com menor consumo de energia e especialmente a vantagem de maior flexibilidade de produção e desenvolvimento de ligas devido ao uso de pó no núcleo. Uma vantagem adicional é a probabilidade de encher seu núcleo com partículas cerâmicas, algo impraticável com fios sólidos. Em um futuro cenário industrial 4.0 em que a produção tende a ser mais personalizada e descentralizada, os arames tubulares certamente expandirão sua participação no mercado de matéria-prima WAAM.

Os arames tubulares não são comumente empregados em mais estudos devido ao preço mais alto dos arames tubulares, em comparação com os arames maciços padrão de aço ou alumínio, desencorajando seu uso em estudos dos aspectos gerais da WAAM. Embora não

sejam a primeira escolha para estudos gerais sobre WAAM, mas podem ser mandatórios em alguns projetos de peças com exigências de resistência ao desgaste.

Os passos iniciais para enriquecer este campo de estudo são a análise do desempenho dos arames tubulares do tipo metal-cored com as variantes de processo GMAW tipicamente usadas para a WAAM. A maioria das variantes de GMAW aplicadas são baseadas na transferência de metal em curto-circuito controlado por corrente, com alimentação dinâmica do arame, concebido para arames maciços. Como estas variantes GMAW funcionam para arames tubulares? Para caracterizar esta combinação de matéria-prima e fonte de calor, a fabricação de amostras juntamente com a filmagem termográfica são experimentos necessários. Os resultados ajudam a correlacionar a dinâmica térmica durante a fabricação com o resultado metalúrgico da amostra, que é obrigatório para determinar a aplicabilidade e a qualidade da peça.

**Objetivos**

Este trabalho tem como objetivo analisar as características e contribuir para estabelecer os fundamentos para a manufatura via Wire + Arc Additive Manufacturing (WAAM), utilizando variantes de soldagem GMAW com baixo aporte de calor, combinada com arame tubular metal-cored como matéria-prima, uma combinação ainda não muito abordada na literatura. A maioria das informações disponíveis aplica programas de soldagem sinérgica dedicados a alimentação de arame, predominantemente para arames metal-cored. Devido à relevância técnica dos arames tubulares metal-cored para a indústria de manufatura aditiva, foram estabelecidas metas para investigar sua resposta à estabilidade do processo (poça de fusão, transferência de metal, comportamento do arco), influências térmicas e metalúrgicas, bem como o desempenho geral sob procedimentos não-sinérgicos de GMAW.

**Metodologia**

Para avaliar as respostas desta combinação de condições de soldagem (arames tubulares + GMAW) na manufatura aditiva tipo WAAM foi realizado a deposição amostras com uma liga de aço com alto teor de manganês (15%) utilizando-se o processo de soldagem GMAW com a variante tecnológica Cold Metal Transfer (CMT) com dois modos de transferência: modo curto-circuito e pulsado. As amostras consistiam em estruturas espessas similares a paredes, com dimensões esperadas de 100 mm de comprimento, 40 mm de altura e 15 mm de largura. As paredes espessas foram depositadas com estratégia de deposição intermitente, na qual ao término de cada camada a fonte de calor/alimentação era extinta e

retornava para o ponto inicial de deposição da camada anterior. Deste modo criou-se um tempo de resfriamento equivalente ao tempo de deposição (60 s). Foram necessárias 20 camadas para alcançar a altura estipulada. Para depositar uma espessura de 15 mm foi necessário a utilização de técnica de espalhamento lateral com padrão trapezoidal.

Cada modo de transferência utilizou diferentes correntes médias, sendo o modo pulsado superior ao modo curto-circuito.

Durante a deposição das amostras foi aquisitado os sinais elétricos do processo de soldagem bem como a velocidade alimentação por meio de um transdutor acoplado a saída de arame do carretel. Foi feito a filmagem termográfica durante a deposição e posterior resfriamento das amostras até 100 °C. Os dois modos de transferência foram posteriormente caracterizados por meio de filmagem em alta velocidade, utilizando uma taxa de aquisição de 5000 frames por segundo.

As amostras foram então seccionadas transversalmente, na qual se realizou um perfil vertical de dureza, análise química e macrografia.

Uma posterior parte do trabalho foi realizada na empresa DURUM Verschleiss-Schutz, na Alemanha. A empresa foi fornecedora dos arames tubulares utilizados no trabalho. No ambiente industrial da empresa foram realizados testes de validação das práticas desenvolvidas no trabalho.

**Resultados e Discussão**

Os arames tubulares apresentaram excelente soldabilidade dentro das condições de manufatura WAMM no laboratório e no ambiente industrial, para todas as variantes GMAW utilizadas (CMT, CMT Pulse e RMD). Este resultado destaca a possibilidade de prospecção do uso de WAAM para a fabricação de peças com exigências de resistência ao desgaste que depende do uso de arames metal-cored com núcleo cerâmico-metálico.

A transferência de material durante a variante CMT Pulse ocorreu principalmente pelo modo de curto-circuito, em vez de voo livre e curto-circuito, como esperado. O pulso de corrente não foi alto o suficiente para alcançar a corrente de transição. A transferência de massa ocorreu preferencialmente durante o curto-circuito, consistindo em uma gota de alto volume formada durante os períodos de pulso, no qual não houve destacamento. Durante o período de pulso, houve uma ejeção contínua de pequenas partículas sólidas e gotas minúsculas do núcleo metálico. Esta transferência de material diferente ocorreu devido ao comportamento do fluxo de corrente intrínseca do arame tubular metal-cored, no qual a corrente flui preferencialmente através da banda metálica externa em vez do núcleo em pó.

De acordo com a análise de filmagem de alta velocidade, o núcleo do arame ainda em sua forma sólida mergulha na poça de fusão em ambas as variantes de processo. Pode-se entender que ao entrar na poça de soldagem, o núcleo sólido na forma de pó agregado influencia a dinâmica térmica da poça de soldagem, de fato, resfriando-a. Este comportamento age como outro artifício para remover o calor do processo de deposição, o que é comumente desejado na WAAM. Entretanto, ainda não foram feitos estudos específicos para avaliar a relevância do efeito sobre a solidificação do depósito.

A variante CMT Pulse resultou em um aporte de calor 23% maior do que a variante CMT para a mesma velocidade de deslocamento (10 cm/min) e velocidade de alimentação de arame (3,5 m/min). Esta diferença de aporte de calor leva a uma diferença média de temperatura de 50˚C entre as duas variantes de processo.

A análise da temperatura média durante a deposição mostrou que em aproximadamente 960s, ou 8 camadas, as amostras entraram em um estado quase estável de fluxo de calor com seus arredores. Até o final da deposição, a temperatura média das amostras aumentou a um ritmo lento em comparação com o regime transitório inicial independente da variante de processo utilizado, quase atingindo um platô de temperatura constante.

A amostra de validação proposta foi fabricada com sucesso na oficina da DURUM com equipamentos convencionais para revestimento duro com duas estratégias de construção diferentes. A primeira estratégia, com múltiplos pontos de percurso, forneceu um grande envelope de trabalho, mas com menos robustez e facilidade de programação do que a segunda estratégia. Com esse maior envelope de deposição é possível a produção de pequenos lotes de peças similares simultaneamente, utilizando o tempo ocioso entre camadas como estratégia para esfriar uma peça enquanto depositava uma nova camada em outra região da mesa que já estava resfriada até a temperatura necessária entre camadas. Por outro lado, o uso da segunda técnica, a estratégia de mesa giratória, forneceu uma solução melhor para um aparelho de pesquisa com uma mentalidade de prototipagem rápida com fácil programação do percurso de deposição em vez de produção flexível de banhos de tamanho médio.

**Palavras-chave:** Manufatura Aditiva, Impressão 3D, FCAW, Arame Tubular, Aço Hadfield.

## ABSTRACT

This work studies the application of conventional materials and equipment of the arc cladding and welding industry aimed to the manufacturing of metallic components by additive manufacturing. The combination of using these conventional arc processes and wire as feedstock matches the manufacturing technique known as Wire + Arc Additive Manufacturing (WAAM). The performance of metal-cored wires for WAAM application was studied in this study, in contrast to conventional solid wires. A 1.2 mm diameter metal-cored Manganese steel wire (0.4 % C, 15 % Mn) was chosen. Two variants of the GMAW process with dynamic feed and current control (CMT and CMT Pulse) were used, both with constant feed speed (3.5 m/min) and travel speed (10 cm/min). As a study methodology, it was proposed the deposition of thick-walled samples (15 mm x 40 mm x 100 mm). To achieve the proposed geometry, 20 layers were deposited, with an average height of 2 mm, for each sample. The deposition strategy consisted of overlapping layers with constant origin and height increments. At the end of each layer the arc is turned off and a constant idle time between layers were imposed while the torch goes back to the origin. The thermal dynamics of the construction of the specimens were analyzed using the infrared thermographic filming technique. Acquisition of the process electrical signals, high-speed filming of material deposition, analysis of the chemical composition profile and microhardness were performed. No difficulties were observed in the use of metal-cored wires compared to conventional solid wires. The metal-cored wire showed good weldability in the chosen welding conditions and deposition strategy, even using a non-dedicated synergic program. Samples with similar dimensions to the objective were achieved for both process variants. As a validation phase, samples were built in an industrial environment at the German company DURUM Verschleiss Schutz. The results showed that, although adjustments in movers and workbenches were necessary, there is the possibility of using the conventional equipment of a welding and cladding company for WAAM parts manufacturing.



**Keywords:** Additive Manufacturing, 3D Printing, FCAW, Tubular Wire, Hadfield Steel.

## LIST OF FIGURES

## LIST OF TABLES

# LIST OF ABREVIATIONS

WAAM Wire + Arc Additive Manufacturing

GMAW Gas Metal Arc Welding

CMT Cold Metal Transfer

SM Subtractive Manufacturing

FM Formative Manufacturing

AM Additive Manufacturing

CAD Computer Aided Design

ASTM American Society for Testing and Materials

3D Three Dimensional

DED Directed Energy Deposition

GTAW Gas Tungsten Arc Welding

CSC Controlled Short Circuit

DWF Dynamic Wire Feeding

RMD Regulated Metal Deposition

SMAW Shielded Metal Arc Welding

FCAW Flux Cored Arc Welding

FTC Fused Tungsten Carbide

HSF High-Speed Filming

HF High Frequency

A/D Analog-to-Digital

IR Infrared

SAP Sistema de Aquisição Portátil

CNC Computer Numerical Control

HMI Human Machine Interface

ISO International Organization for Standardization

CTWD Contact Tip to Work Distance

WS Weaving Speed

TS Travel Speed

WFR Wire Feed Rate

$O_s$ Oblique Speed

IT Interlayer Temperature

CRA's Corrosion Resistant Alloys

## TABLE OF CONTENTS

# 1 INTRODUCTION

The first three industrial revolutions brought mass production, assembly lines, electricity, and information technology, raising workers' incomes and making technological competition the heart of economic development. The fourth industrial revolution, which will have a deeper and more exponential impact, is characterized by a set of technologies that allow the merging of the physical, digital, and biological world. One of the hype technologies that walks through the 4.0 industry wave is the additive manufacturing, popularly known as 3D printing. This new manufacturing concept provides manufacturing solutions once impracticable with former subtractive and formative manufacturing technologies. The principle of additive manufacturing is established on the fact that any object can have its digital geometrical concept sliced into layers and rebuilt using these 2D layers coordinates as a material deposition path, regardless of the complexity of its geometry. One of AM's technological variants for the construction of metal parts is called Directed Energy Deposition (DED). This categorization agglomerates the set of AM practices in which a thermal source is focused on the fusion of a feed material simultaneously with its deposition on a previously defined path, forming layers. Within this category, the process can still be classified according to the energy source used in the fusion of the feedstock. Concerning the form of feedstock two main forms can be observed: powder feed and wire feed. Within the DED category lies the AM variant that combines an electric arc as the thermal source and wire as feedstock, called Wire + Arc Additive Manufacturing (WAAM). Currently, plenty of researching centers around the world have been studying the WAAM technology, but only a few have published about the use of tubular wires, as feedstock. Differing from the conventional solid wire, tubular wires consist of thin tubes, with similar diameter and length as solid wires, filled with matter in form of powder. The employment of this type of feedstock for WAAM can bring benefits like higher deposition rates with less power consumption and especially the advantage of higher flexibility of production and development of alloys due to the use of powder in the core. The most usual manufacturing method used to produce metal-cored wires consists of folding a thin metal strip into a “U” shape, filling it with flux constituents, closing the “U” to form a circular section, and reducing the diameter of the tube by drawing or rolling. The core constituents in this fashion of tubular wires are predominantly alloying elements, even though arc stabilizers, deoxidizers, and slag inducers may also be present for improved weldability. When the core is filled mainly with metal alloying powder, it is called

metal-cored wire. An additional advantage is the likelihood of filling its core with ceramic particles, something unpracticable with solid wires. Another advantage of tubular wires over solid ones is the easiness of producing small batches of tailormade alloys for prototypes or repairing of parts made of non-conventional alloys. This flexibility also powers the growing application of functionally graded materials, that require the gradual deposition of different compositions of materials in the same structure to achieve gradual material properties. In a future 4.0 industry scenario in which the production tends to be more customized and decentralized, the metal-cored wires certainly will expand their share in the WAAM feedstock market.

The metal-cored wires are not employed in more studies due to the conventionality use of solid wires. The metal-cored wire's higher price, compared to standard steel or aluminum solid wires, discourages its use in studies of the general aspects of the WAAM.

Metal cored wires might not be the first choice for general studies about WAAM, but it can be mandatory in some projects of parts with wear resistance requirements. The studies about metal-cored wires in WAAM are important to support the buildup of parts with wear resistance needs. Parts like drilling heads and pipe fittings have high attractiveness to be manufactured by WAAM due to their geometric complexity and customization appeal.

Initial steps to enrich this field of study are the analysis of the metal-cored wires' performance with the GMAW process variants typically used for WAAM and to evaluate the necessity of developing synergic programs for metal-cored wires or if using non-specific programs would result in acceptable results. Most applied GMAW variants are based on current-controlled short-circuiting metal transfer, with dynamic wire feed (reciprocating wire), conceived for solid wires. How do these GMAW variants perform for metal-cored wires? To characterize this combination of feedstock and heat source, the manufacturing of samples along with thermographic filming are necessary experiments. The results aid to correlate the thermal dynamics during the manufacturing with the sample metallurgic outcome, which is mandatory to determine the part applicability and quality.

## 1.1 OBJECTIVE

This work aims to analyze the characteristics and contribute to lay the fundamentals for Wire + Arc Additive Manufacturing (WAAM) while using low heat input Gas Metal Arc Welding (GMAW) variants, combined with metal-cored wire as feedstock, a combination not

yet deeply approached in the literature. Most of the information available apply synergic welding programs dedicated to the wire-electrodes being fed, predominantly solid wires. Due to the technical relevance of metal-cored wires for the AM industry, goals were set to investigate their response to process stability (molten pool, metal transfer, arc), thermal and metallurgical influences, as well as overall performance under non-synergic GMAW procedures.

## 1.2 SPECIFIC OBJECTIVES

Specific objectives were proposed to achieve the main objective, being these:

- To build wall like samples using GMAW process with two different heat inputs and metal transfer modes, while keeping the same wire feed rate: controlled short-circuit mode (CMT) with lower heat input and pulse mode (CMT Pulse) with higher welding energy.
- Analyze the weldability of a hardfacing steel alloy with high Manganese content (~15% in weight) in form of metal-cored wire during the WAAM.
- The additive manufacturing of the samples must be thermographic recorded to acquire the thermal cycles of the samples during the deposition.
- The deposition must be recorded with a high-speed filming camera technology to analyze the material transfer characteristics for each process variant.
- Characterize the properties of the deposited walls by mapping its chemical composition and microhardness.
- As a validation stage, a sample must be additively manufactured with the know-how acquired in this work in an industry workshop using conventional hardfacing/cladding equipment.

# 2 STATE OF THE ART

## 2.1 MANUFACTURING PROCESSES OVERVIEW

The development of manufacturing processes has been one of the main foundations of human society as we know it. The modern economy lies on that constant progress, with the advances of technology changing the processes and production capacity severely for many vital industries from Agriculture to Healthcare and Oil & Gas. For instance, even human history can be outlined by the control of new manufacturing techniques it achieved, from the Stone Ages to the Industrial Revolution. Where it will go shortly and beyond will depend on many unpredictable aspects like the economic crisis and the Earth environment changes, but a look at where it began and where it currently stands helps to estimate the trendline of the future manufacturing processes.

The term manufacturing first known use dates 1567 from a Middle French writing. Its etymology denotes that it comes from the Latin words “manu” for hand and “factus” for make, meaning made by hand. Even though, the term nowadays widened its meaning for “to make from raw materials by hand or by machinery” (WEBSTER, 2020).

In 1836, when the industrial revolution was already discussed in London, the writer and philosopher Thomas Carlyle smartly stated:

> “*Man is a Tool-using Animal. Weak in himself, and of small stature, he stands on a basis, at most for the flattest-soled, of some half-square foot, insecurely enough; has to straddle out his legs, lest the very wind supplant him. Feeblest of bipeds! Three quintals are a crushing load for him; the steer of the meadow tosses him aloft, like a waste rag. Nevertheless, he can use Tools; can devise Tools: with these the granite mountain melts into light dust before him; he kneads glowing iron, as if it were soft paste; seas are his smooth highway, winds and fire his unwearying steeds. Nowhere do you find him without Tools; without Tools he is nothing, with Tools he is all*.” (CARLYLE, 2001).

Even though we see ourselves surrounded by objects, we unusually fully recognize that they become part of the humanity meaning itself, and most people do not recognize the harsh path that leads us to develop the skills and technology to control and invent the

manufacturing technologies required to produce these objects, especially in the quantities and quality we attained.

The manufacturing processes can be classified by a geometrical concept in three fundamental clusters: Subtractive, Formative and Additive (GEBHARDT; HÖTTER, 2016). More complex and detailed subdivisions can be found, like the DIN 8085 that states six general groups: cutting, changing material properties, joining, coating, casting/molding and forming (FÖRSTER; FÖRSTER, 2018).

The first fashion of manufacturing developed by our early ancestors was the Subtractive Manufacturing (SM), in other words, the subtraction of parts from a whole raw structure (e.g., rock boulders, tree branches) to achieve a designed useful tool out of it (e.g., chipped stone knife, wood fishing spear). The first findings of man-made tools date around 3,3 million years ago (ERLANDSON; BRAJE, 2013). They were, however, very rudimentary tools made from chipped stones, like Figure 1 shows. The drastic upgrade of human manufacturing control during the time is clear when one compares the former mentioned Neolithic tool with a contemporaneous micro-wall-like structure presented in Figure 2. Both are example of SM.

Figure 1: Chipped stone tool. 3 million year old, East Africa (ERLANDSON; BRAJE, 2013).

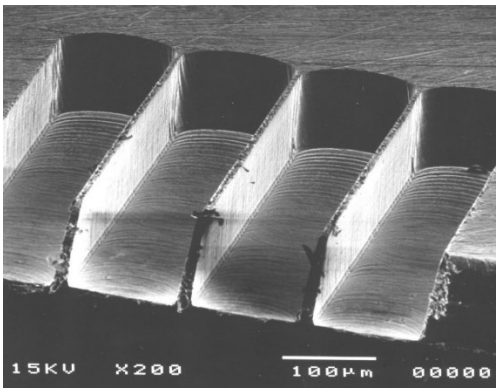

Figure 2: Micro walls machined using a 100-micron endmill on a stainless workpiece. (SHIN).

Opposing to the SM, the Formative Manufacturing (FM) processes require superior setup. Its subdivision covers processes like casting, bending, and forging that require external forces or heat to define the part geometry. Although, FM does not change the volume of the part. On the other hand, Additive Manufacturing processes, which this thesis covers, produces the chosen part shape by adding material, preferably by staggering contoured layers on top of each other (FÖRSTER; FÖRSTER, 2018). Therefore, it is also called layered technology. It`s important to highlight that the industry that demands advanced solutions like AM is an industry that also demands strict dimensional tolerances. Therefore, post-processing by SM is still required in most applications. The same is true for many processes of FM, like casting (VEVERS *et al.*, 2018). The AM main aspects and classifications will be cover more specifically in the next subchapter.

## 2.2 ADDITIVE MANUFACTURING

The principle of additive manufacturing (AM) is based on the fact that any object can have its digital geometrical concept (3D CAD) sliced into layers and rebuilt using these two dimensional (2D) layers coordinates as a material deposition path, regardless of the complexity of its geometry (FÖRSTER; FÖRSTER, 2018). According to the technical nomenclature standard offered by the American Society for Testing and Materials (ASTM), AM is “a process of joining materials to make objects from 3D model data, usually layer upon layer, as opposed to subtractive manufacturing methodologies.” (ASTM, 2012). Following this concept, the technology is now popularly known as three-dimensional (3D) printing. This additively perspective could already be seen in works from the late 80`s with the name of Stereolithography (LEVY; SCHINDEL; KRUTH, 2003), but only in the last two decades it

became a reality within specialized manufacturing industries, especially for metal components (DEBROY *et al.*, 2018). AM has been referred to as the third industrial revolution by the influential media, The Economist, in 2012, claiming a possible “sea of change in the contemporary culture” (PRINCE, 2014), due to its advantages comparing to conventional manufacturing processes.

The AM’s processes provide advantages in both business and technical facets, over traditional SM and FM technology. One of the main points is the possibility of manufacturing parts with complex geometries and, even so, with a high buy-to-fly ratio (ALBERTI *et al.*, 2014; DING, D *et al.*, 2015). Another advantage of AM over SM is the ability to produce prototypes on a reduced time scale with lower capital expenditure and operational expenditure, a feature that has already been utilized for decades by the automotive industry, especially for polymeric parts. Currently, AM has also called the industry's attention to the manufacture of parts in metal alloys, focusing on more complex alloys based on titanium, nickel and aluminum, mainly because it saves material costs by producing the components in their net shape or near-net shape (DING, DONGHONG *et al.*, 2015). The possibility of producing parts with composition or microstructure gradients and, consequently, gradual variations in their properties, known as Functionally Graded Materials (FGM), can also be highlighted (BOBBIO *et al.*, 2017). Positive aspects in sustainability aspects can also be pointed: better energy efficiency (e.g. lower consumption of raw materials), increased useful life of parts and machines (e.g. repairs, higher degree of customization), and the reconfiguration of the value chain within the production scope (e.g. smaller plants, local supply) (FORD; DESPEISSE, 2016).

The AM technologies can be subdivided into several categories. The ASTM F2792 standard classifies it in seven big clusters, each one covering some variants with the same principle of heating source, joining aspects and feedstock fashion (ASTM, 2012). One of AM's technological variants for the construction of metal parts is called Directed Energy Deposition (DED). This categorization agglomerates the set of AM practices in which a thermal source is focused on the fusion of a feed material simultaneously with its deposition on a previously defined path, forming layers (ASTM, 2016). Within this category, the process can still be classified according to the energy source used in the fusion of the feedstock into two categories: electric arc welding processes and high intensity welding processes such as laser and electron beam (ASTM, 2016). In relation to the form of feedstock two main forms can be observed: powder feed and wire feed. Within the DED category lies the AM variant

that combines an electric arc as thermal source and wire as feedstock, called Wire + Arc Additive Manufacturing (WAAM) which was addressed in this work and will be explained in the next subchapter.

### 2.2.1 **Wire + Arc Additive Manufacturing**

WAAM presents potentially the higher deposition rate amongst the DED group (DEBROY *et al.*, 2018), providing higher productivity compared to the other high intensity processes (laser and electron beam), being especially superior for the manufacture of parts with larger build volume and fewer dimensional complexity (compared do AM). A large build volume is considered as a volume superior to 1000 $mm^3$ (ASTM, 2016). There are three main arc welding processes that currently showed to fit the WAAM needs: Gas Metal Arc Welding (GMAW), Gas Tungsten Arc Welding (GTAW) and Plasma Transferred Arc (PTA). The most suitable welding process in the current state of the art seems to be the GMAW (DAHAT *et al.*, 2020). This assumption takes in account specially the inherent coaxiality of the electric arc with the feedstock in form of wire. The heating source coaxiality with the additive material provides a higher tool displacement degree of freedom, compared to the GTAW, per example. The use of wire as feedstock facilitates the process comparing to the use of powder, like in PTA.

The use of well stablished and inexpensive equipment from the welding industry is also a key factor for the use of GMAW in WAAM. The main difference lies on the fact that these equipment usually are used for joining/coating whereas for WAAM it is used for layer by layer deposition to make functional parts (DAHAT *et al.*, 2020). However, there are also challenges to be overcome, especially regarding the processability of materials. The main deleterious effects of the WAAM are the residual stresses formed in the built part as well as the anisotropy in the mechanical properties (CUNNINGHAM *et al.*, 2018; HU *et al.*, 2018). Currently, there is a lack of techniques aimed at mitigating these defects, and the most common solutions are focused mainly on variations in the strategy of deposition (CUNNINGHAM *et al.*, 2018), control of the heat input (DA SILVA *et al.*, 2020) and alternating layer depositions with in situ post-processing techniques, like high-pressure rolling (COLEGROVE *et al.*, 2013).

The conventional GMAW process, in its less energetic working range of short-circuit metal transfer mode, presents a metal transfer that is customarily inconstant (KVASOV,

2000). On the other hand, in its most energetic array, through free-flight metal transfer mode, the GMAW features high heat input and pressure on the welding pool. Both situations are deleterious for WAAM. However, conventional GMAW processes are still able to be used for WAAM, although other paraphernalia, like active cooling, must be used to surpass the intrinsic cons of the conventional mode. That metal transfer dilemma, however, can be surpassed with advanced variants of the GMAW process. These advanced variants offer deposition conditions within the upper mentioned extreme situations.

These modern equipment offers more controlled wire feeding dynamics and metal transfer modes (e.g. pulsed mode) through the advent of intelligent electric waveform design. These advanced welding power sources can provide faster response times that have allowed better control of the imposed electrical waveform, weakening the heat input and smoothing the droplet transfer from the wire tip to the weld pool. The next subchapter disserts about the advanced GMAW processes that improved the metal transfer conditions to allow better results in WAAM.

## 2.3 ADVANCED GMAW PROCESSES

The origins of the GMAW process lies on the creation of H.E. Kennedy in 1948. Although, at that time low control over the process dynamics were possible. The use of protective gas dates 10 years later, in 1958, when the use of $CO_2$ led to the development of short circuit metal transfer, allowing affordable quality weldments in all positions, which has popularized the GMAW process (CARY, 1988). With a technology development overview, until the late 60's the equipment used for the GMAW can be named as conventional. That early stage apparatus provided the electric power to the arc by means of a control based on electromagnetic effects, such as variation of inductance and regulated transformers by shunt, iron or moving coil (SCOTTI; PONOMAREV, 2008; RODRIGUES, 2016). Advances in power electronics have made conceivable the emergence of a new group, named after electronic power sources. In this group lies the power sources that benefits from the use of thyristors and transistors. The transistorized power sources started with the analogical and linear approach. That development allowed higher response times and low electrical wave noise (MODENESI; MARQUES; SANTOS, 2005), enabling an upgrade in metal deposition smoothness and repetitiveness. The disadvantages lie on the transistors high power dissipation (GOHR, 2002). A group of power sources that also uses transistors but with higher energy

efficiency and that enable smaller transformer sizes, is the switched-mode transistorized power sources (GOHR, 2002). Within time, around 2000, the power sources were connected to PC's and the GMAW process deeply benefited from this digitalization (RODRIGUES, 2016).

The digital controlled transistorized power sources enabled the possibility of acting directly on the welding current, the variable with most influence on welding results. A collection of current controlled waveforms was developed since then, benefiting low heat input applications that used the short circuit metal transfer mode. These processes can be classified as Controlled Short Circuit (CSC). Three main characteristics of the CSC processes that directly benefit it to the application in WAAM can be highlighted: reduced heat input, higher metal transfer stability and decrease in spatter formation (SCOTTI; PONOMAREV, 2008). The CSC working principle is based on the regulation of the current and its control in real time. To obtain such control, the monitoring and feedback strategy are used, so that the power source can respond to the instantaneous operating condition (voltage) according to what was previously programmed (current). Per example, when the metal droplet is almost detaching from the wire tip, the controller reads the voltage rise and instantaneously refeed the information to reduce the current, resulting in a smother detaching behavior.

One of the state-of-the-art technologies that uses the previously cited CSC technology and that is widely used in WAAM is the process variant known as Dynamic Wire Feeding (DWF). These processes combine the CSC benefits with another refined control of metallic transfer: the synchronized wire electrode backward movement with current controlled waveforms. The next subchapter will dissert about the use of the DWF correlated with CSC and how it can benefit the WAAM application.

### 2.3.1 **Dynamic Wire Feeding**

Advances in the welding equipment were mainly aimed at the electro-electronic field of the welding power sources or new torches design until the Austrian company Fronius International GmbH, in 2005, patented the first equipment with an additional servomotor in the wire feeder (SCHÖRGHUBER, 2015). This equipment introduced the electromechanical control of wire feeding in the field of welding, presenting the concept of Dynamic Wire Feeding, or, at least, turning the concept in a fully commercial solution. Prior to this innovation, the wire feeding systems for GMAW consisted merely of a DC motor, promoting

the wire feed at a constant speed. Therefore, the servomotors, integrated with micro controlled digital source systems, made it possible to implement wire trajectories in different speed profiles and orientation (BRUCKNER, 2005; RODRIGUES, 2016). The direct control of wire movement enables the not possible before backward movement of feeding wire. The backward movement happens at the instant the short circuit is detected, mechanically assisting the droplet detachment by breaking the surface tension force between the droplet and weld pool, as the Figure 3 schematic drawing presents.

Positioned in the torch there is a high dynamic response servomotor which allows high frequencies of movement orientation inversion. This wire behavior, composed with the welding current control, provided the CMT with a very smooth metal transfer, with virtually no spatter and low fumes generation (MARQUES, 2013) being held as the GMAW process variant with lowest global heat input (POSCH *et al.*, 2014) what made it the first process choice for GMAW in WAAM applications. The functioning of the CMT can be understood with the help of the idealized oscillograms and images associated with the moments indicated in Figure 3.

The starting point is showed by the frame number 1, corresponding to the instant when the arc is opened. Although the wire continues to be pulled, this is also the moment that the torch motor begins to slow down to reverse the movement. The instant recorded by the frame 2 indicates the point where the wire stops. After reopening the arc, the power source imposes a current pulse to fuse the wire and form the droplet on its tip. With the wire in forward movement and the drop formed, the arc current is then reduced in the instant 3 until the short circuit 5. Reducing the current before the short circuit contributes to the reduction of spatter formation. The short circuit is detected by a decay in the voltage value levels near 0 V (zero Volt). This moment marks the beginning of the wire deceleration, so the orientation inverts. The frame 6 records the point where the wire speed passes again by zero and starts the backward movement. In the moment of detection of the short circuit, the current is reduced again. The metal transfer happens, fundamentally, by the action of the surface tension force and by the recoil movement of the wire. The reduction of current in the short circuit also contributes to the reduction of fumes and spatter. At moments near the arc reopening, the metal bridge becomes very thin. A high current density in these conditions can cause metal vaporization, with a tendency to create fumes and micro explosions in the moment of the breakup. The frame 7 indicates the imminence of metal bridge rupture, where later the arc is reopened and a new cycle begins (RODRIGUES, 2016; MARQUES, 2017).

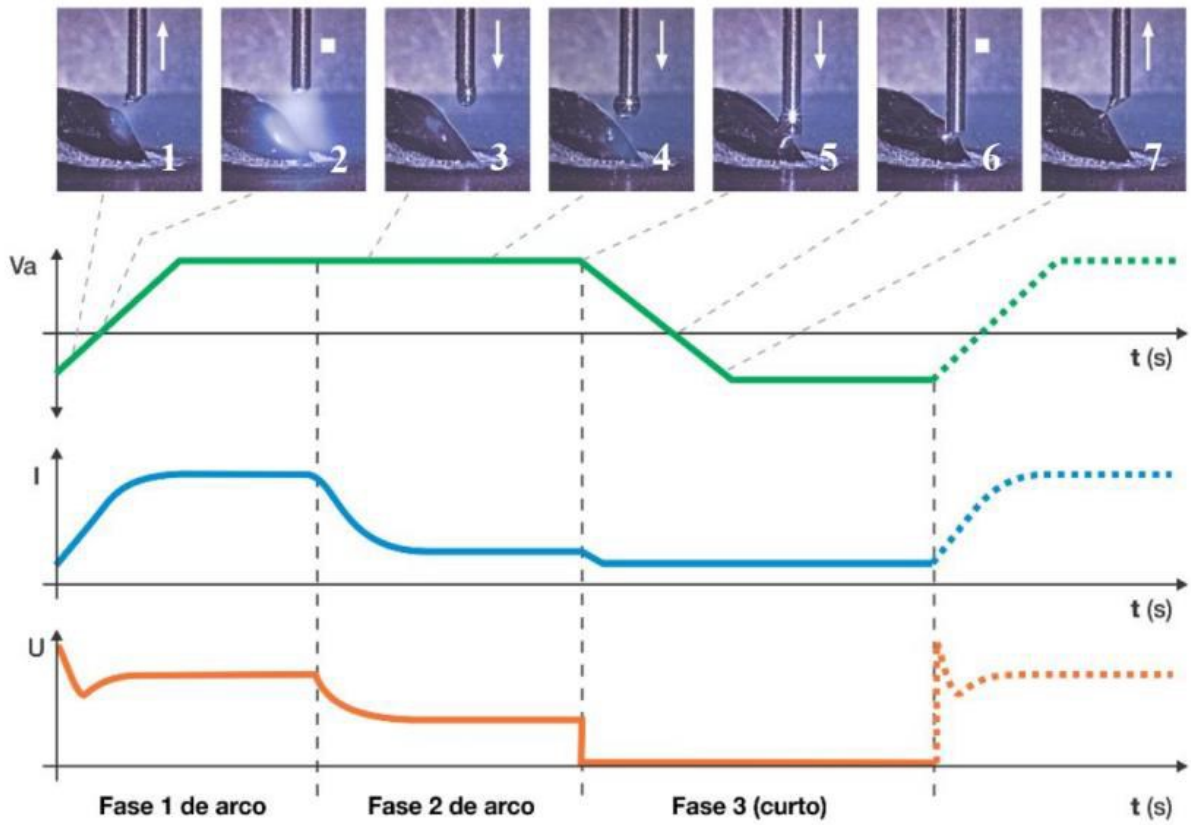


Figure 3: CMT oscillograms of wire feed speed (Va), current (I) and voltage (U) (MARQUES, 2017).

The LABSOLDA Welding and Mechatronics Institute, together with fellow companies, seeks to develop a complete DWF version, that, in opposite to the commercial CMT version, will provide fully open architecture mode (RODRIGUES, 2016). The DWF version will offer total freedom in the modification of the electric welding parameters (waveforms), wire dynamics, logic, and control parameters. This allows the creation of customized waves and synergic programs for each application, without the need to adapt non-optimized parameters to limited synergic programs available in currently commercial versions. The superior system openness is an appreciable advantage to WAAM, since an optimized wave can be created for each welding condition, per example deposition strategy and material. The LABSOLDA DWF version allows a refined manipulation of the process thermal efficiency over the formation of the beads (and consequently over layers geometry) by manipulating the waveform and wire movement patterns, with the wire plunging more or less, faster or slower into the weld pool. The possibility of such a sensitive energetic refining allows an even better control of the molten pool dynamics, a primordial factor in the WAAM success. The dynamics of the weld pool has great importance for the WAAM since the

dimensional stability of the deposited layers is causally linked to the solidification conditions of the weld pool. But what makes this development even better is the freedom to optimize thermal input conditions for many different combinations of welding conditions (e.g., additive material, welding gas, building strategy) including non-conventional wire type like metal-cored wires with tailormade alloys.

Since the LABSOLDA DWF equipment is still in development, it was chosen to use the CMT power source and peripherical in the first experiments of this work. The next subchapter will elucidate the concept of another CSC process used in the validation stage of this work. The process used was the Regulated Metal Deposition (RMD).

### 2.3.2 **Regulated Metal Deposition (RMD)**

Developed in 2004 by the American company, Miller Electric, the RMD technique is one of the GMAW processes with CSC waveforms commercially available. The Figure 4 introduce the idealized current oscillogram for the RMD process and the metal transfer condition in each waveform stage (DAS; VORA; PATEL, 2019).

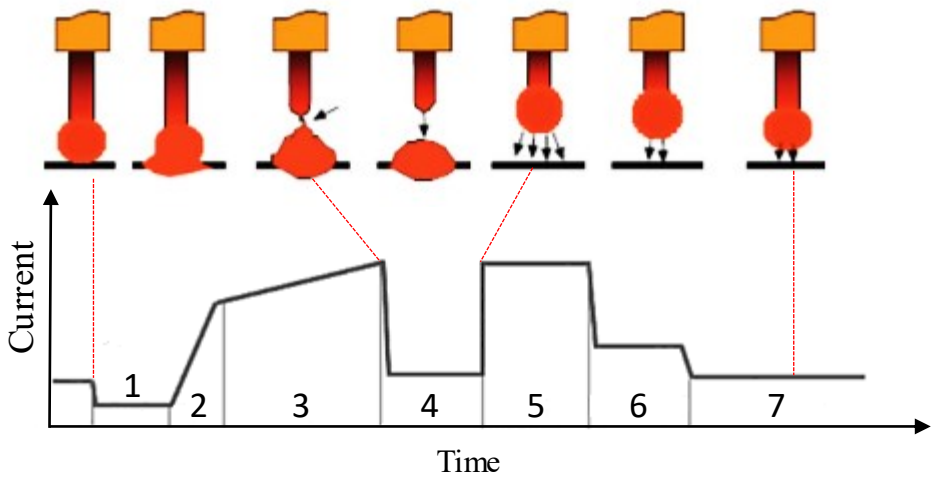


Figure 4: Typical RMD cycle. Adapted from (KAH; SUORANTA; MARTIKAINEN, 2013; DAS; VORA; PATEL, 2019).

According to the manufacturer, the RMD software program, working with an inverter-based welding system and closed-loop feedback, closely monitors and controls the electrode current at speeds up to 50 µs. Moreover, the software accurately adjusts the required speed and gas combination for a specific wire diameter. Thus, based on the heat history of the tips, it predicts future arc conditions and controls the droplet transfer accordingly. The RMD

approach is illustrated in seven steps as follows (KAH; SUORANTA; MARTIKAINEN, 2013). At step (1) the metal drop on the end of the wire wet-out to the molten pool. Step (2) refers to the Pinch phase. An Increase in current level aid the pinch effect. In the step (3) the current slightly increase to clear the short circuit while simultaneously watching for pinch detection. In the step (4), the pinch detection occurs before the metal bridge breaks the current is set to a low level. After the arc reopening, at the step (5) an increase in current is imposed to form again a droplet on the wire's tip. In the step (6) the current level drops to a low enough level to allow a short circuit to occur. Then the current level goes back to its pre-short circuit level in step (7). If the background current of step (6) exists for a relatively long time, the pre-short period drops current to an even lower level to make sure arc force does not push the weld pool back, preventing excessive pool agitation. (KAH; SUORANTA; MARTIKAINEN, 2013)

The use of advanced GMAW processes like RMD and CMT are commonly seen in the WAAM research. Despite that fact, few works combine these processes with the advantages of adopting Metal-cored wires as feedstock. This novel approach was explored in the present thesis. The next subchapter brings enlightenment support about metal-cored wires for an adequate awareness of the benefits of the association between these processes' variants and nonconventional feedstock for WAAM purpose.

## 2.4 METAL-CORED WIRES

The most common used GMAW feedstock consists in solid wires with circular section throughout its continuous length. However, wires can feature different geometry, conditional on its conformation process. Around 1957, a wire with tubular cross-section was introduced to the GMAW market (MYERS, 2002). Relating the previously known gains of Shielded Metal Arc Welding (SMAW) fluxing elements, the tubular wires were filled with similar content (AWS, 2004).

Over time, the flux evolved to refined mixtures of inorganic and metallic elements that act to deoxidize (Si, Mn), stabilize the electric arc (Na, K), to aid the alloying elements transfer, to form protective gas atmospheres (CaF2, CaCO3) and to form the protective slag (TiO2, CaO, K2O, Na2O) (FORTES; ARAÚJO, 2004). The slag covers the molten pool as it solidifies, protecting it from the O2 rich atmosphere and reducing the bead cooling rate (FORTES; ARAÚJO, 2004). The flux improves the metallic transfer smoothness, reducing

spatter and improving the wire fusion rate compared to the solid wires (AWS, 2004). The Figure 5 diagrammatically exemplifies the difference between metal-cored and solid wires, showing the cross- and transversal-sectioning, the metallic transfer behavior and penetration profile (D'ARCY, 2012).

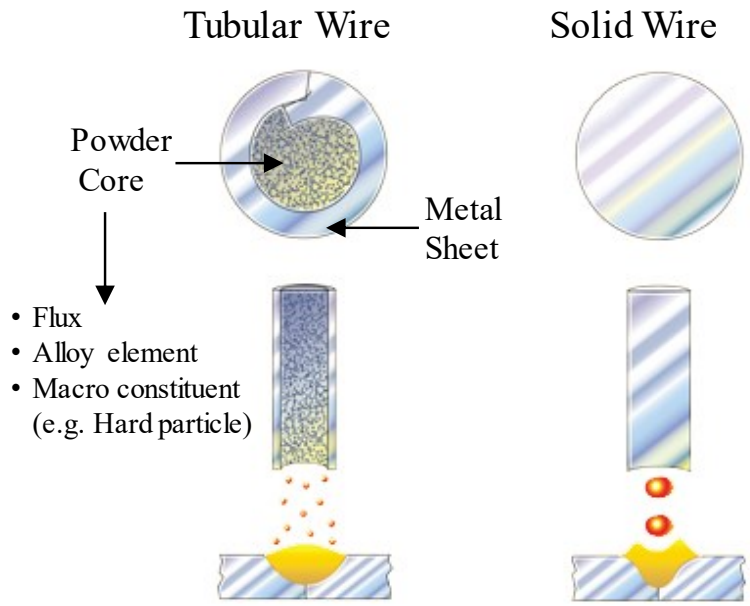


Figure 5: Idealized comparison between Metal-Cored and Solid Wires. Adapted from (D'ARCY, 2012).

The most usual producing technique used to manufacture tubular wires consists in folding a thin metal strip into a “U” shape, filling it with the flux constituents, closing the “U” to form a circular section and reducing the diameter of the tube by drawing or rolling (NORRISH, 2006). The Figure 6 diagrammatically explains the production process.

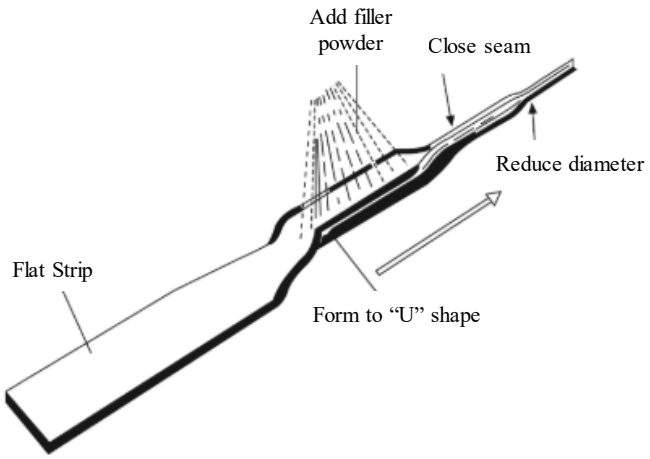


Figure 6: Production of flux-cored wire. Adapted from (NORRISH, 2006).

The American Welding Society (AWS) states that if the GMAW equipment is performed with flux-cored wires the process is referred as Flux-cored Arc Welding (FCAW) (AWS, 2004). Although not all tubular wires are filled only with fluxing elements. Per instance, the category named Metal-Cored Wires have its core filled with metal alloying powder elements or even filled with ceramic particles, or a mix of protective flux, metal and ceramic particles. Frequently, the term FCAW is used without distinction, disregard the core material, especially in the commercial and industrial environment. For the material used in this work the more accurate term is metal-cored wire.

Regarding the advantages of metal-cored wires, the higher deposition rate and production flexibility can be highlighted. In metal-cored wires the electric current flows only partially through the core due to its powder dispersive nature. Indeed, the current is conducted mainly through the metallic band. With a thinner active conductive cross section, the tubular wires undergo superior Joule effect compared to solid wires (WIDGERY, 1994; FORTES; ARAÚJO, 2004). This explain the higher fusion rates seen in metal-cored wires, allowing higher wire feeding speeds (CARY, 1988) and higher deposition rates for the same power input (WIDGERY, 1994). Although, the productivity is debatable (BRITO, 2019), depending on many factors as welding gas mixtures, per example (WIDGERY, 1994). Therefore, for WAAM applications, where productivity may not be the first challenge to overcome, the possibility of depositing more material weight compared to solid wires, with the same heat input, is of great value (LIN *et al.*, 2019).

The most useful advantage of metal-cored wires employment in WAAM, however, lies on its superior production and development flexibility. Currently, only a limited number of institutions and specialized wire manufactures, like DURUM Verschleiss-Schutz, are starting to develop alloys dedicated to WAAM, even though in small scale. The current small market demand does not allow high production volumes of special alloys designed for WAAM applications due to lack of commercial attractiveness (FRAZIER, 2014; LIN *et al.*, 2019). On the other hand, the WAAM market is in ascendency, and it will eventually increase in volume. Since the production of solid wires of specific alloys is only economically feasible for large volumes, the use of metal-cored wires can be a solution for the WAMM consumable boost at early stages of this technology. Notwithstanding, the R&D of adequate additive material chemical composition is benefited by the metal-cored wire production method. Small batch productions of tailormade alloys for prototypes or repairing of parts made of non-conventional alloys can easily be made with metal-core wires, compared to solid ones (LIN *et*

*al.*, 2019). This flexibility also impacts the growing application of functionally graded materials, that require the gradually deposition of different compositions of materials in the same structure to achieve gradual material properties. Another advantage of metal-cored wires over solid wires is the possibility of filling hard ceramic particles in its core, as the metal-cored cross section showed in Figure 7 exemplifies.

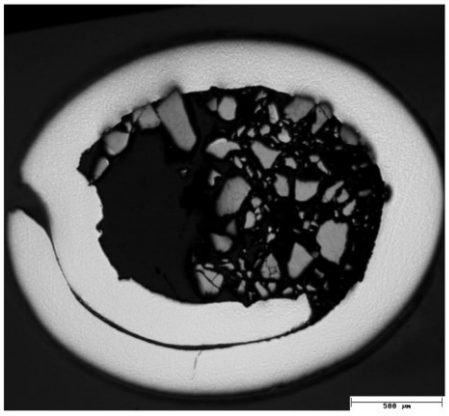

Figure 7: Ni basis Metal-cored wire filled with Fused Tungsten Carbides (55% wt.) (WILDEN *et al.*, 1999).

These extreme hard particle (reaching over 2900 $HV_{0,1}$ ) do not melt during the deposition process, rather precipitating in a metal matrix, forming a Cermet composite material (LAMPKE *et al.*, 2011), usually applied for Hardfacing applications. The Figure 8 demonstrate a hardfacing bead with embedded Fused Tungsten Carbides (FTC) in a Ni-B-Si rich matrix.

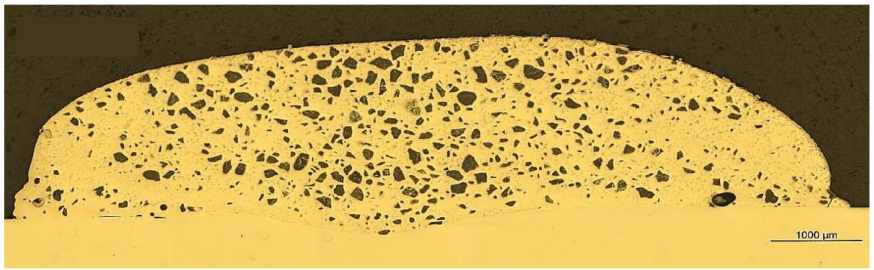


Figure 8: Ni-basis hardfacing deposit with FTC particles embedded. Adapted from (ROCHA, 2017).

The actual GMAW integrated solution offers only few specific waveform and synergic programs for metal-cored wires. Moreover, the offered programs are aimed to high deposition applications where excessive heat input is not an issue, like joining and coating of thick plates or repairing components of large dimensions and volume. This condition supports even more the need for an open architecture advanced power source that would allow the

sensible parametrization of metal-cored wires of a wide range of welding condition like non-conventional combination of materials, wire diameters and gas mixtures.

# 3 MATERIALS, EQUIPMENT AND METHODOLOGY

The next subchapters will bring the information about the materials, equipment and methods used in this research work. The work was done in four stages, as presented in the topics below. Since this work was done not only in one research facility, but some stages were also done in the LABSOLDA Welding and Mechatronics Institute and other in the German company DURUM Verschleiss-Schutz.

- **1st Stage – Pre-parameterization and Setup**: during this stage, the research requirements were first set. The working bench was arranged, and the pre-parameters and welding conditions set. The main bibliography research about the theme was doing along this phase. *Completed in LABSOLDA*.

- **2nd Stage – Samples Manufacturing:** during this stage, wall-like samples were built, and the process data was acquired. Thermographic, and high-speed filming also took place in this stage. *Completed in LABSOLDA*

- **3rd Stage – Data Treatment and Analysis:** during this stage, the samples were prepared and analyzed. The acquired process soft data (electric signals, thermal behavior, deposition characteristics) were treated and analyzed. *Completed both in LABSOLDA and DURUM.*

- **4th Stage – WAAM Part Validation:** during this stage, a representative part was built by WAAM with the background know-how developed in the former stages. *Completed in LABSOLDA and DURUM*.

This chapter will be subdivided in subchapters according to the stage of interest. Firstly, materials and equipment used will be presented. The methodology of the pertinent stages will be posteriorly exposed, after the materials and equipment are already known by the reader. It is important to highlight that some measuring units are not according to the

International Unit System due to the easiness of use of other units in the welding research context. Per example, the deposition rate is stated in [kg/h] instead of [kg/s].

## 3.1 MATERIALS AND EQUIPMENT

The materials and equipment will be presented according to the research stage. Primarily, the materials and equipment used to accomplish the 1st, 2nd and 3rd Stages will be listed in tables, for easiness of consulting. Furthermore, the 4th Stage's material and equipment will be presented with similar tables of content. This split was made once there is a considerable change in equipment and materials between the first three stages and the last one.

### 3.1.1 **Samples Manufacture and Analysis (1st, 2nd and 3rd Stages)**

The materials and equipment are divided by subtopic according to the main content.

#### *3.1.1.1 Welding Equipment*

The Table 1 brings the equipment, and their model specifications.

Table 1: Welding equipment.

| Equipment | Model |
|---|---|
| Welding Power Source + Wire Feeder | -Fronius CMT Advanced 4000R |
| Configuration Interface | -RCU5000i |
| Handling Device | -Yaskawa-Motoman, HP20 Antropomorfic Robot |
| Handling Device Controller Unit | -DX 100 |
| Pendant (HMI) | -NX 100 |

For the deposition rate analysis, a scale specified in the Table 2 was used.

Table 2: Scale specifications.

| Equipment | Specification | |
|---|---|---|
| Precision Scale - BEL S3201 | -Class: | II |
| | - Resolution: | 0.1 g |
| | - Max. weight: | 3200 g |

### *3.1.1.2 High Speed Filming Equipment*

Table 3 presents the equipment used for the high-speed filming (HSF) acquisition. Along with the cutting-edge equipment, the expertise developed by the LABSOLDA's design specialist, Marcelo Okuyama, was essential to the recording and image digital treatment of the acquisitions.

Table 3: High Speed Filming Equipment.

| Equipment | Specification | |
|---|---|---|
| High Speed Camera IDT Y4-S2 | - Max. Resolution: | 1024 x 1024 |
| | - Max. Acquisition rate: (in the max. resolution) | 5100 fps |
| | - Min. Exposure time: | 1 µs |
| Laser Lightinning System Cavitar CAVILUX HF | -Laser Class: | 4 |
| | - Pulse power: | 500 W |
| | -Pulse time: | < 50 ns |
| | - Wavelenght: | 810 nm |
| Data Acquisition System IDT, DAS MotionPro | - Analogic input chanel: | 16 |
| | - A/D conversor resolutior | 16 bits |
| | - Max. Acquisition rate: | 500 kHz |
| | - Input tension range: | ±10 V |

### *3.1.1.3 Thermographic Filming Equipment*

The infrared (IR) thermographic analysis was made with the equipment presented by Table 4.

Table 4: Thermographic Camera Equipment and Specification.

| Equipment | Specification | |
|---|---|---|
| Thermographic Camera FLIR SC 7000 | -Spectral range: | 7.7 to 9.3 µm |
| | -Resolution: | 320 x 256 |
| | -Pixel size: | 29 µm |

### *3.1.1.4 Electric Signal Acquisition Equipment*

The Table 5 present the equipment used for the electric signal acquisitions. For the Wire Feed Speed measurement, a speed transducer was attached to the interior of the wire feeder head. The data acquisition and treatment were made with its dedicated software.

Table 5: Electric Signals Acquisition Equipment.

| Equipment | Specification | |
|---|---|---|
| IMC Portable Acquisition System - SAP - Version 4 | -Signal Acquisition rate: | 5 kHz |
| | - Chanels number: | 4 |
| | -Signals Measured: | -Voltage; |
| | | -Current; |
| | | -Wire Feed Speed. |

### *3.1.1.5 Microhardness*

A microhardness HMV Shimadzu equipment was used. The microhardness test was made according to the Vickers standard, with pyramidal indent and 1.961 N (~200g) of load, during 10 s. The measurements were made starting from the bottom, at 2.5 mm from the base. Subsequent measurements were made every 2.5 mm until reaching the top.

### *3.1.1.6 Metallography*

Semi-automatic grinding (80 – 1200 mesh) and polishing (Alumina, 3 μm) rotative table was used. As etchant, a marble reagent was employed (total submersion, time of 7 s) for the macro analysis. The micrographs were made with two different etching: Adler and Behara 2.

### *3.1.1.7 Chemical composition analysis – Arc Spark Spectrometer*

A mobile metal analyzer by arc spark optical emission spectroscopy, model SPECTROTEST, was used. Three measurements points were analyzed: base, middle and top. The base and the top correspond to 2.5 mm from the extremes, while the middle point is located in the middle of the sample height.

#### *3.1.1.8 Feedstock, Substrate and Shielding Gas*

As feedstock, a high manganese steel alloy was employed in form of metal-cored wire, with diameter of 1.2 mm. The Table 6 presents the specifications of the metal-cored wire. During the work, the alloy was referred by its popular name for a better exhibition and comprehensibility.

Table 6: Metal-Cored Wire Specification.

| Metal-Cored Wire Commercial Designation | DIN EN (14700) | Popular Alloy Name | Chemical Analysis According to Material Certificate (%) | | | | | | | |
|---|---|---|---|---|---|---|---|---|---|---|
| | | | C | Si | Mn | Cr | Ni | Mo | Co | Fe |
| DURMAT FD 250 K | (T Fe9) | Mangalloy | 0.32 | 0.40 | 14.90 | 12.25 | 0.53 | 0.28 | --- | Bal. |

As substrate, carbon steel bars were used, with the specifications as shown in the Table 7. Each test used a sample bar with dimensions of 200 x 50 x 12,7 $mm^3$. As shielding gas, industrial pure Argon was employed with a flow of 15 L/min.

Table 7: Substrate Specification.

| Substrate | DIN EN (WN) | ASTM | Chemical Analysis According to Standard (%) | | | | | | | |
|---|---|---|---|---|---|---|---|---|---|---|
| | | | C | Si | Mn | Cr | Ni | Mo | Co | Fe |
| Carbon Steel | C22 (1.0402) | 1020 | 0.18 - 0.23 | < 0.40 | 0.30-0.60 | < 0.40 | < 0.40 | < 0.10 | --- | Bal. |

### 3.1.2 **WAAM Part Manufacture (4th Stage)**

The materials and equipment used in the fourth stage, the validation stage, are presented by subtopics according to the main content as follows below.

#### *3.1.2.1 Welding Equipment*

The Table 8 brings the welding equipment, and model specification.

Table 8: Welding equipment.

| Equipment | Model |
|---|---|
| Welding Power Source + Wire Feeder | -Miller Auto-Continuum 500 |
| Handling Devices | -CNC Table (3 Axis)<br>-Turn Table (1 Axis) |
| Handling Device Controller Unit | -Siemens SIMATIC<br>-Mach3 (PC) |
| Human-Machine Interface (HMI) | -Siemens SIMATIC HMI Touch |

#### *3.1.2.2 Feedstock, Substrate and Shielding Gas*

In this stage, the Mangalloy metal-cored wire with 1.2 mm of diameter was chosen, similar to the first stages. The Table 9 shows the chemical content specification.60

Table 9: Metal-cored wire specification.

| Metal-Cored Wire Commercial Designation | DIN EN (14700) | Popular Alloy Name | Chemical Analysis According to Material Certificate (%) | | | | | | | |
|---|---|---|---|---|---|---|---|---|---|---|
| | | | C | Si | Mn | Cr | Ni | Mo | Co | Fe |
| DURMAT FD 250 K | (T Fe9) | Mangalloy | 0.32 | 0.40 | 14.90 | 12.25 | 0.53 | 0.28 | --- | Bal. |

As substrate, carbon steel bars were used, with the specifications as shown in the Table 10. Each test used a plate with dimensions of 400 x 180 x 24,5 mm3. As shielding gas, a gas mixture of 18% $CO_2$ in Argon, branded Corgon 18, was employed with a flow of 15 L/min.

Table 10: Substrate Specification.

| Substrate | DIN EN (WN) | ASTM | Chemical Analysis According to Standard (%) | | | | | | | |
|---|---|---|---|---|---|---|---|---|---|---|
| | | | C | Si | Mn | P | S | Mo | Co | Fe |
| Structure Steel | S235JR (1.0038) | A36 | 0.22 max | 0.05 max | 1.60 max | 0.05 max | 0.05 max | --- | --- | Bal. |

## 3.2 METHODOLOGY

Similarly, to the previous subsection, the methodology will be split in subsection for each stage of work.

### 3.2.1 **First Stage – Sample geometry definition and welding parameterization**

At the first stage of this research the specific objectives were:

- Define a representatively geometry for the samples;
- Define the deposition strategy;
- Define the welding parameters for the combination of metal-cored wires and welding equipment.

The methodology of each specified objective is presented above in subtopics.

#### *3.2.1.1 Sample's geometry*

The first step to manufacture a part by WAAM is the definition of its geometry. To represent a thick section of a part, wall-like structures were concepted as representative samples that would reflect real parts deposition behavior, following this work main objective. The adjective "thick" has a relative connotation, thus it`s meaning must be clarified. In this work, the term "thick layer" is meant as a layer with a wide width that would not have its dimension reachable merely by the deposition of single beads as the whole section, as occurs to thin sections. GMAW processes could be adjusted to achieve larger widths only by deposition single beads by adjusting its welding conditions and parameters (wire diameter, welding energy, WFR and gas flow rate), resulting in beads with even over 14 mm of width (KIM; KWON; PARK, 1996). However, these parameters do not suit the WAAM requirements, since to achieve large width single beads, high energy input is mandatory. Regardless novel experimental cooling techniques that could solve the former related issue, GMAW process with lower energy input has proven to be the most suited options for WAAM application. Using the GMAW low energy range permit less heat input into the part, however, implying in single beads with reduced welding pool size, that would further solidify in beads of small width. Thus, in this work a thick width was considered a width of at least 15 mm.

The width of 15 mm was chosen, along with 100 mm of length and 40 mm of height. The Figure 9 brings the drawing concept, with the geometry of the idealized wall-like structure (in blue), deposited over the substrate.

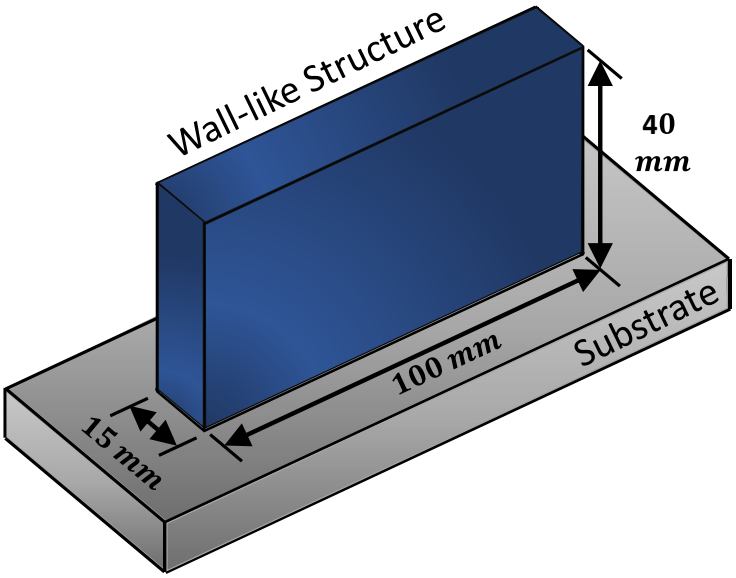


Figure 9: Sample drawing: Thick layered wall-like structure.

*3.2.1.2 Deposition Strategy*

The deposition strategy, in the WAAM context, is a term that states to the combination of factors regarding the processes variants one can elected to build a part additively. Other terms are used interchangeably. Terms as WAAM strategy (YUAN *et al.*, 2020), process planning strategy (ZHAO *et al.*, 2020) , build strategy (OJO; TABAN, 2020), layering strategy (CHEEPU; LEE; CHO, 2020) are used, regarding to the author choice. The ASTM and ISO terminology standards do not bring reference to this issue (ASTM, 2012; ASTM, 2018). The term, though, seeks to determine, at least, but not only, the following items:

- **Deposition path** - The path which the torch will be displaced while depositing the feedstock, how the material will be spread if needed.
- **Cooling strategy** - Cares about how to keep the thermal behavior of the deposit. Define strategy to achieve the aimed geometry and properties along with the deposition path planned.

The deposition strategy features adopted in this work are also listed in the Table 11. The wall-like structure proposed was sliced in 20 layers of equal height. This slice number was set to match the layer height average of 2 mm. This average layer height value was

defined according to previous works done in recent works with similar methodology (ROCHA *et al.*, 2020).

Every layer was deposit in the same direction. Right after reaching the end point, the arc extinguished and returned to the original starting point. As it reached the start point, a vertical "z" increment was programmed to happen with the value of the average layer height, thus, starting again over the precedent layer with the same contact tip to work distance (CTWD) in every new layer. Although the layers did not have always the same exact height, no distance feedback control to correct the CTWD was employed.

Idle time between the deposition of every layer was used as the cooling strategy, aimed to avoid overheating the structure while it was being built. The idle time period was set to be the exact time of the deposition of the layers, 60 s. This idle time happened during the torch displacement to the starting point of the new layer.

Table 11: Deposition Strategy main characteristics.

| **Structure type** | **Layer height average (mm)** | **Path Planning** | **Tranversal Material Spreading** | **Cooling Strategy** | |
|---|---|---|---|---|---|
| Multi-layer | 2 | Unidirectional | Weaving | Idle time between every layer | |
| Total height (mm) | Layers to reach part height | Fixed Arc Start/Stop Point | Trapezoidal Pattern | Idle time (s) | Layer Deposition time (s) |
| 40 | 20 | PA (flat position) | stop time= 1s<br>f = 1 Hz<br>A= 14.7 mm | 60 | 60 |

To achieve the 15 mm layer width, a transversal periodic movement was set to the torch travel trajectory. This practice is usually employed to spread the additive material as it is deposited. The weaving is extensively used in the welding context, especially for coating applications. That technique is known as weaving, or, more technically as oscillatory movement. Different patterns of weaving trajectories are used, as the Figure 10 shows. In this work, a Trapezoidal pattern was programed. The linear trajectory is related to single beads deposition.

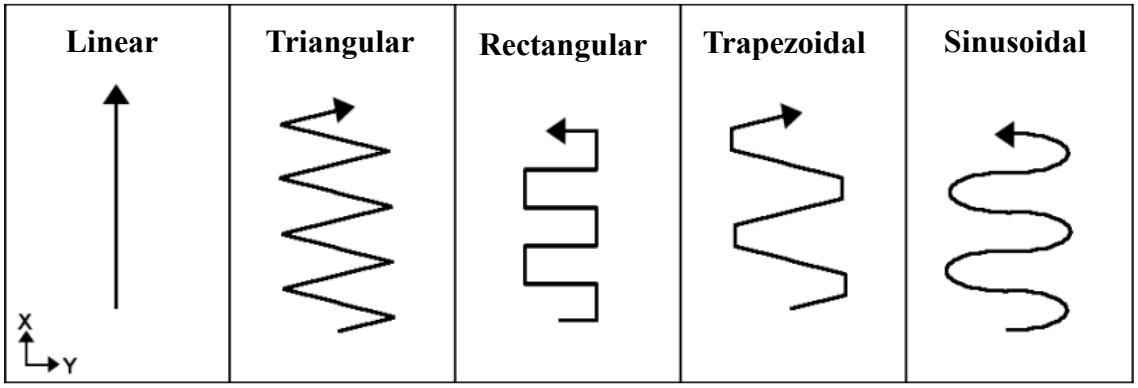


Figure 10: Trajectory patterns. Adapted from (SILVA, 2012).

The Figure 11 shows a schematic drawing of the weaving technique used. The red path represents the trapezoidal oscillation pattern imposed. Other weaving aspects like period (T), Weaving Speed (WS) orientation, Travel Speed (TS) orientation, Weave Pause (stop time) and Oscillation Amplitude are schematically exposed.

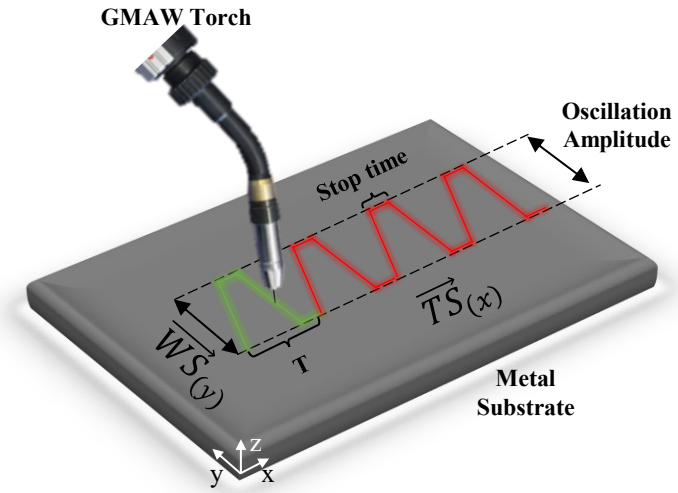


Figure 11: Schematic Drawing of the oscillation movement.

The pattern has an amplitude of movement that periodically repeats within a chosen frequency. The arc is lit through the movement, so the material deposition never stops. Thus, the feedstock is spread to the laterals forming a thick molten pool that will consequently solidify with similar width from the oscillation movement. At the edges of its amplitude, when the movement changes its orientation, a pause in the weave is set to assure the material deposition on the border. The use of weaving showed to be the best method for this particular

geometry and material, other works relate similar conclusion (XU *et al.*, 2019; ROCHA *et al.*, 2020).

The Figure 12 brings the drawing concept of the deposition strategy with the sample sliced and its main aspects.

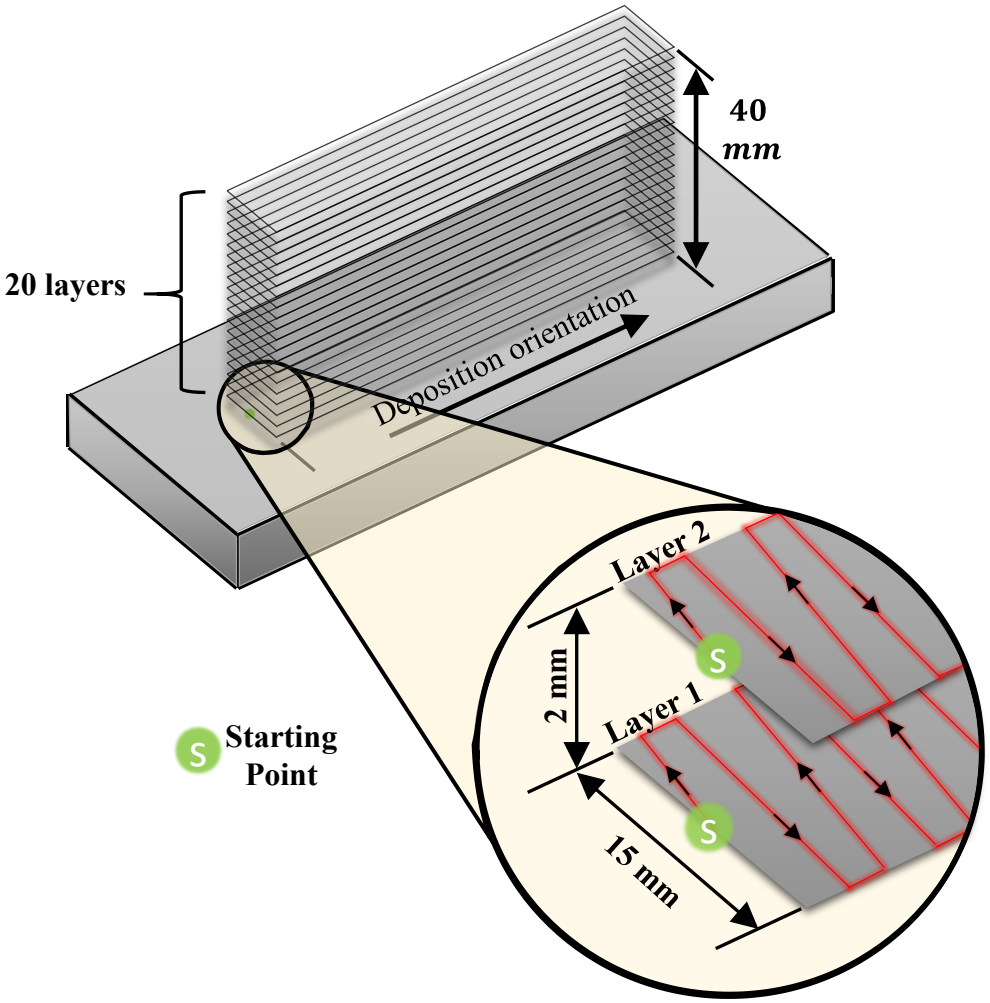


Figure 12: Deposition strategy overview.

### *3.2.1.3 Sample's Welding and Electric Parameters*

The subsequent step in the first stage was to define welding and electric parameters to achieve the desired geometry aimed at the deposition strategy step. Single beads were first used for choosing a power source synergic program that allowed a regular deposition with minimal spatter level and with low heat input. Previous works with metal-cored wires and non-dedicated synergic programs demonstrated a suiting results with the use of wave patterns dedicated to aluminum alloys, but using metal-cored wires (ROCHA, 2017). Confirming the

previously thought, between the available programs, the AlSi5 synergic program showed the best results (metal transfer smoothness, deposits surface aspects). Therefore, this synergic program was chosen.

Part of this work main objective was to compare the deposition of thick walls in two distinct energy inputs, one with a minimal energy input and a second more aggressive, with a high energy range. This comparison was meant to provide information about the thermal behavior influence on the WAAM general aspects, like deposit surface quality and its causes. Two different electric current wave patterns were used to achieve this energy input variation. The AlSi5 synergic program allowed the use of two different forms wave patterns, a low energy with short-circuiting material transfer only and a pulsed mode. Each mode presented different features of material transfer, welding pool pressure and electric power. The combination of factors resulted in different heat input towards the substrate and previously deposited structure. Parameters for both modes were set with a constant Wire Feed Rate (WFR), that was constantly measured with a wire speed transducer. The differences of each mode are described as follow.

- **CMT wave pattern**, with short-circuiting metallic transfer mode. This mode is referred simply as CMT in this work. This mode is expected to input less heat and less pressure on the welding pool. The Figure 13 shows the electric oscillogram combination of current and voltage along 100 ms ($10^{-3}$ s).

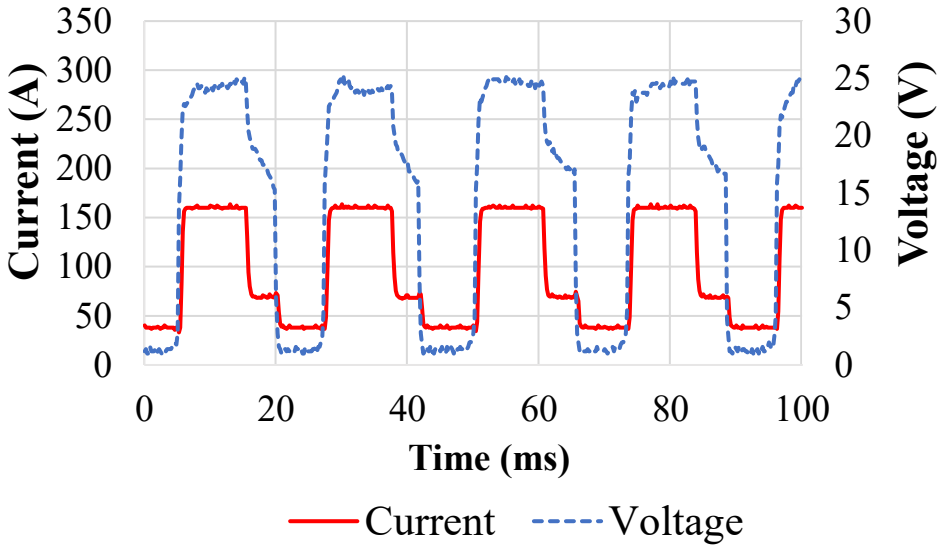


Figure 13: Combination of current and voltage oscillogram. AlSi5 CMT waveform.

- **CMT Pulsed wave pattern**, with alternating short-circuiting metallic transfer mode and free-flight metal transfer during the pulses. This mode is expected to impose more pressure towards the molten pool because of the pulses. At every 7 pulses, a short circuit occurs. This mode is referred as CMT Pulse in this work. The Figure 14 shows the electric oscillogram combination of current and voltage for the Pulse mode.

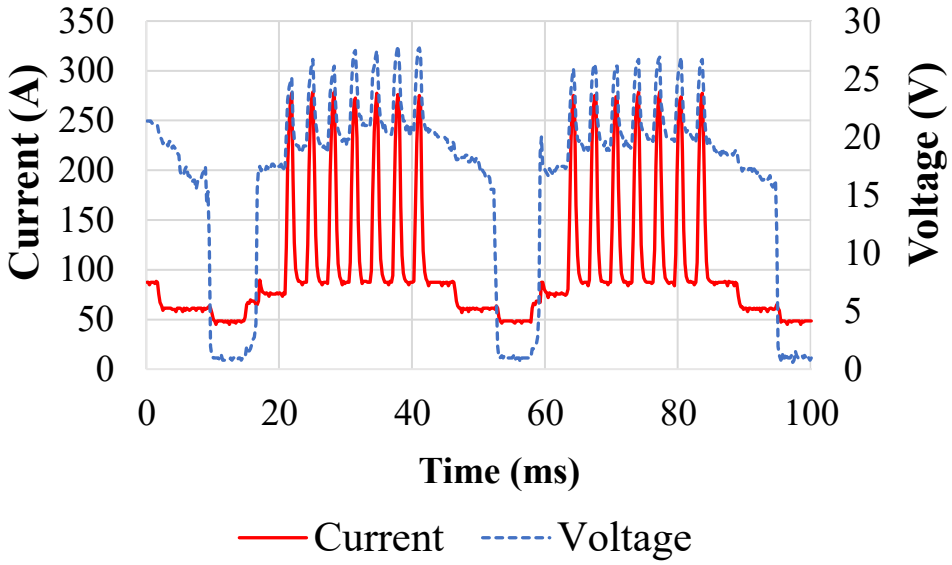


Figure 14 : Combination of current and voltage oscillogram. AlSi5 CMT Pulse waveform.

To determine adequate travel speed (TS) for a WFR it was chosen to use lower deposition rates, that would facilitate the study. Its decision was based in recent studies that indicate that higher deposition rates impact negatively in the surface quality. High deposition rates causes further increase in post processing steps, even though it is highly dependable of multiple factors like target geometry, material selection and heat source (YEHOROV *et al.*, 2019). A productivity analysis in WAAM context is relative and complex. Although, an array of tests was made concerning the influence of WFR, TS and its ratios as the Figure 15 shows. An estimated deposition rate, calculated by Equation 1, was superposed to the measured values. The measured deposition rates follow straight under the estimated values ($D_e$) until an upper limit of around WFR= 9 m/min, when its starts decreasing its values compared to the calculated. As expected in the GMAW processes a feedstock waste was seen. The highest materials waste happened for the highest TS/WFR ratio, in which it was deposited 15.4 % less material than estimated. The ratio that resulted in the most forgiving material waste, was the 5.6 ratio, which led to 4.6 % less material. The average material waste was 7.4 %.

Equation 1: Estimated deposition rate [kg/h]. WFR [m/h]. $\rho_w$= wire mass [kg/m].

$$D_e = (WFR \cdot \rho_w)$$

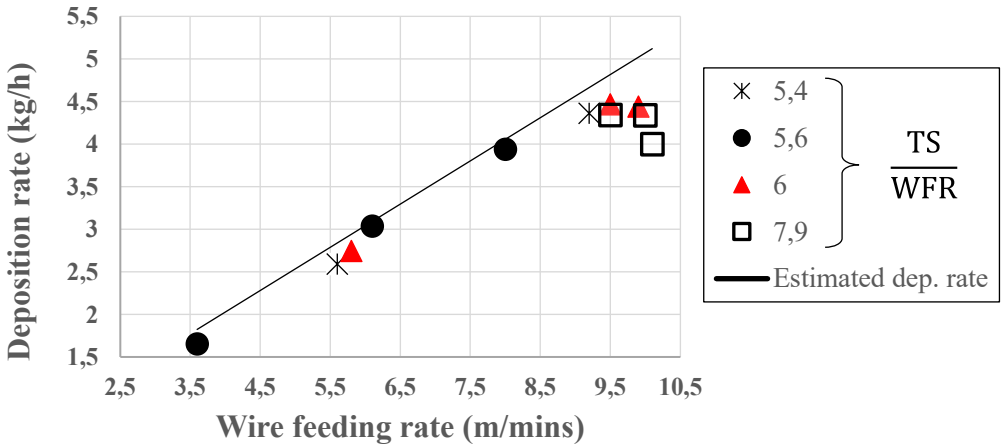


Figure 15: Behavior of deposition rate according to WFR with different TS.

The welding parameter chosen matched with the lowest material waste TS/WFR ratio. Among this ratio's possibilities, a reduced TS was appropriated to reduce effects of humping and to facilitate a smoother metallic transfer from the wire electrode to the melting pool. Higher WFR, along with higher TS induce melting pool disturbances, thus more defects can be expected. The parameters used for the single beads are showed in the Table 12.

Table 12: Single bead pre-parameters.

| Process | Wire Feed Rate (m/min) | Current (A) | Travel Speed (cm/min) | TS/WFR (cm/m) |
|---|---|---|---|---|
| CMT | 3.5 | 90 | 20 | 5.7 |
| CMT Pulse | 3.5 | 110 | 20 | 5.7 |

Once the synergic programs slightly correct the chosen parameters, in order to provide a smooth transfer rather than keeping them constant throughout the deposition, the WFR set in the power source's HMI had to be adjusted so the measured value resulted constantly in 3.5 cm/min. This was taken in account since the beginning of the experiments. The use of the SAP with the WFR transducer was of high importance to the parameter's reading reliability. The parameters of the work were attached by the WFR. Per example, at Table 12, the WFR shows the measured value acquired from the wire speed transducer, whilst, in this same table , the current values are only representative values showed in the HMI. The TS, on the other hand, was set in the robot trajectory program and did not change along the deposition.

After defining stable parameters for single beads, the parameterization of the weaving beads was made. The correlation between TS for single beads and weaving beads is not direct. This incongruence occurs due to the formation of different welding pool size. During the weave, the material is deposit over a bigger welding pool which changes considerably the deposition dynamics. Per example, an oblique speed of 217 cm/min was needed to assure the oscillation movement frequency with the given amplitude. This value is considered of high-speed for GMAW single beads, however the displacement length is only 14.5 mm, which do not permit the formation of high-speed related defects, like humping. Thus, it allies the benefits of high velocity without its intrinsic deleterious effects. As a matter of fact, the speed might be lower, once mechanical hysteresis dynamic was not taken in account for the speed estimation. It is known that the robot has to reduce the speed gradually for changing it orientation or stopping.

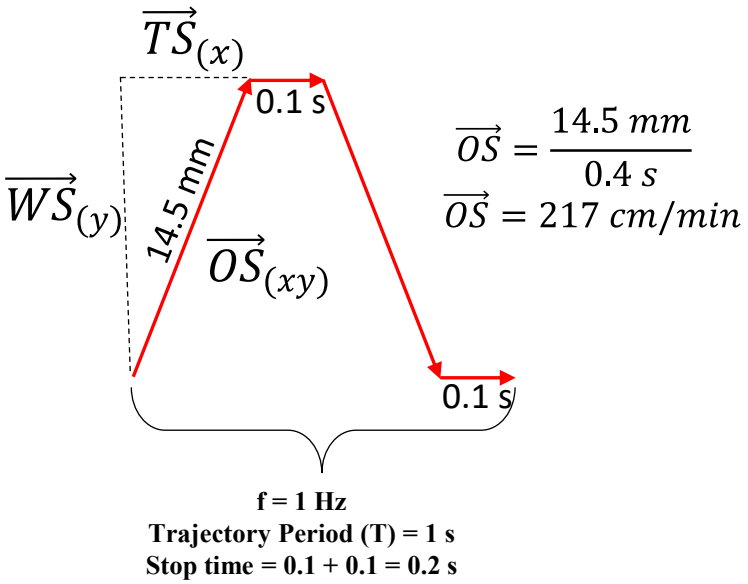


Figure 16: Oblique speed ($\overrightarrow{OS}$) composition.

The WFR used for the single beads were kept constant for the weaving beads, once it had demonstrated to be the main agent of deposition rate influence, as Figure 15 indicates. The parameters used for the weaving beads are presented in the Table 13. The same parameters were used to the manufacture of the wall-like structures in the second stage of the research.

Table 13: Electric and welding parameters for weaving beads.

| Material | Process | WFR (cm/min) | Current (A) | TS (cm/min) | Frequency (Hz) | Amplitude (mm) | Stop time (s) | CTWD (mm) |
|---|---|---|---|---|---|---|---|---|
| Mangalloy | CMT | 3.5 | 90 | 10 | 1 | 14.5 | 0.1 | 15 |
| | CMT Pulse | 3.5 | 110 | 10 | 1 | 14.5 | 0.1 | 15 |

A stop time of 0.1 s (100 ms) was defined for the weaving pattern. This time allowed an occurrence of 5 short-circuits in the CMT mode, whilst for the CMT Pulse mode, 2 cycles of 7 pulses alternating with 1 short-circuit were possible, as the oscillograms of the Figure 13 and Figure 14 presents. This stop time boost the welding pool stabilization in the bead flanks. Once the electric arc lies for a moment in this region, more heat transits, promoting more dilution between the feedstock and substrate. The stop time was imposed in both sides of the weaving bead.

Before the deposition, the substrate was superficially grinded, with care to result in a continuous flat surface without the presence of mill scale (iron oxide), originated from the hot-rolling process. This was made to prevent discontinuities of current flow for the first layer's deposition. Although. between layers the same care was not done, and the layers were deposited over possible oxide layer that may have formed, even though the pool solidification happened in a shielded atmosphere provided by the torch nozzle gas flow of 15 L/min of pure argon. The first layer's deposit resulted in a width of 15.1 mm and height of 3.8 mm. The average layer height of 2 mm defined in the deposition strategy includes the prediction of higher height in the first beads.

### 3.2.2 **Second and Third Stages – Samples Manufacturing**

The second stage of the methodology is focused on the manufacturing of the sample and the acquisition and analysis of the process in terms of electric signals, thermography by IR camera and high-speed filming of the material deposition.

#### *3.2.2.1 Depositing the samples*

The substrates were fixed on the turn table by means of one transversal steel bar on each extremity of the sample substrate. The fixture bars were bolted to a support attached to the turn tabletop. The turn table axes were not used in this work. The Figure 17 shows the working bench with all the equipment used for the manufacture of the wall-like structures.

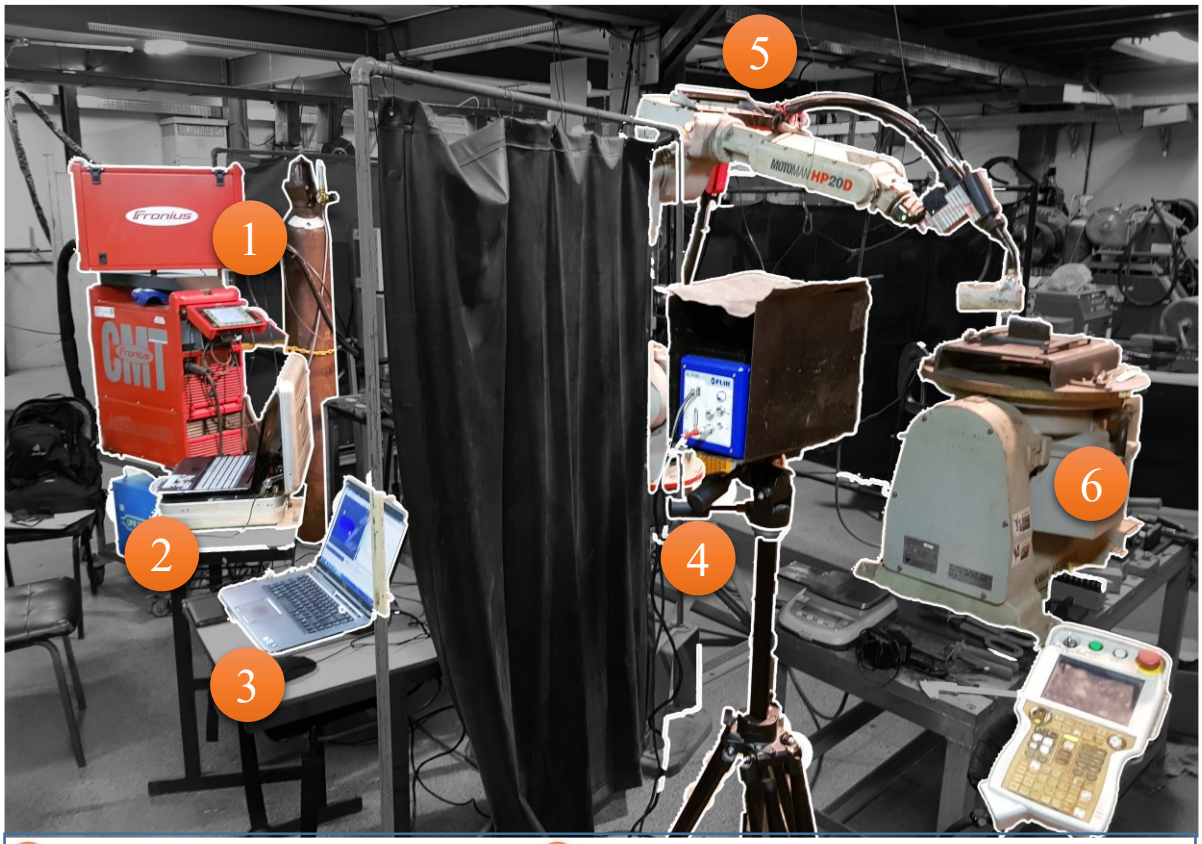


1 CMT power source + Gas Flask
2 SAP.
3 Thermographic Acquisition Laptop.
4 Thermographic Camera.
5 Robot with CMT torch and wire buffer case.
6 Turn table and sample fixture device.

Figure 17: Working bench during stage 2.

The samples were built according to the experiment matrix presented by the Table 14, following the sequence of the samples reference number.

Table 14: Experiment matrix.

| Material | Process Mode | Thermographic Temp. range (°C) | Sample Reference Number |
|---|---|---|---|
| Mangalloy | CMT | 5-300 | 1 |
| | | 300-1500 | 2 |
| | CMT-Pulse | 5-300 | 3 |
| | | 300-1500 | 4 |

### *3.2.2.2 Sample Electric Signals Acquisition and Analysis*

During all the sample manufacturing the electric signals of current and voltage and wire feed speed were measured. Since two samples of the same combination of parameters were built, it was possible to measure the mean values of signals in the first sample and the instantaneous values during the second sample. The mean values are calculated with a 1 sample/second rate, still with a 5 KHz signal reading. The Figure 18 shows an example of the mean current value for the deposition of a CMT Pulse mode. In this example a mean current value of 110 A was measure through the deposition. Each layer takes 60 s to be deposited. Between the layers a null mean value is seen, once the arc is extinguished while returning to the start point of the next layer.

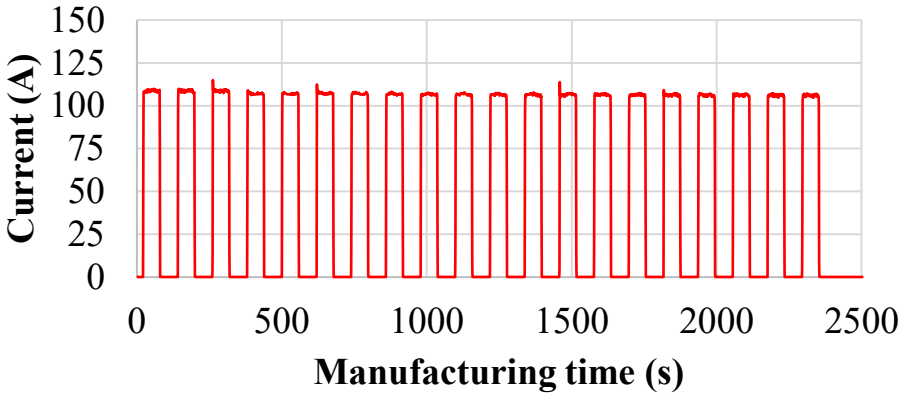


Figure 18: Mean value of current over time. CMT Pulse.

The data from the instantaneous values acquisition has a time limitation of 600 s. That means the whole deposition process cannot have it full electric signals records saved. Though, it can act as an on-line monitoring system, during the deposition, to check the parameters behavior. The Figure 19 brings instantaneous values of current during 1 s, for the same sample showed above, in the Figure 18. It means that one point in the mean value acquisition is the average of the whole acquisition presented in the Figure 19.

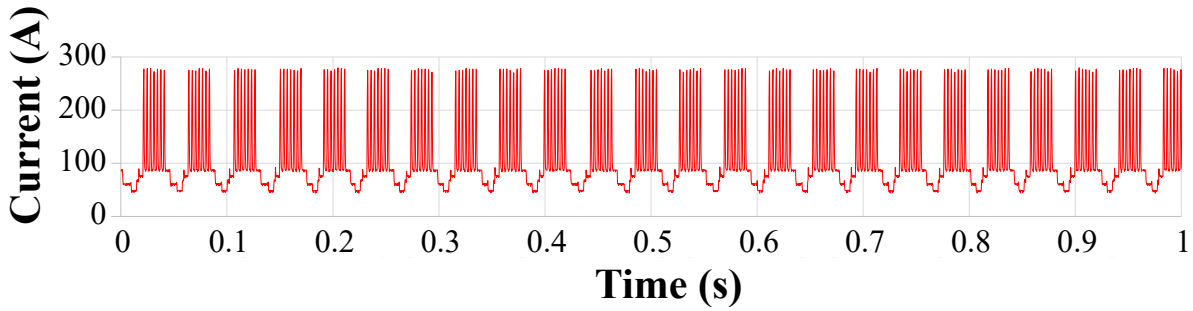


Figure 19: Instantaneous value of current over time. CMT Pulse.

### *3.2.2.3 Sample Thermographic Acquisition and Analysis*

The temperature is the measurement of how hot something is related to its surroundings, indicating the heat flow orientation, from hot to cold (RADI; RASMUSSEN, 2012). One can see a part, like the wall-like sample, as a system with its respective internal energy. Due to the basic WAAM concept of additively depositing new layers of matter, a new layer can be seen as a new thermal system that will somehow exchange heat to its surrounding systems. This heat transfer with the formerly deposited layers happens mainly by conduction. Then, the formed structure will successively transfer heat to the substrate and to the table where it is fixed. The Figure 20 schematically elucidate the simplified idea of heat flow during WAAM.

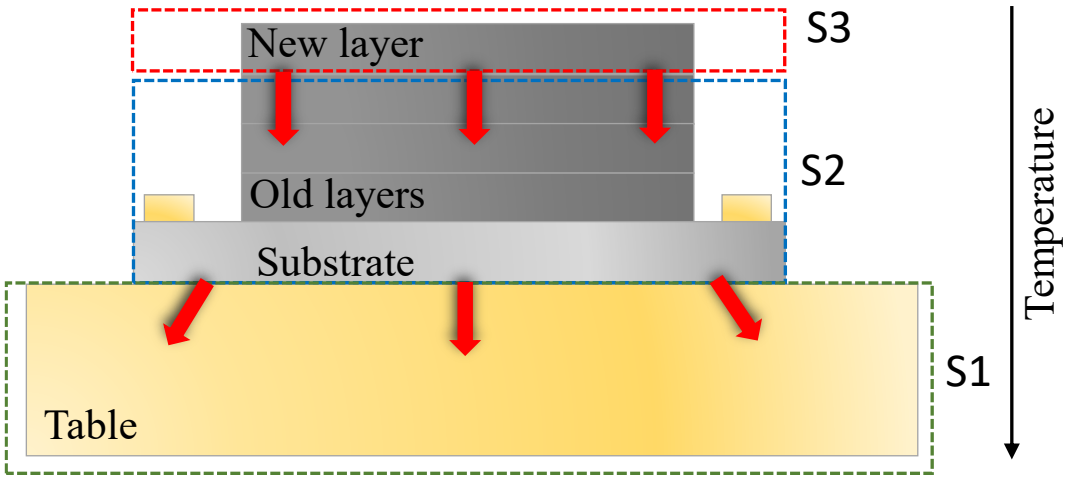


Figure 20: Heat flow behavior during WAAM. System (S)

The simplified one-dimension model given by the law of heat conduction states that heat flow (H) is mainly influenced by the temperature gradient (differential thickness “dx”

and differential temperature difference “dT”), the material thermal conductivity (k) and the contact surface area (A) between the systems, following the Equation 2 proportion (RADI; RASMUSSEN, 2012).

Equation 2: Law of heat conduction [ W/m C°]

$$H = -kA\frac{\Delta T}{\Delta x}$$

This concept is important in the WAAM practical activity because every new layer act as a new heat input in the global system, so the hotter heat reservoir is in constant increase, implying in an inconstant thermal cycle, in which a temperature gradient steady state is not reached until certain number of layers are deposited. The physical properties (e.g., molten pool viscosity) of the deposited layers change with the change of thermal energy. With time, the cooler system will eventually warm up, decreasing the heat flow. It means that the upper structure will reach higher temperatures with time, meaning that its thermal energy increased with every new layer, until reaching the temperature steady state.

The measurement of the part temperature is important in WAAM to analyze how this increment in thermal energy influences the deposit geometry (e.g., width, height), how this influence in layer geometry impacts the macrostructure of the part (e.g. surface quality, defects) as a whole, and also how does it affect the microstructure of the resulted structure.

In terms of process, a constant thermal gradient in the structure is pursued. It means that the deposit conditions could be hold constant during the whole process, facilitating the operation of the process.

A usual method in welding is to measure the temperature of the deposited surface area immediately before the next pass or layer. This temperature is known as interlayer temperature (IT) or interpass temperature (FUNDERBURK, 1998). The IT provides an approximation of the structure thermal energy, acting as an indirect control parameter. Monitoring the IT improves predictability of characteristics of the next deposits, like its geometry.

Two main option to measure the IT are the contact method and the noncontact method. The contact method uses thermometers and thermocouples in contact to the surface of interest. The noncontact method analyses the surface temperature by mean of its thermal

radiation, in infrared wave length (TSURUMAKI *et al.*, 2019). The infrared thermography (IR) method was used in this work.

Some difficulties of using the IR thermography are the definition of the emissivity coefficient of the focused object and how to avoid the interference of the welding arc radiation in the results.

To minimize the arc interference two differing techniques were used. The first was to film the reverse side of the substrate with a setup as shown in the Figure 21. This setup is interesting for single layer deposits once in which the temperature gradient is still high. The other method to reduce the arc interference is to position the camera perpendicular to deposit orientation but with a certain slope degree (HUANG *et al.*, 2007; YANG; WANG; ZHANG, 2017). The Figure 22 shows the setup for this recording condition. The camera height is higher than the substrate height.

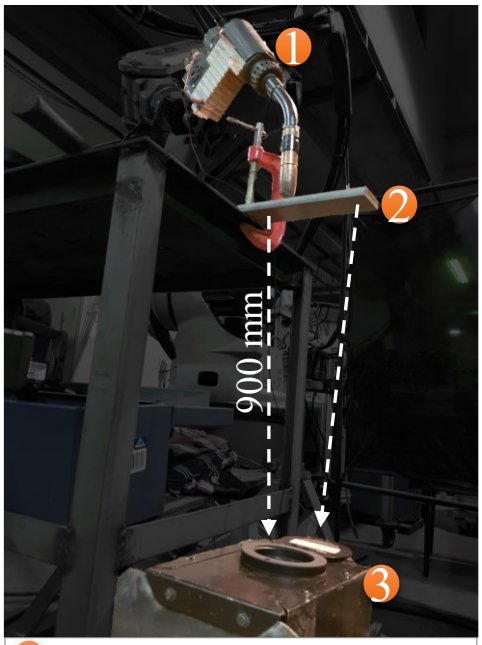


Figure 21: Thermographic acquisition method: substrate reverse side.

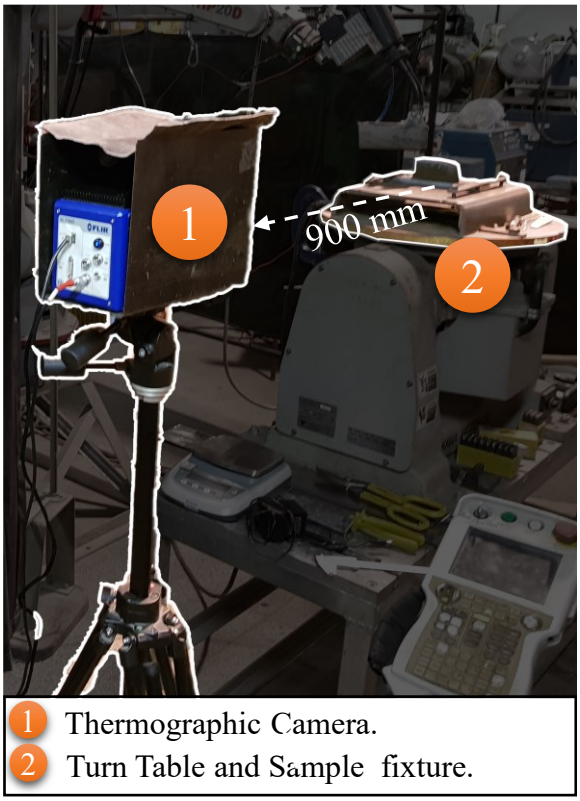


Figure 22: Thermographic acquisition method: sloped perpendicular.

The second difficulty was to define the optimal object emissivity. To do so, a sample consisting of three layers only was built and used as probe to the emissivity calibration. After the deposition, its lateral side was aimed by an IR pyrometer followed by its contact thermocouple to the same spot at temperature of approximate 150 °C. A mean value of both was used to adjust the emissivity in the IR camera. Even with this calibration, an optimal emissivity is hard to define once it fluctuates with the temperature and surface finish in WAAM also varies (BAI; ZHANG; WANG, 2013). An emissivity coefficient of 0.88 was defined, following similar methodology of former works (YANG; WANG; ZHANG, 2017; RODRIGUES *et al.*, 2019; ROCHA *et al.*, 2020).

To acquire the thermal cycle during the sample buildup, it was required to use two temperature ranges, set in the recording software in a PC connected to the IR camera. The first temperature range (300 to 1500 °C) was used to obtain the thermal film during the deposition of material, with the electric arc still lit. The second range (5 to 300 °C) was used to obtain the thermal data after the arc extinction and in the previous layers where the structure is still in lower temperatures. Two samples of each combination of parameters was fully recorded with both temperature ranges and the recording only stopped after reaching a global part temperature of 100 °C.

The recording parameters were configured in the dedicated software Altair. The data acquired was processed using the same software to measure the temperature at any point during the sample additive manufacture. A transmission coefficient of 0.97 was set due to the use of a proper lens that protect the camera from spatter. The parameters used in the thermographic data acquisition are described in the Table 15.

Table 15: Thermographic Camera Parameters.

| Parameter | Value |
|---|---|
| Emissivity | 0.88 |
| Acquisition Range (1) | 5 - 300 ºC |
| Acquisition Range (2) | 300 - 1500 ºC |
| Transmission Coefficient | 0.97 |
| Room Temperature | 26 ºC |
| Camera-Substrate Distance | 0.9 m |

The thermographic acquisition was made in two steps. The first was an analysis of the heat input from each process (CMT or CMT-Pulse) while depositing only one bead and filming the substrate reverse side, using the method of the Figure 21. The substrate had dimensions and material identical to the used for the deposit of the wall-like structures. Its position was kept strictly identical for all the samples with aid of a fixture on the table that restrained the alignment with the camera, that also was not moved during the whole acquisition. The start and end point, as well as deposition time was kept constant.

The mean temperature line method was used to compare the heat input towards the substrate and deposit. The method consisted in drawing a horizontal line in the center of the sample, as the Figure 23 presents. This line of mean temperature over time can be estimated to represent the thermal cycle of the deposit. Measuring the mean temperature is one method to quantify the heat input difference between the two process modes, CMT and CMT Pulse. Although, the real temperature value is not reliable due to the former mentioned issue of emissivity. However, when comparing experiments with identical conditions it is of great value. The color pallet and temperature scale do not affect the results that were extracted and analyzed in the Excel software.

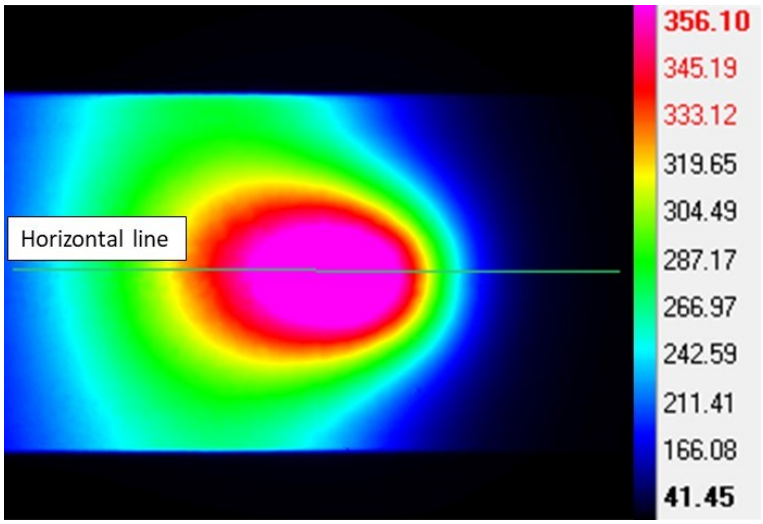


Figure 23:Thermographic image of substrate reverse side. Temperature scale in ˚C.

The second step of the thermographic acquisition methodology was made during the manufacture of the wall-like structures. The same analysis methods were used: mean temperature.

To film the buildup process, the camera was positioned to frame the whole sample dimension, and still caring to prevent from potential spatter and arc radiation interference. To measure the part's mean temperature a method of composing lines was used. This method consists in add two measurement line, one vertical and other horizontal to the sample. The lines are modified every time the arc extinguish. The mean temperature was acquired with a acquisition rate of 2 measurements per layer, right before the arc extinction and before the arc opening. After the end of deposition, the acquisition was made until the mean temperature cooled to 100 ˚C. The Figure 24 shows the how the lines were set in the video. An automatic gain control in the temperature scale was used to better visualize the sample, however, the scale does not reflect in the thermal data.

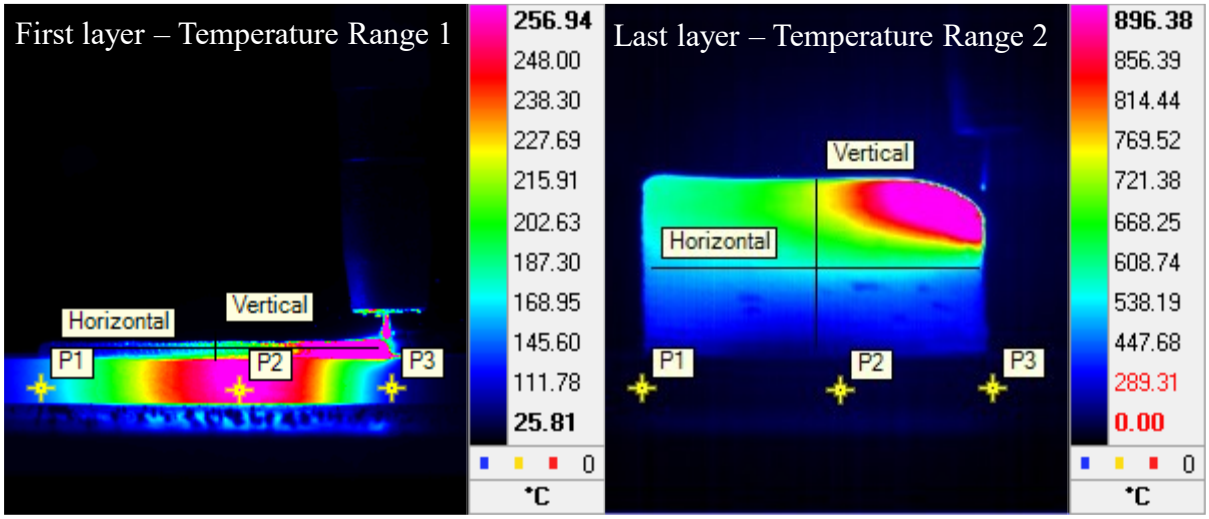


Figure 24: Mean Temperature Line method.

### *3.2.2.4 High Speed Filming*

The high filming speed of the deposition happened with the setup schematically showed in the Figure 25. The substrate was clamped to a moving table. Therefore, the torch remained motionless during deposition. This method is used so that the focus of filming does not change during deposition. For this, only single beads were deposited, avoiding loss of focus during oscillation.

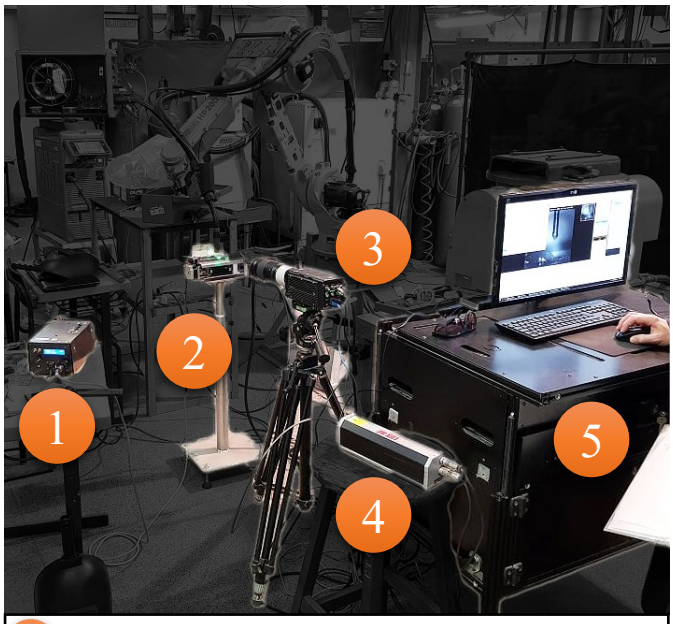


1 Table controller.
2 Table with substrate.
3 High-speed filming camera.
4 Laser source.
5 System integrated box.

Figure 25: High-speed filming setup.

### *3.2.2.5 Metallography*

To analyze the macrostructure and microstructure of the deposited samples, a cross section was extracted from the middle of the wall-like structures, like the Figure 26 demonstrates.

The cut was made by means of an automatic cut-off with use of abrasive disks. The sample had its face grinded, polished, and then etched with the Adler, Behara 2 or Marble reagents, depending on the stage. The sample were analyzed by means of an optical microscope, from which analysis, a 25x amplification was made from three regions: the top, the middle, and the bottom of the sample.

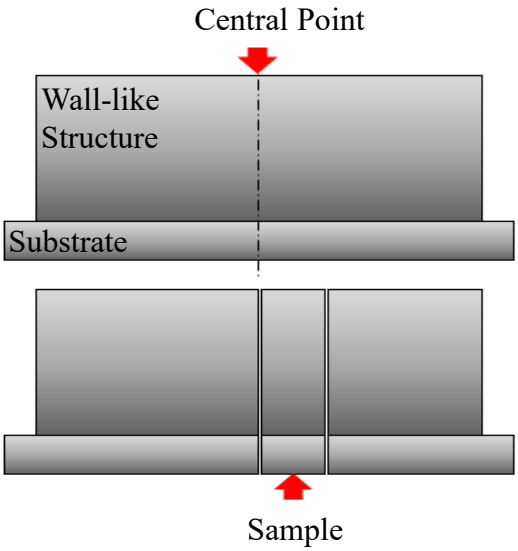


Figure 26: Schematic representation of sample cut in wall center point

### 3.2.3 **Stage 4 – Validation**

The methodology of the validation part manufacturing will be presented within the results section.

## 4 RESULTS

### 4.1 GEOMETRY

The Figure 27 presents the side view of the Sample 1, made with the CMT variant. The wall presents an integer bond with the substrate and good geometric accuracy with the proposed sample geometry. Some slope in the beginning and end of the deposition can be observed. The slope is caused the by the opening and extinction of the electric arc. There was no special care with opening and ending ramps. Some spatter was aggregated to the walls after the deposition, but with no metallic bonding with the structure. The layers showed to keep constant aspect, especially in the middle of the wall. The first three layers showed superior height and smaller width once the deposit was still in its lower energy stage allowing a faster welding pool solidification.


Figure 27: Sample 1, side view. CMT variant, as welded.

The Figure 28 shows the Sample 3, welded with the CMT Pulse variant. This sample presented inferior geometric accuracy compared to the Sample 2, but still with appreciable repetitiveness in the layer's geometrical aspects. It can be inferred by the material overflow in the end of the deposit that the energy used to deposit the layers was excessive, or at least a ending ramp should have been used. At the end of the deposition path the welding pool needs to solidify fast enough to maintain a continuous layer height. When the deposition stops the tendency of the welding pool is to keep moving. Depending on the welding pool inertia and viscosity it will overflow. In the Figure 28, the right side of Sample 3 shows the end of the deposition path with the layers overflow.


Figure 28: Sample 3, side view. CMT Pulse variant, as welded.

The Figure 29 shows the height distribution chart comparison made with 18 measurement point along the wall. The chart shows that both walls did not reach the aimed height. The results show that the mean layer height was inferior of the 2.0 mm estimated. The height profile along the wall showed small dispersion, with a standard deviation of 0.27 mm for the CMT and 1.00 mm for the CMT Pulse.

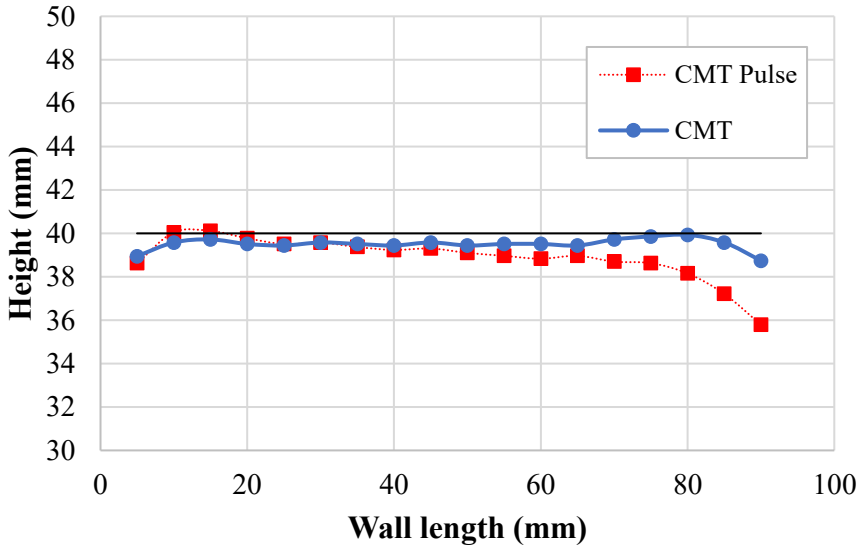


Figure 29: Height profile along the sample. Comparison between CMT and CMT Pulse.

The Figure 30 and Figure 31 presents the walls perspective from a top view, one for each process variant, CMT and CMT Pulse. In this way the width of the wall can be better

examined. The background of the above-mentioned figures was extracted for better measurement of the wall thickness profile and to support the easiness of comparison between each process. The Figure 30 shows the top view of the Sample 1. The scales are well noted along the deposit. Some slag stains lie on the surface, especially in the end.

Figure 30: Wall top view. CMT.

The Figure 31 shows the top view of the Sample 3. Some scales are visible but with inferior geometrical repetitiveness. Slag stains are present in almost all the surface with big bubble stains in the end. Once the sample 3 was made with a superior energy level, it is presumable that the surface was more exposed to oxidizing.

Figure 31: Wall top view. CMT Pulse.

The Figure 32 shows the width distribution along the deposit for both variants. As expected, the CMT Pulse variant resulted in a wider width profile due to its higher welding pool fluidity. Again, the beginning and end of the wall have the biggest inaccuracy. Both the walls presented lower width in the beginning and higher width in the end of the wall.

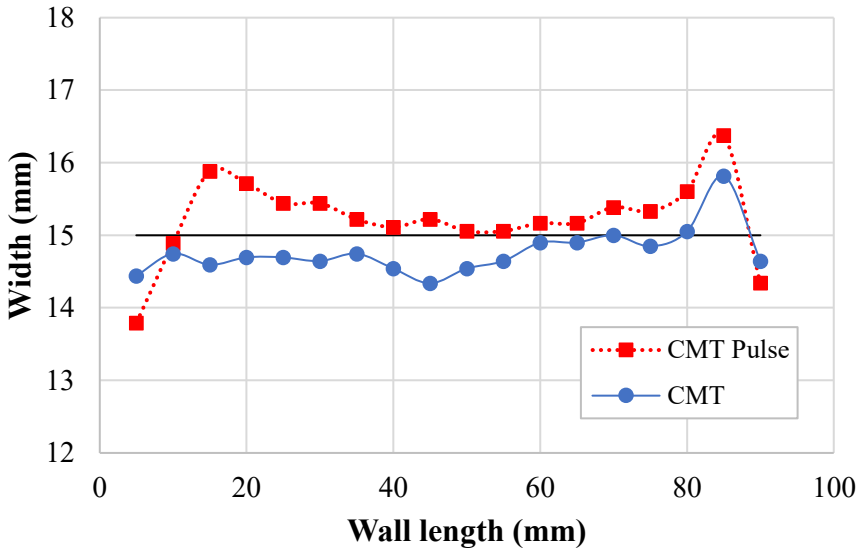


Figure 32: Width profile along the sample. Comparison between CMT and CMT Pulse

The Figure 33 shows a macrography of the cross sections from the middle of the Sample 1 and Sample 3. In the Figure 33 four threshold lines were set to indicate the surface roughness. In both variants the inner lines were limited by the first layers as the arrows show. The outer lines are limited by the regions with the biggest width. In both samples the outer layer was set in both sides at the same, indicating that the material overflow affects both sides of the structure. In the Sample 3, a possible explanation for the overflow is the reduced width of the first layers. The first layers could not support the welding pool size. After two or three overflowing layers a stable base was formed allowing the next layers to solidify in a constant width until the last layer. A thicker base could have avoided this irregularity.

Both process variants resulted in similar surface roughness. A mean roughness of 1.9 mm was measured for the Sample 1 and 2.1 mm for the Sample 3.

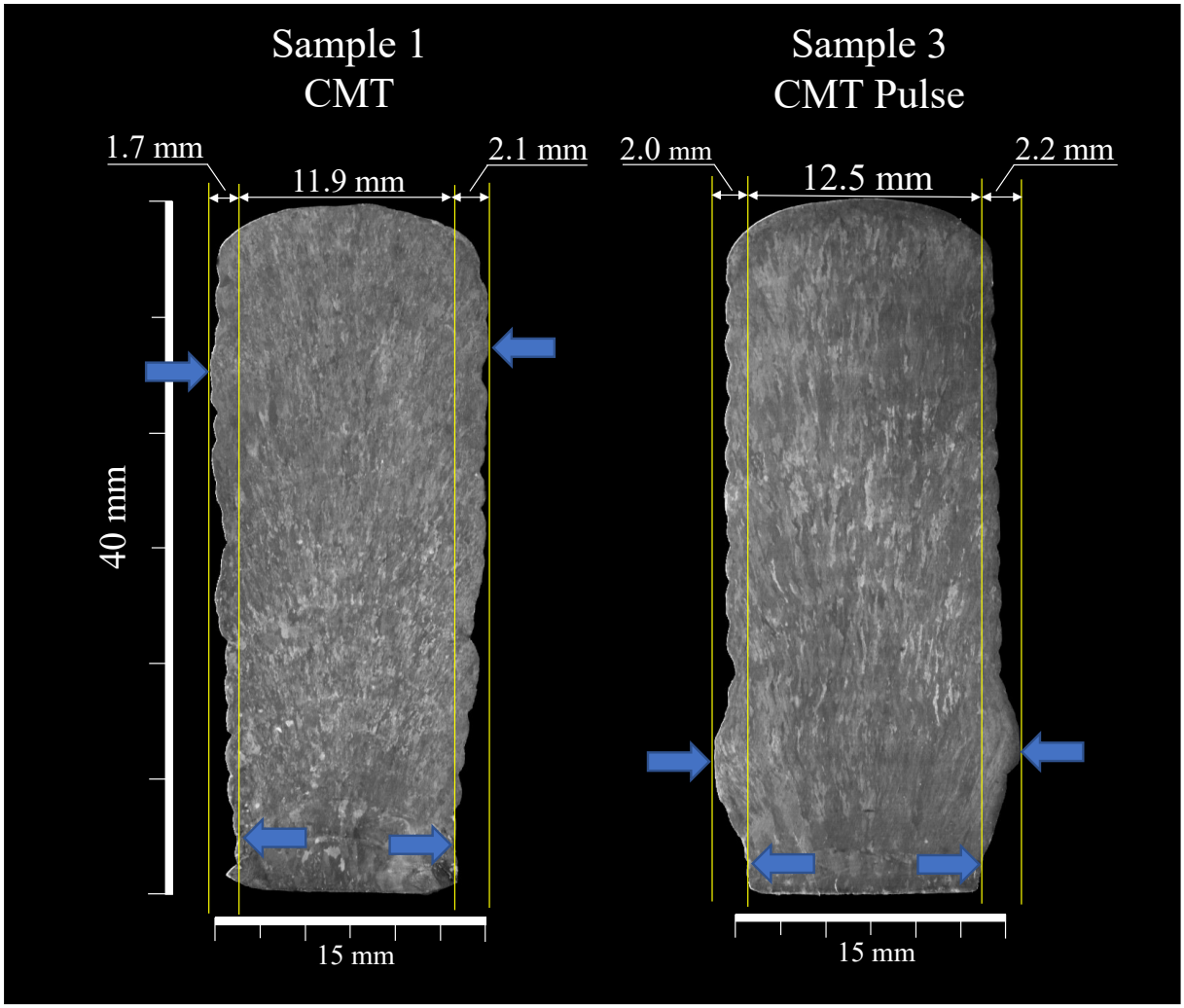


Figure 33: Samples cross sections macrography. Surface roughness.

The macrography of the Sample 1, presented in the Figure 34 shows the Mangalloy austenitic matrix with the presence of (Fe, Mn)$_3$C carbides. Defects such as macroporosity and cracking are not found on the presented surfaces. The grains grow nearly along the vertical direction forming a columnar pattern with a dendritic structure. As the micrography of the Figure 34 shows, the bottom of the wall presented a coarser grain size compared to the middle and top, indicating a lower cooling rate that resulted in superior grain growth in this region. The very top of the wall presents a fine microstructure due to the rapid cooling of the deposition and because the last layer is not affected by any new heating cycle.

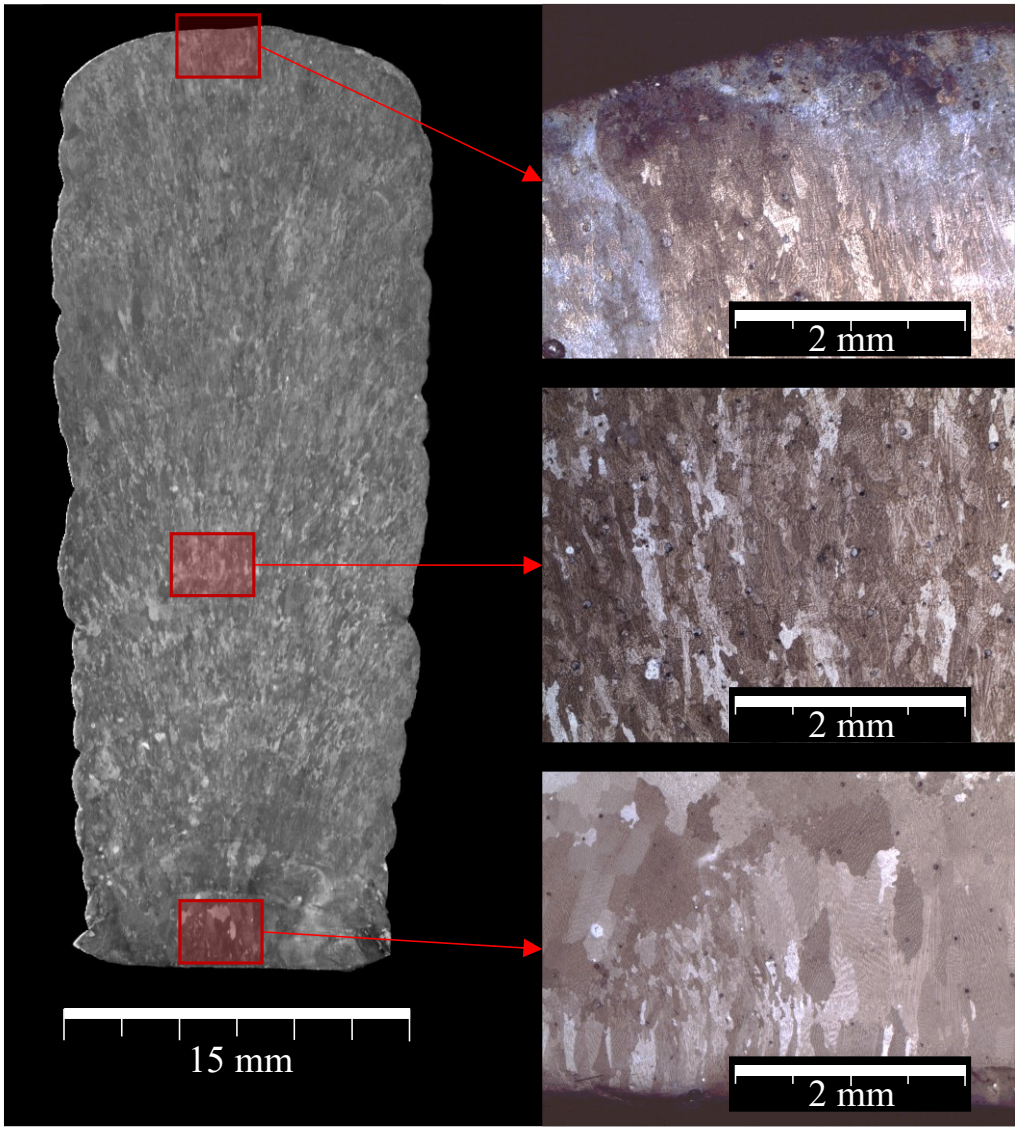


Figure 34: Sample 1. CMT. Macro and micrographs. 25x, etched with Behara 2.

The Sample 3 presented in the Figure 35 shows similar columnar grain orientation, following the heat flow that happens during the deposition. The Sample 3 was etched with the Adler reagent helping to visualize the dendritic formation with primary branches in the vertical orientation.

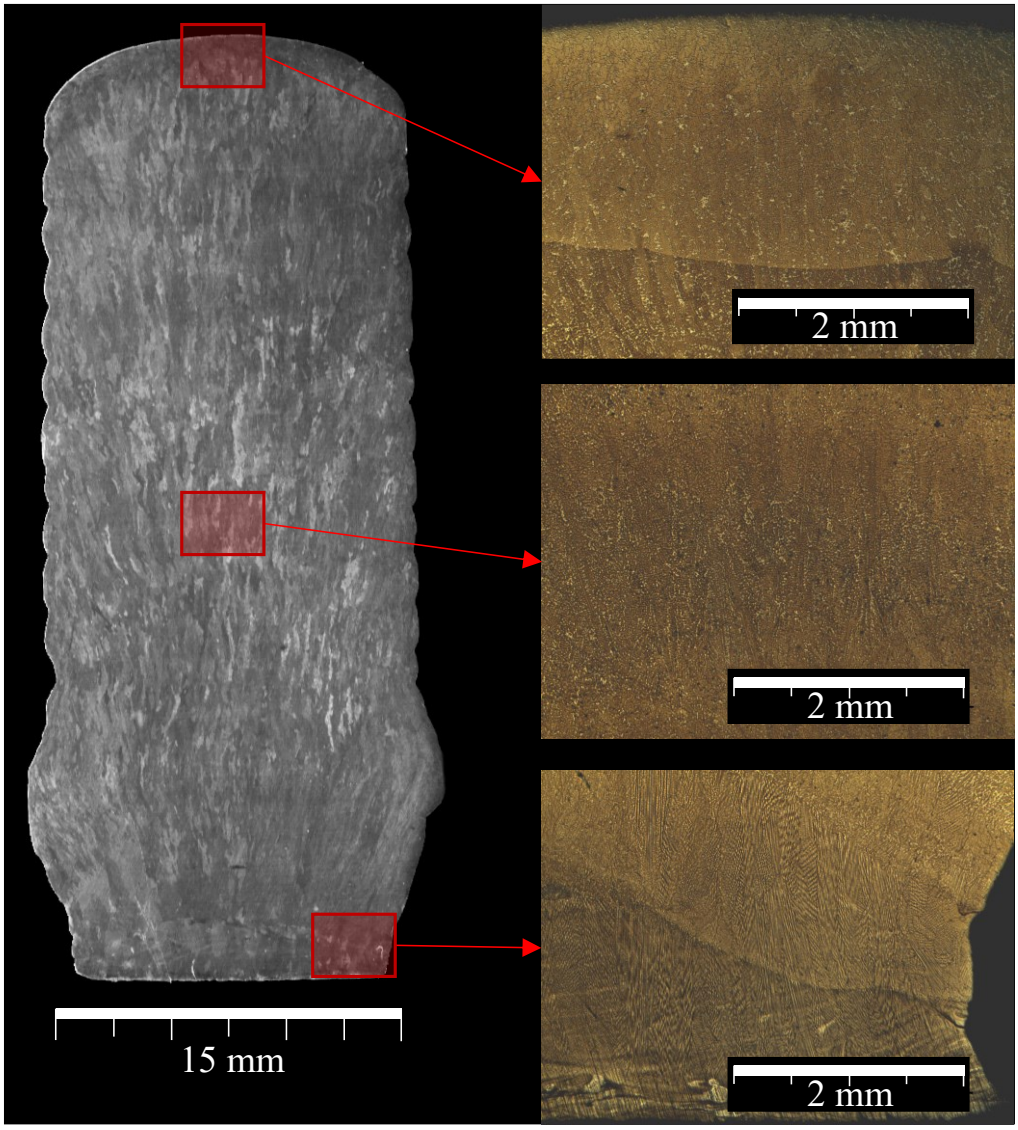


Figure 35: Sample 3. CMT Pulse. Macro and micrographs. 25x, etched with Adler.

## 4.2 ELECTRIC SIGNALS ANALYSIS

The electric signals of the welding process were recorded during the sample's deposition. As explained in the methodology, the mean values were recorded with a acquisition rate of 1 Hz during the whole deposition while the instantaneous values were recorded with 5 KHz but during only the last 600 s of the deposition.

With the electric signal mean values important information about the process can be visualized. The Figure 36 presents the voltage, current, power and wire feed speed mean values during the deposition of the Sample 1, while the Figure 37 for the Sample 3. Each pulse represents the deposition periods of one layer and the valleys represent the idle time between layers.

The charts of the Figure 36, showing the CMT variant oscillograms, presents an increase in the mean voltage after the second layer. The mean voltage rises until the sixth layer until reaching a homogeneous value. The mean power oscillogram follows the same behavior once it is calculated by the voltage. This voltage rise can be explained by the rise of the contact tip to work distance as the layers are being deposited. During the deposition, the sample's temperature grows tending to form layers with reduced height. If the torch "z" increment is constant the electric arc tension will differ depending on the layer. In this case the power input oscillation did not impacted in the wall overall geometry and surface roughness. The wide layer width and the weaving movement also helps in the support of the welding pool, decreasing the probabilities of lateral material overflow during excessive heat input periods. Still in the voltage chart, it is possible to see the mean voltage rise in the end of the layer deposition. This signal shows the electric arc rise as the deposition reaches the lower part of the wall. As the process is current controlled the current mean values showed almost no dispersion in the results. The wire feeding rate showed more dispersion in the mean values which can be explained by the normal dynamic feeding oscillation causing dimples in the speedometer.

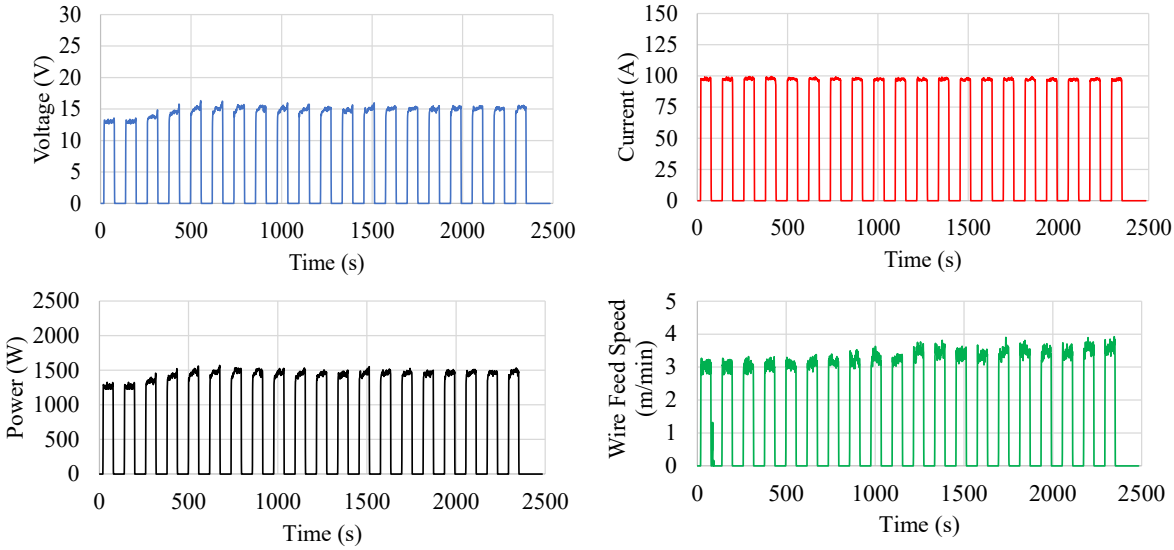


Figure 36: Sample 1, CMT variant. Mean value electric signal.

The charts of the Figure 37, showing the CMT Pulse variant oscillograms, presents the same mean voltage and power increase along the layer's deposition as the CMT variant supporting the explanation that this behavior was caused due to the deposition strategy employed. The current mean values showed some dimples in the beginning of the deposition periods, indicating the material transfer difficulties that are better visualized in the high-speed

filming section. The wire feeding speed showed similar behavior as the CMT, with an fine increase along the deposition of the layers.

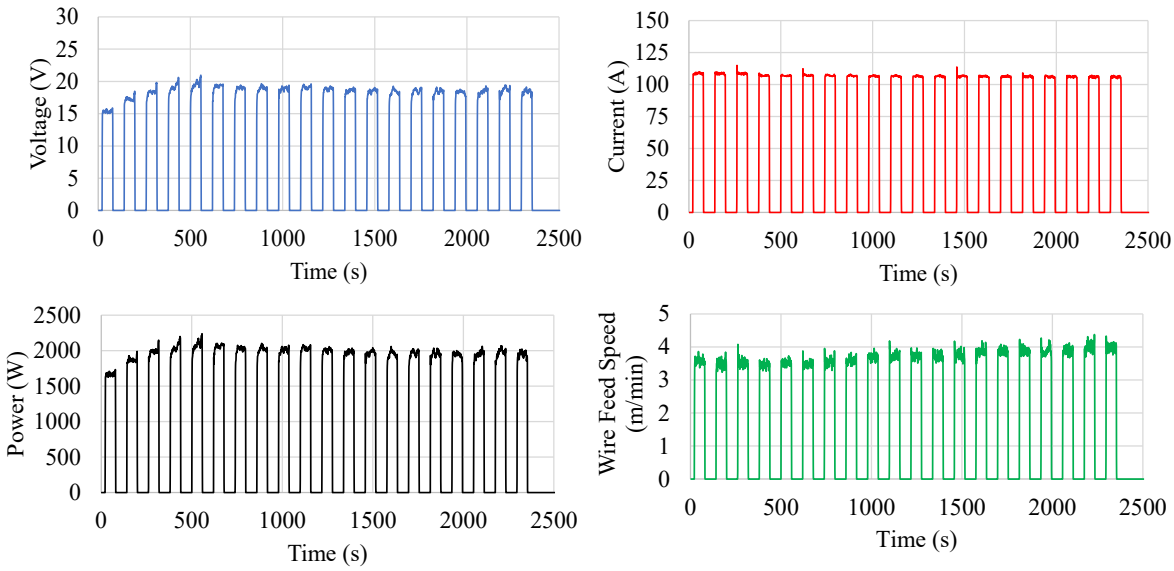


Figure 37: Sample 3. CMT Pulse. Mean value electric signals.

The welding energy can be estimated by the mean power during deposition divided by the travel speed. The Table 16 shows the comparison of maximal and minimal layer heat input for both process variants with an energetic efficient of 76% for the CMT and 70% for the CMT Pulse (VILARINHO, 2012). The CMT Pulse resulted in higher heat input in all conditions, with a max heat input 23% higher than the CMT max, and minimal heat input 20% higher than the CMT minimal. The next section of thermographic analysis shows how the temperature of the samples diverged with this heat input difference between the variants.

Table 16: Maximal and minimum heat input per variant.

| Sample | Process | Power (W) | | Travel Speed (cm/min) | Heat input (KJ/cm) |
|---|---|---|---|---|---|
| 1 | CMT | max. | 1485 | 10 | 113 |
| | | min. | 1227 | 10 | 93 |
| 3 | CMT Pulse | max. | 2086 | 10 | 146 |
| | | min. | 1670 | 10 | 117 |

The instantaneous electric signals oscillograms, presented in the Figure 38 and Figure 39, bring the tension and current signals over 100 ms during the first layer deposition.

The oscillograms of Figure 38 shows the short-circuit wave of the CMT variant with the expected decay of voltage during the short-circuit with posterior rise of voltage during the arc reignition. The upper voltage level refers to the arcing period in which the arc oscillation is noted by certain irregularities. The current chart shows almost no dimples once it the process is current controlled.

The Figure 39 shows the CMT Pulse wave pattern. In the voltage chart it is possible to see that the pulses respect constant periods but oscillates in its voltage magnitude. The post pulse period in which occur the short circuit indicated high irregularity. This behavior is explained by the high-speed analysis in which the material transfer can be analyzed. The films showed that the bigger portion of material that melts during the pulse phase do not detach from the electrode tip, supplying a droplet growth until it is finally transferred to the molten pool during the short circuit period.

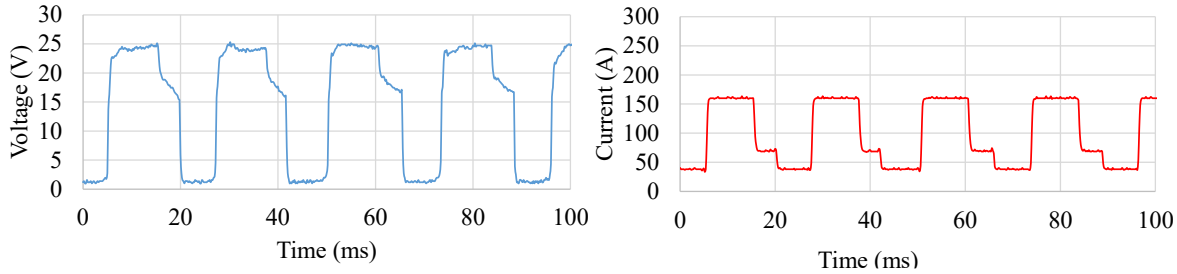


Figure 38: Sample 1, CMT. Instantaneous voltage and current.

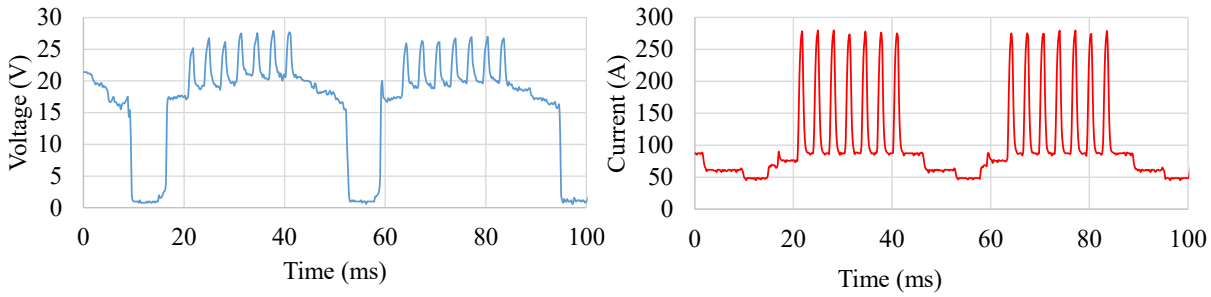


Figure 39: Sample 3, CMT Pulse. Instantaneous voltage and current.

Once the synergic program used was not specific for the combination of feedstock and welding gas, it was already expected variations in the droplet transfer rate. The expected analysis of the free-flight mode impact in the deposition was not possible once it did not occur during the test. Rather a mix of preheating with pulses to form a big droplet and detach it during the forward wire movement. This observation supports the assumption that there are plenty combinations of wire movement and wave forms that can be combined to reach very

refined thermal input conditions and non-conventional material transfer modes. Posterior works aimed in developing dedicated synergic programs for metal cored wires will widen the WAAM controllability, increasing the quality of the deposits.

## 4.3 THERMOGRAPHIC FILMING

To better evaluate the influence of heat transfer in the additive manufacturing with the different CMT versions, infrared filming of the wall under construction was performed. The Figure 40 illustrates the thermal gradient obtained while thermographic filming the reverse side of the substrate during the deposition of one layer. This test was made to compare the heat input between the variants in a more controlled experiment condition. According to the results, the CMT Pulse runs to a maximal mean temperature 22.1 ˚C higher than the CMT variant. This difference costed to the CMT Pulse sample a 1000 s delay to cool to the same temperature as the CMT variant. In fact, depositing with higher energy conditions results not only to instantaneous higher temperature deposit but also tend to accumulate more energy at every new layer.

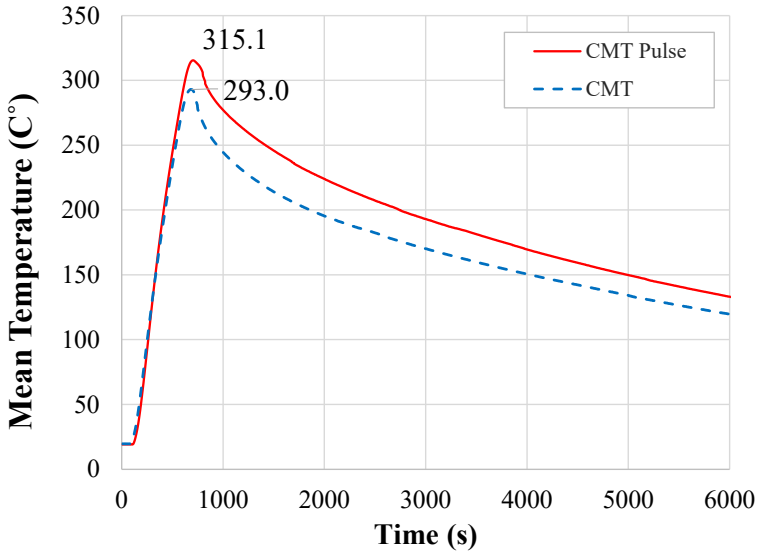


Figure 40: Thermal cycle. Substrate reverse side method.

The Figure 41 graphic was constructed from the infrared filming data by the mean temperature line method explained in the methodology. It was verified that all variants reached a regime temperature around 960 s of operation, enough time for the construction of 8 layers. In this transient phase it is perceived that the CMT Pulse variant heats up at a

relatively higher rate than the CMT. In the continuous regime, the CMT Pulse variant reaches a higher value than the CMT, about 570 °C, while for the CMT variant the average was 506 °C. At the end of deposition, a difference of about 50 °C was measured between the two samples mean temperature.

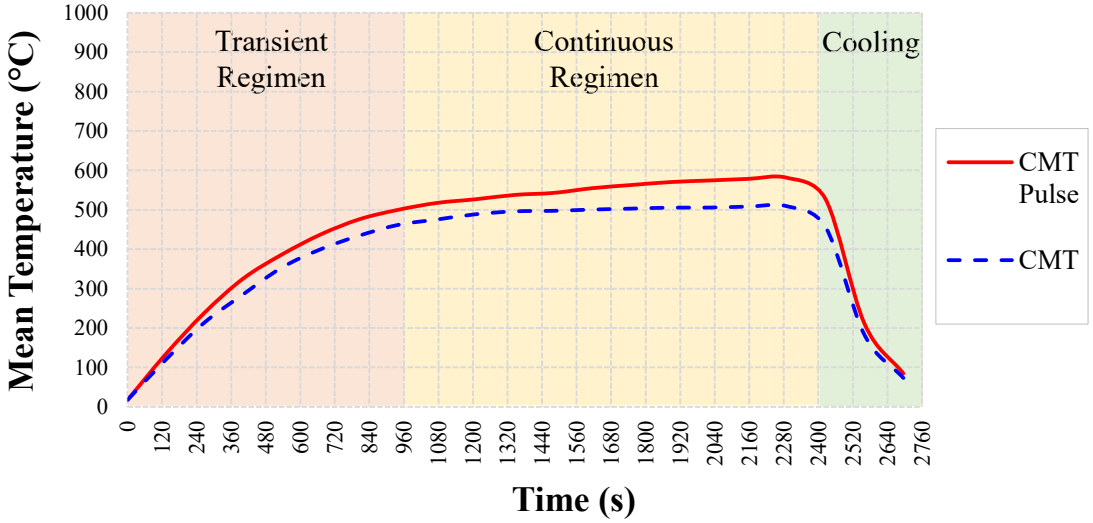


Figure 41: Mean temperature of the samples under construction.

## 4.4 MICROHARDNESS PROFILE

The microhardness results showed similar values with the literature for the alloy and low dispersion along the profile. The regular hardness profile along the section can be explained by the long time in which the structure was kept at a constant temperature in the continuous regimen. The samples were cooled as welded in air environment. The Figure 42 shows the microhardness profile analysis with the results of both process variants. The CMT Pulse presented a mean hardness of 271 HV. The CMT presented a mean hardness of 263 HV.

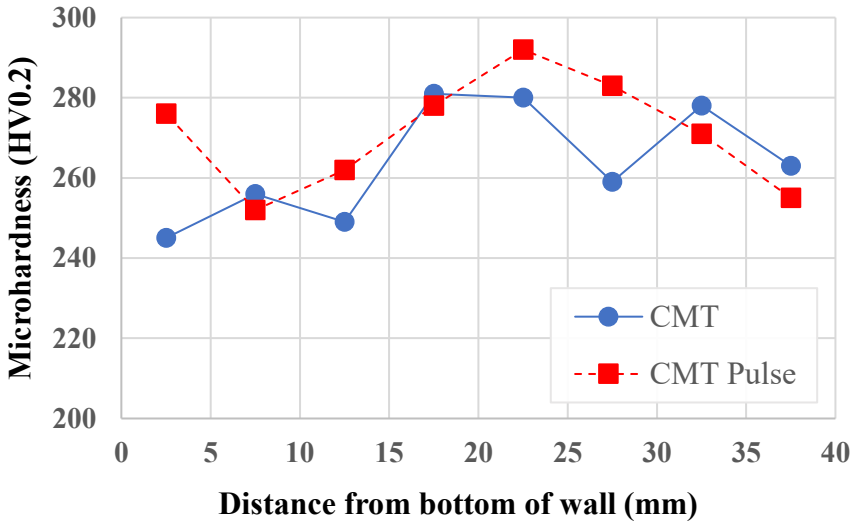


Figure 42: Microhardness profile. CMT and CMT Pulse comparison.

## 4.5 CHEMICAL COMPOSITION

The chemical composition of the samples was evaluated measuring three points of the cross section (base, middle and top). The Figure 43 brings the comparison of chemical elements content for the samples of CMT and CMT Pulse. The elements compared are carbon, manganese, iron, and chromium.

The chemical composition showed almost no difference between the process variants. As expected, the measurement of the base showed more iron content and less alloying elements because of the dilution with the substrate. The CMT Pulse showed higher dilution, which is expected due to its higher heat input.

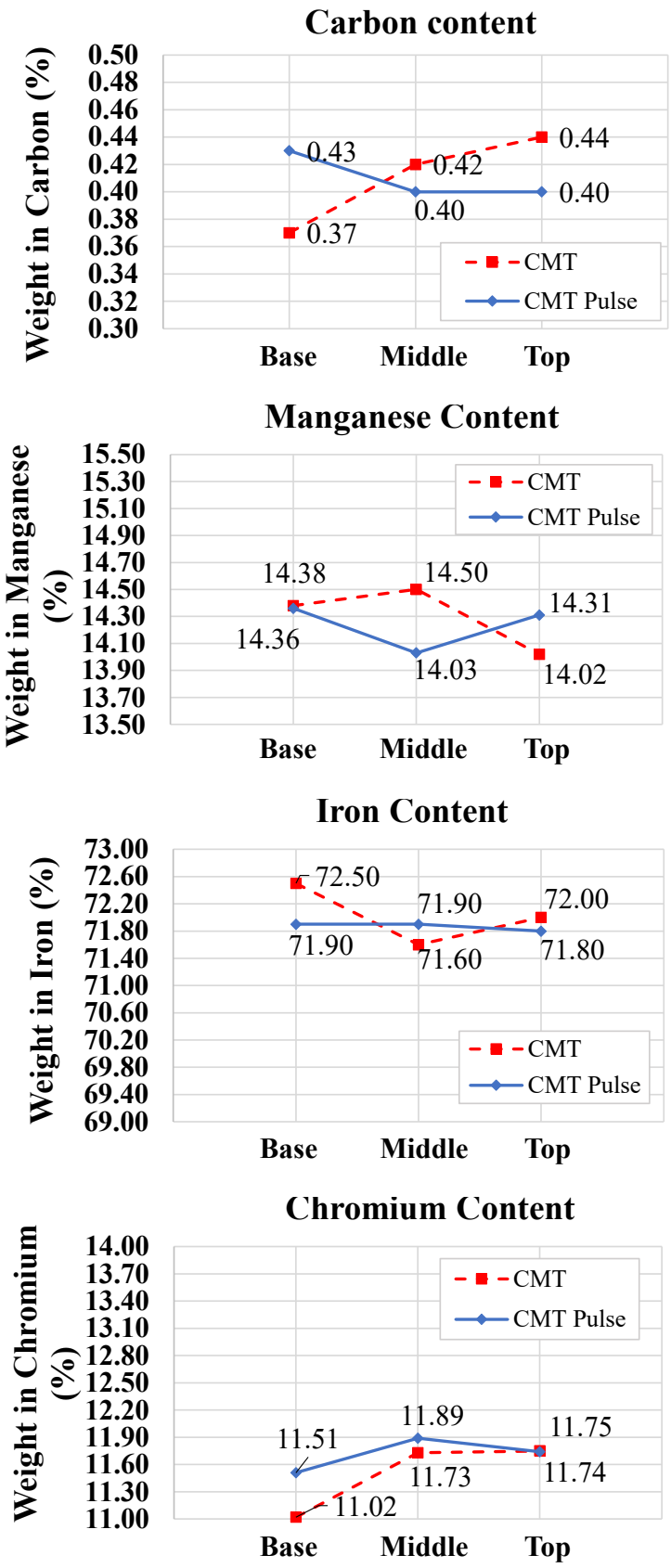


Figure 43: Chemical composition analysis comparing CMT and CMT Pulse.

## 4.6 HIGH SPEED FILMING

By means of a high-speed filming analysis of the process it was possible to evaluate different aspects of the welding conditions applied (process + addition material). Once the analysis was based in a film, the use of snapshots of the video was used. Even though, for a better understanding of the phenomena one can scan the QR codes bellow the snapshots to watch the film in its full length. Together with the QR code is also the link.

Among these aspects of deposition that can be analyzed due to the HSF technique, the following can be highlighted:

**The electrode melting behavior and material transfer from the electrode to the welding pool occurs differently to solid wire under analogous process conditions.** Due to the characteristic of metal cored wires being formed by metallic band that contains a powder aggregate, the conduction of electric current occurs differently to solid wires. In metal-cored wires the electric current flows predominantly through the band since it conducts the electric current more easily than the core. Two main factors lead to this behavior: the presence of non-conductive materials in the composition of the aggregate core and the lower electrical resistance of the metal strip band compared to a conductive powder mixture. This behavior influences the formation of the electric arc and the way in which the material melts and is transferred to the welding pool. The differences between these behaviors can be compared by analyzing the deposition of both wires with similar welding conditions by means of high-speed films as well as frames of the main moments. The Figure 44 shows a sequence of frames of the main events of a deposition with the tubular wire (Mangalloy) in the CMT variant. In contrast, the Figure 45 shows a similar sequence of moments of deposition of a solid wire in similar welding conditions (CMT, 3 m/min), although with Er70S-6 alloy.

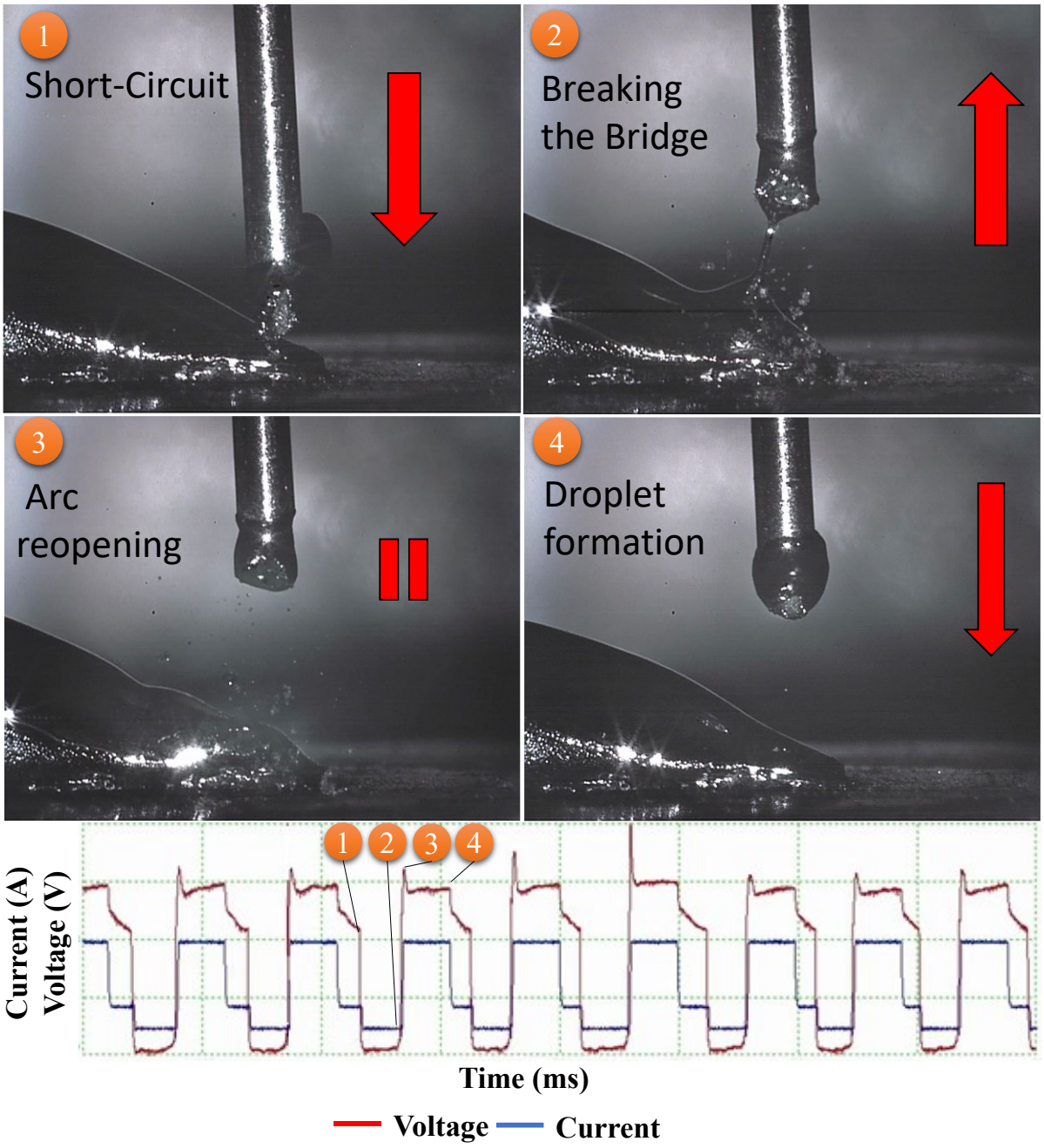


Figure 44: HSF main events of tubular wire deposition. CMT, 3.5 m/min. Mangalloy.
https://youtu.be/o1wtwGgGmyg

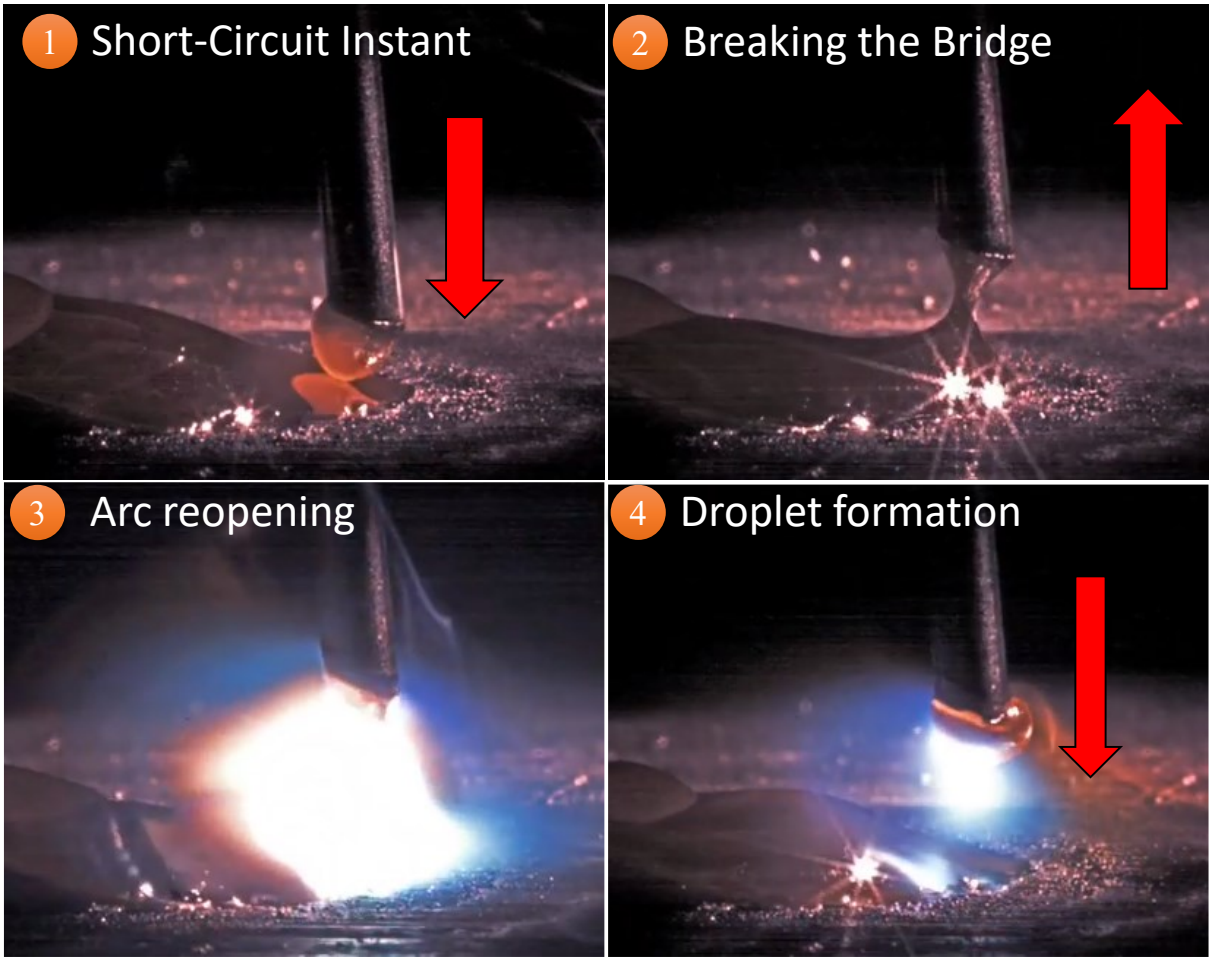


Figure 45: HSF main events of solid wire deposition. CMT, 3 m/min, Er-70s-6.
https://labsolda.ufsc.br/videos/videos-tecnicos/mig-mag/video/mig-mag-cmt-soldagem-em-aco

The same comparison can be done with the CMT Pulse. The Figure 46 shows a sequence of frames of the main events of a deposition with the tubular wire (Mangalloy) in the CMT Pulse variant. In contrast, the Figure 47 Figure 45 shows a similar sequence of moments of deposition of a solid wire in analogous welding conditions to represent the expected behavior of free flight material transfer at every pulse, alternating with the short-circuiting periods. The process variant used was also CMT Pulse, although with the use of an Aluminum alloy and in vertical position (3G uphill).

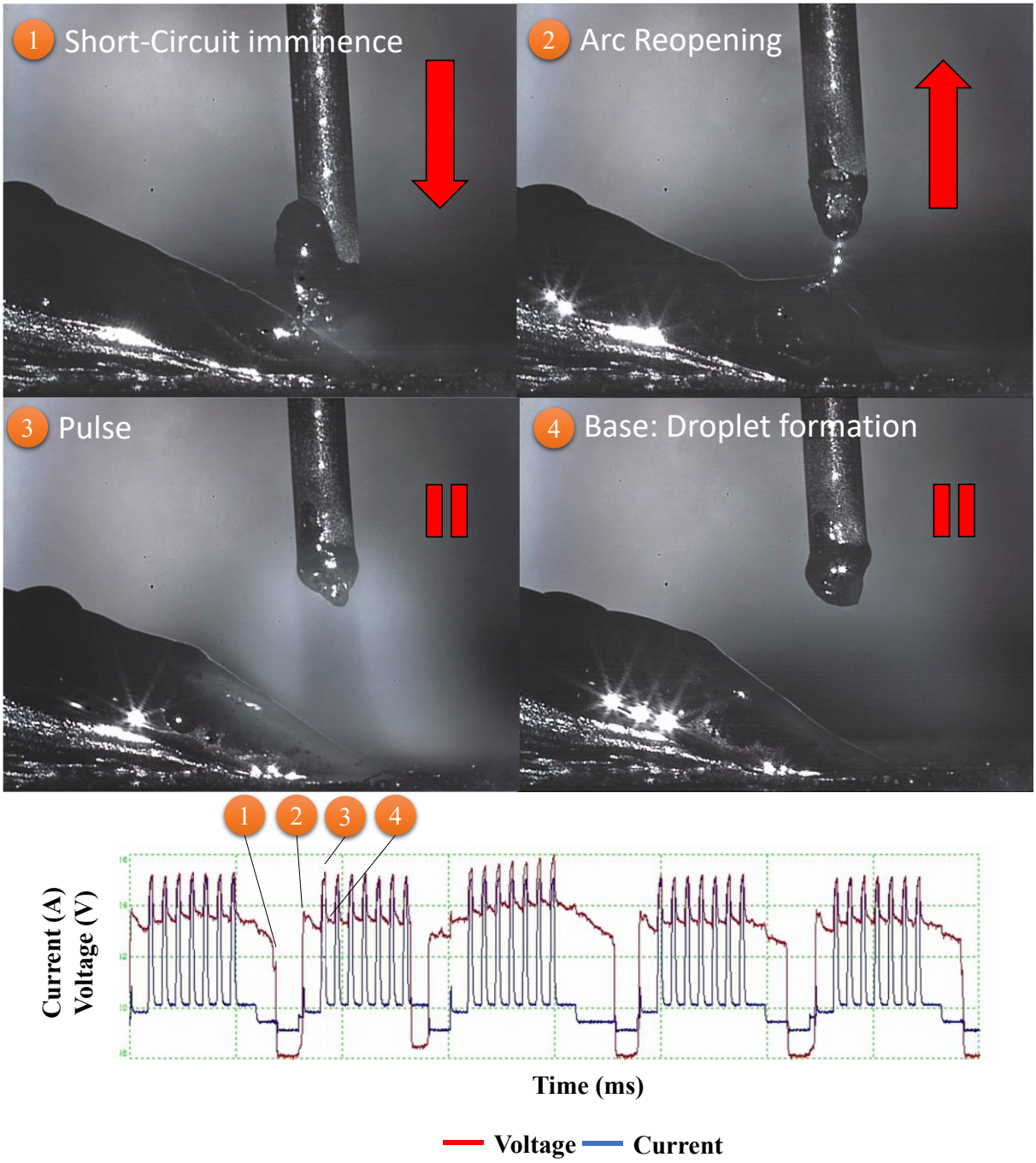


Figure 46: HSF main events of tubular wire deposition. CMT Pulse, 3.5 m/min, Mangalloy.
https://youtu.be/o3jojBoUjfg

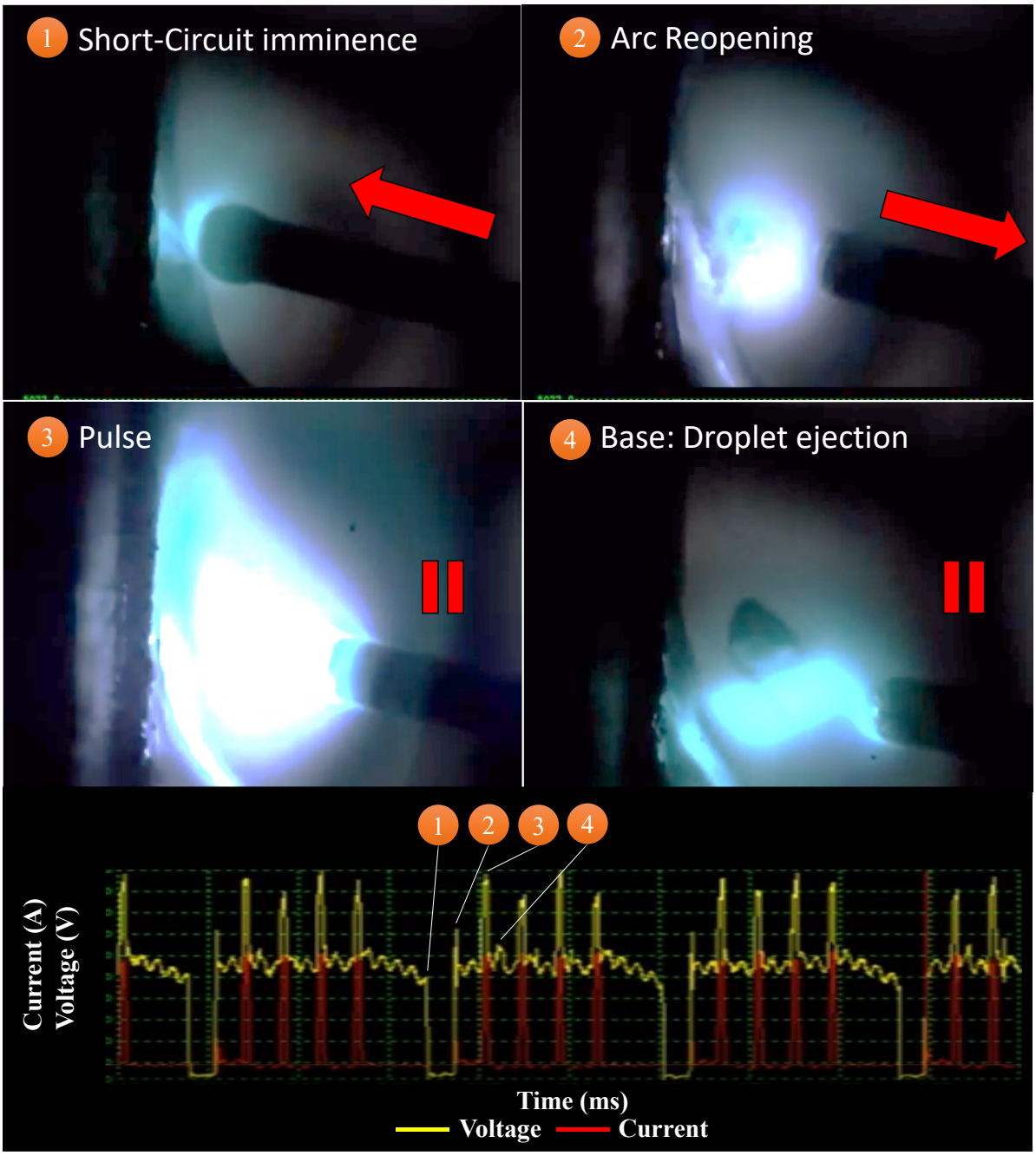


Figure 47: High speed filming main events of solid wire deposition. CMT Pulse.
https://www.youtube.com/watch?v=2lBWBgPna7A

**The droplet formed during the deposition was mainly composed by the wire band, leaving the core in solid state until reaching the welding pool.** In both process

variants was observed that the fusion line escalates quickly through the metal band. Once the band conducts the electric current, it is more exposed to the heating effects than the core. Consequently, the core remains in the solid state, in its aggregated powder form, with some green resistance until it is mechanically detached, as demonstrated by the Figure 48. The same behavior is seen in the CMT Pulse variant as shown by the Figure 49. The visible solid core presents a cone form, like a pen tip, showing that the outer particles of the core have been melted and diluted with the droplet or ejected.

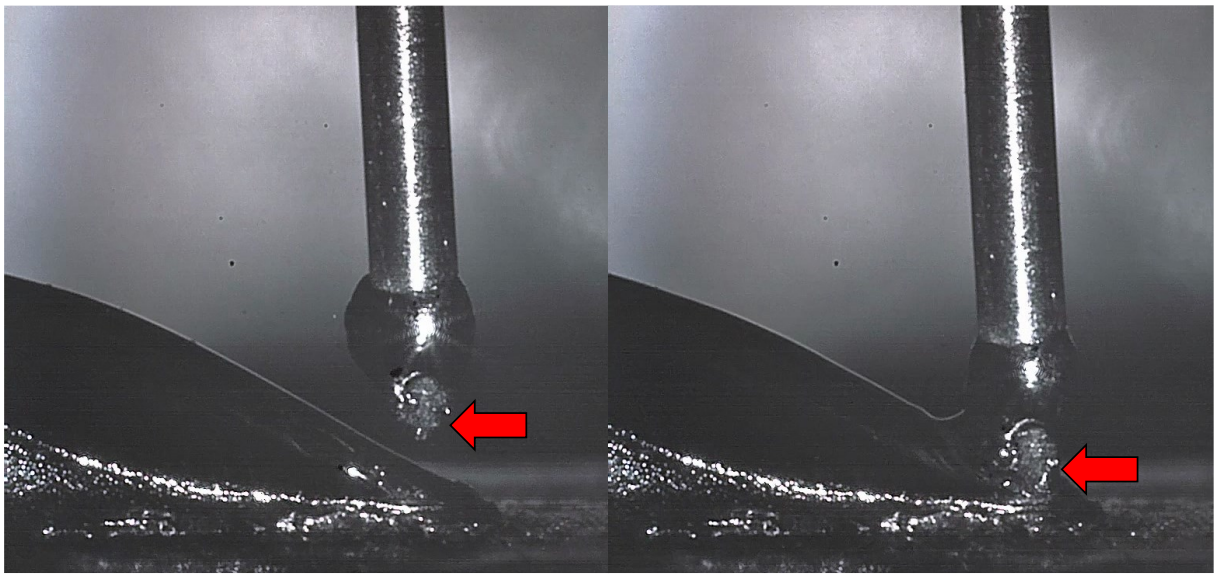

Figure 48: Solid core dives into welding pool. CMT variant.

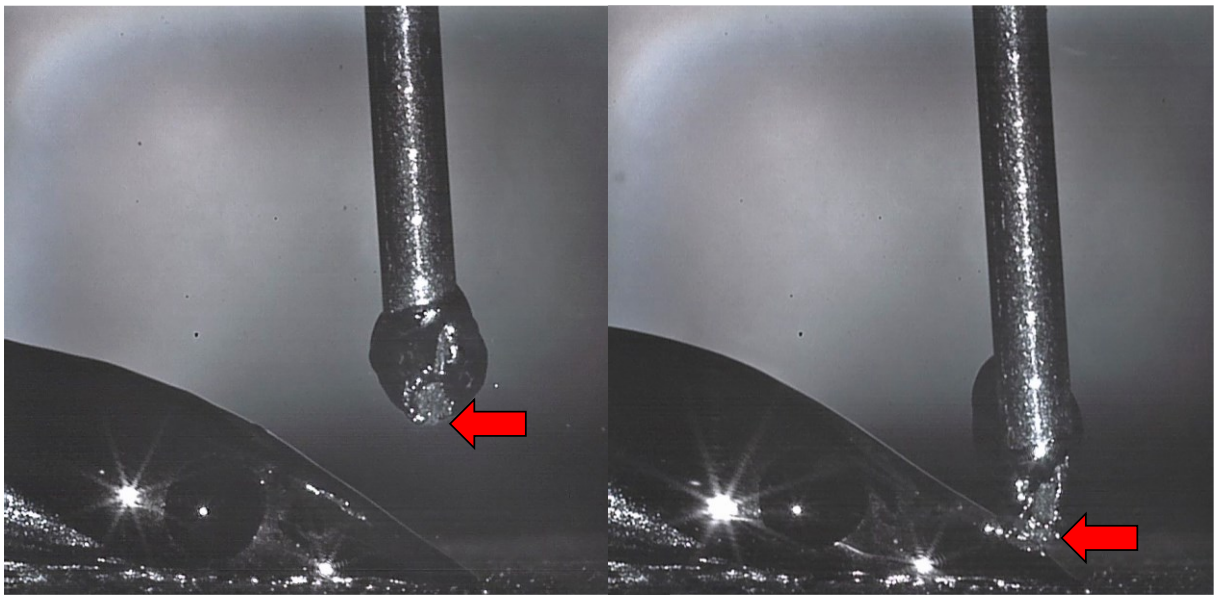

Figure 49: Solid core dives into welding pool. CMT Pulse variant.

**The core material transfer to the welding pool occurs mainly by the constant ejection of small particles and tiny droplets or by the detachment of bigger powder clusters.** During the whole process is possible to see small droplets and particles being ejected from the core. These particles fly mainly toward the welding pool, but also to the surrounding area. Bigger clusters seem to desegregate as the core reaches the surface of the welding pool during the forward oscillatory movement of the wire. The Figure 50 shows some frames of the core material transfer behavior of the CMT variant.

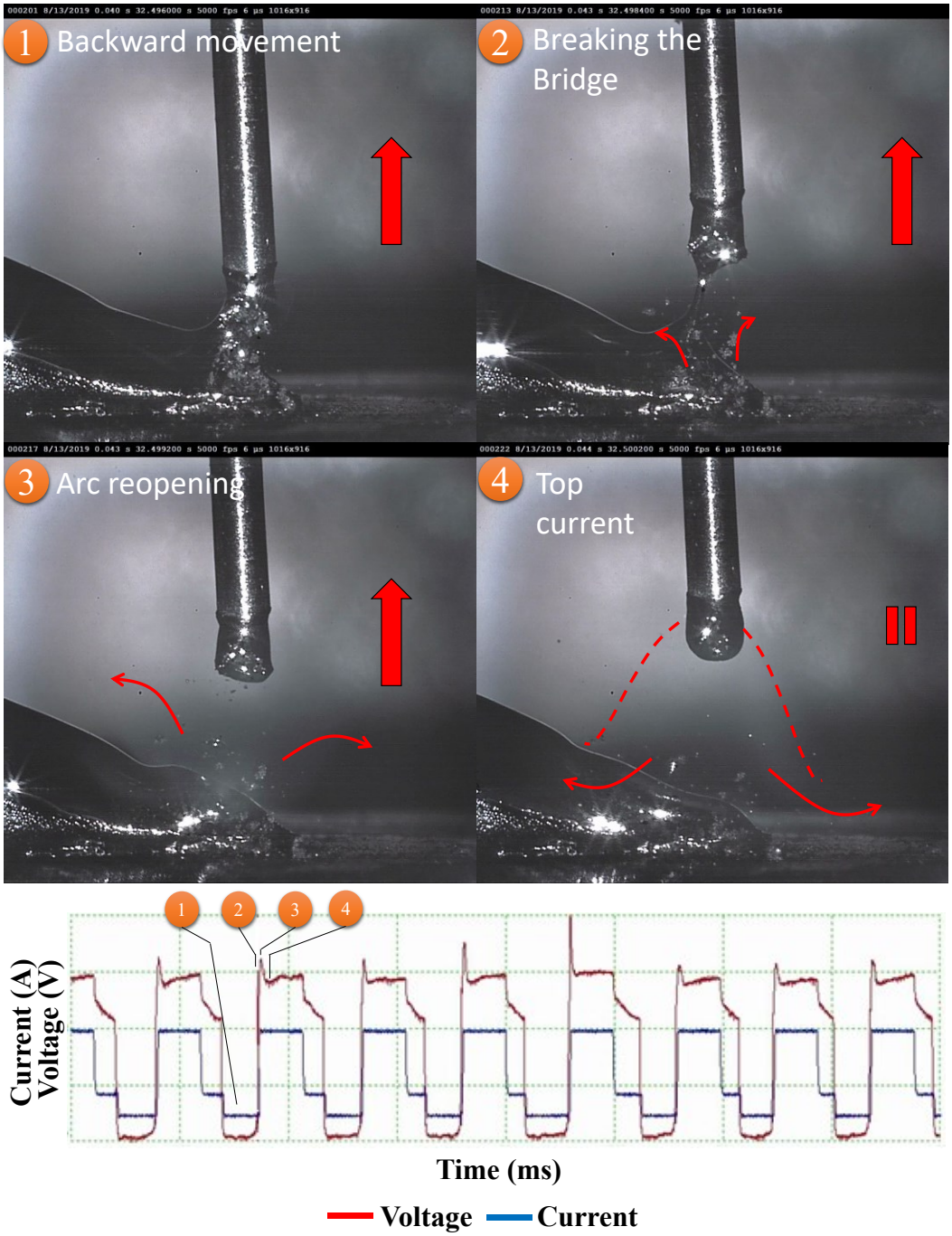


Figure 50: Solid core transfer during deposition. CMT variant.

**In the CMT variant it is possible to see that the core dives through the welding pool and touch the substrate**. Still in the CMT variant, the backward movement showed to cause the ejection of the powder aggregate that was still not melted flowing on the welding pool, as showed in the frame 2. The Figure 51 shows some frames of the core material transfer behavior of the CMT Pulse variant.

The first frame of Figure 51 shows the imminence of the short circuit. At this moment, the massive transfer of material from the electrode to the welding pool has not yet occurred, except for tiny droplets and small particles of the core that are continuously ejected in a dispersed way during the pulse cycle. As the electrode advances towards the welding pool, the core, still solid, is revealed. Analogous to what occurs in the CMT variant, the solid core plunges into the welding pool during the short-circuit stage. Unlike the CMT variant, the ejection of particles due to the wire backward movement was not observed in the film. In the final frame the formation of two drops of slag can be observed floating over the welding pool. A set of solid particles flowing on the welding pool surface is also evident.

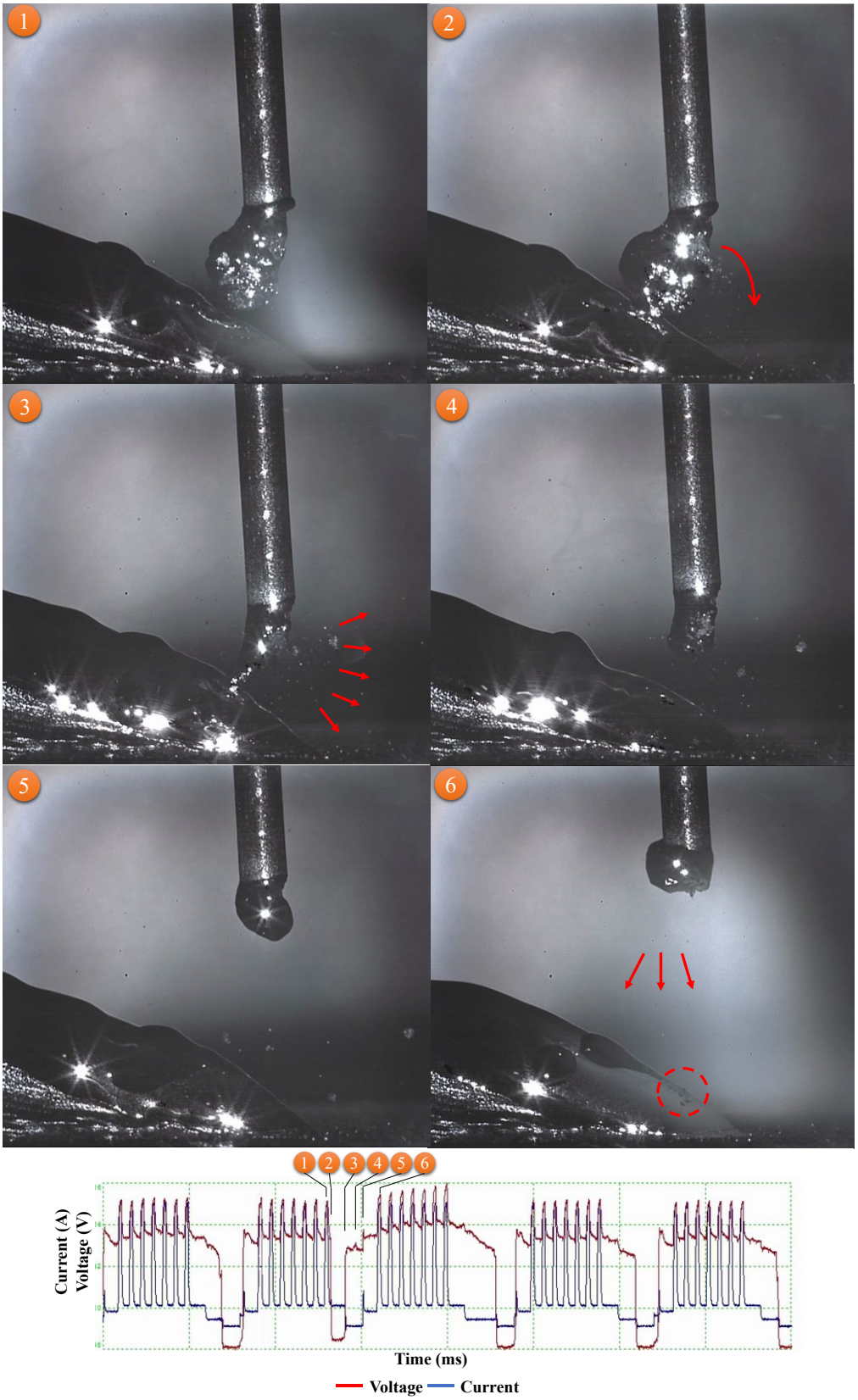


Figure 51: Solid core transfer during deposition. CMT Pulse variant.

**The metal transfer in the CMT Pulse process occurred mainly during the short-circuit cycle** in pulsed GMAW process, it is usually expected that the imposed current pulse will be able to induce the droplet detachment, resulting in a free-flying transfer. However, according to high-speed filming analysis, the material transfer occurred only by short-circuit mode. The Figure 52 shows a sequence of frames demonstrating the lack of massive material transfer during the pulse. At each pulse, the molten volume on the electrode grows, however it does not detach from the wire tip. At the same time, the ejection of small solid particles and tiny droplets is apparent during the whole process.

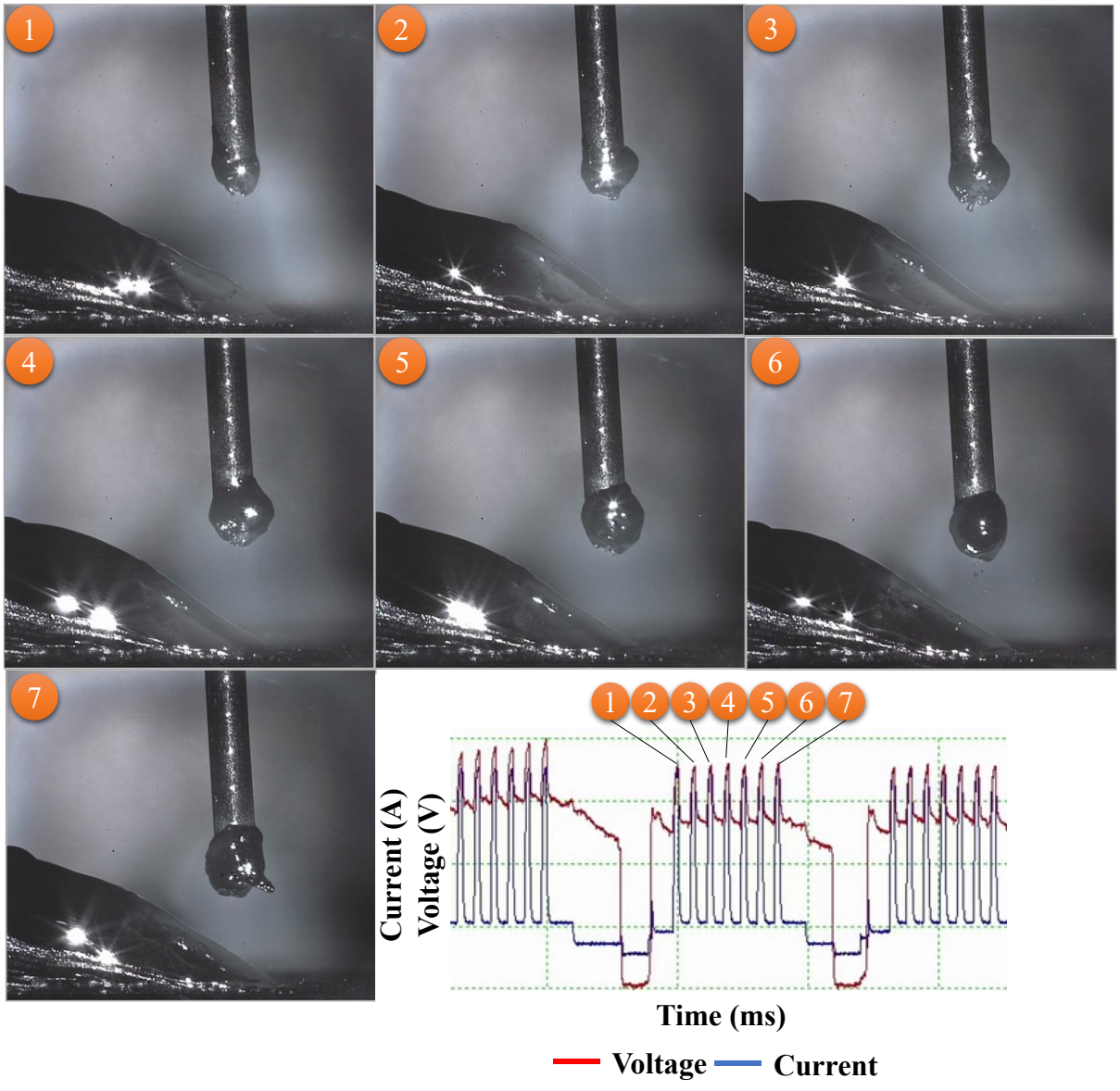


Figure 52: Frame at every pulse of a cycle. CMT Pulse.

## 4.7 VALIDATION SAMPLE

The additively manufacturing of a part with industrial application was proposed in the final phase of this project as a validation test. The objective was to analyze the initial challenges of manufacturing a part by means of WAAM using conventional equipment of the arc cladding and hard facing industry.

This challenge of manufacturing a WAAM made part in a hard-facing industry environment brought some intrinsic equipment limitations. While for the first stages of the research a Fronius CMT technology and a welding robot were used, at the industry, for the validation test, the equipment available with most relatable characteristics was a Miller Auto-Continuum power source with RMD electric wave pattern and a CNC table. During the validation test, no electric signal monitoring apparatus were available.

The geometry chosen for the validation part was a thick-walled pipe, as specified in the methodology. It might be considered a relatively simple structure that can be manufactured by other conventional conformation means, but its geometry is the basis of other more complex structures such as manifolds, pipe sleeves and nonlinear or asymmetrical pipe fittings, like pipe elbows, therefore, it is seem as highly relevant. These two formerly mentioned parts have important application in strategic industries for the Brazilian state: The Mining, Agriculture and Oil & Gas industry. These two sectors often work with raw materials (sand, gravel, crude oil) that can be aggressive in terms of wear, heat and chemical reactivity with the transport structures (e.g. pipelines and conveyors) and specially to the processing equipment. Some parts used in these systems needs to be protected from this aggressive working condition to provide a feasible part lifespan. Coating the parts with advanced materials is commonly made by welding processes either for cladding (protection against corrosion) or hard facing (protection against wear). These overlay process with advanced materials offer improved properties to the surface, like better resistance to abrasion and corrosion or even both. Although, the cladding process of smooth pipe bends can be made impractical or uneconomical in special conditions (WOOD; PIPING, 2008).

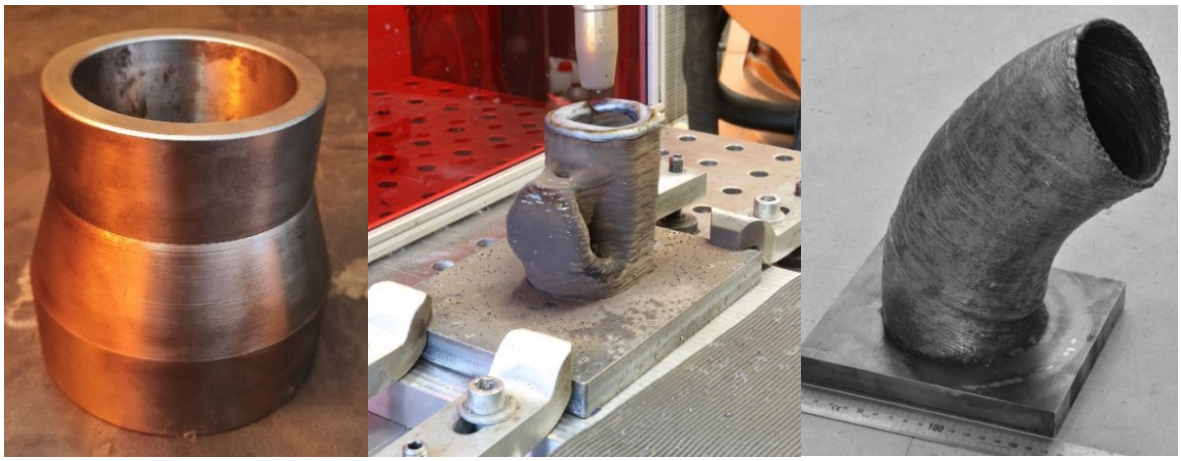

Figure 53: Thick pipe sleeve (VILARINHO, 2020). Pipe Fitting as deposited (REINMANN). Thin Pipe Elbow (HENCKELL, 2019).

Pipes of small diameters or pipes with nonlinear geometry are challenging to internally overlay due to the welding torch/feeder head size, between other factors. It is a problem also for solid-state metal-joining processes, like explosive welding (FINDIK; DESIGN, 2011), due to its geometric nonlinearity condition.

Explosive welding cladded pipes might be bended by induction means latter but it's another extra production cost, comparing to WAAM in which the heat treatment can be made during the deposition. One solution for that problem is manufacturing mitered pipe bends, although it's seen as a vulnerable fitting for wear and corrosion (BHARDWAJ, 2020). The Figure 54 shows a pipe elbow with erosion-corrosion induced failure, showing the most vulnerable region. To manufacture mitered pipe bends, it is first required to internally overlay the pipe, afterwards cut it, and then join the parts together. The Figure 55 shows as example an internally hard-faced mitered pipe elbow made by DURUM Verschleiss-Schutz. Mitered pipe bends results also some internal square tips at the joints reinforcement, lessening the abrasion resistance, and, though, the part lifespan. This manufacturing method has intrinsic disadvantages. The joining of dissimilar materials coated sections is not trivial (GONÇALVES E SILVA *et al.*, 2020), especially for corrosion resistant alloys (CRA's) where the whole surface area needs to be cover with homogeneity to avoid corrosion issues and fulfill its purpose. For wear protection in noncorrosive environment, the surface roughness and homogeneity are not so critical once the overlay acts as a mechanical protection, differing for the chemical characteristic of corrosion attacks. Another disadvantage is the waste of production time, due to the series processes required (coating, cutting, joining, heat treatment). The material waste during the cutting can be also pointed out as a relevant

negative characteristic, especially for advanced costly coating alloys like CRA's and composite high wear resistant alloys. Cutting wear resistant materials is also not a trivial task, and the consume of cutting disks may be elevated.

Figure 54: Failure due to erosion–corrosion in the elbow section (BHARDWAJ, 2020).

Figure 55: Mitered pipe elbow with internal coating by DURUM Verschleiss-Schutz.

Using WAAM to manufacture these nonlinear pipe fittings has been proof feasible by recent research (HENCKELL, 2019). The WAMM technology can mitigate some of the above-mentioned issues. Once the structure grows in layers, there is less concerns with the tool center point reaching all the flanks without the torch bumping on its walls. The possibility of changing the parameters between each layer widen the prospects of altering even more the surface properties. Being possible to change the material type added in each layer provides the ability to make functionally graded pipes with different chemical composition depending on the local requirement (HENCKELL, 2018). Per example, an elbow pipe section which is more severely exposed to wear can be made more resistant by gradually improving the carbon content in its section than the rest of the pipeline. This gradual variation in the material deposited diminished the sudden change in the mechanical resistance, weakening problems of tensile strength overmatch within weldment and base material (RIFFEL, 2018).

The use of metal-cored wires as material feedstock increases even more the flexibility of WAAM inner cladded/hard faced pipes. Per example, metal/flux-cored wires can carry wear resistant ceramic powder particles, like fused tungsten carbides (FTC) in its core (SCHREIBER, 2000), which is not possible with massive wires. With WAAM, one can built a multiple torch apparatus with more than one wire feeder assembled, each with different wire alloys. One wire feeder would feed the material for the outer layer while the other wire feeder, the inner layer alloy. This way, it would be possible to manufacture complex pipe fittings with internal coating/ functional graded deposits without the need of using pipe miters. The Figure 56 brings the concept with two different depositing strategies, named by the author as "layer wise" and "parallel" strategies. Both utilizes different materials with some alternating deposition dynamic .

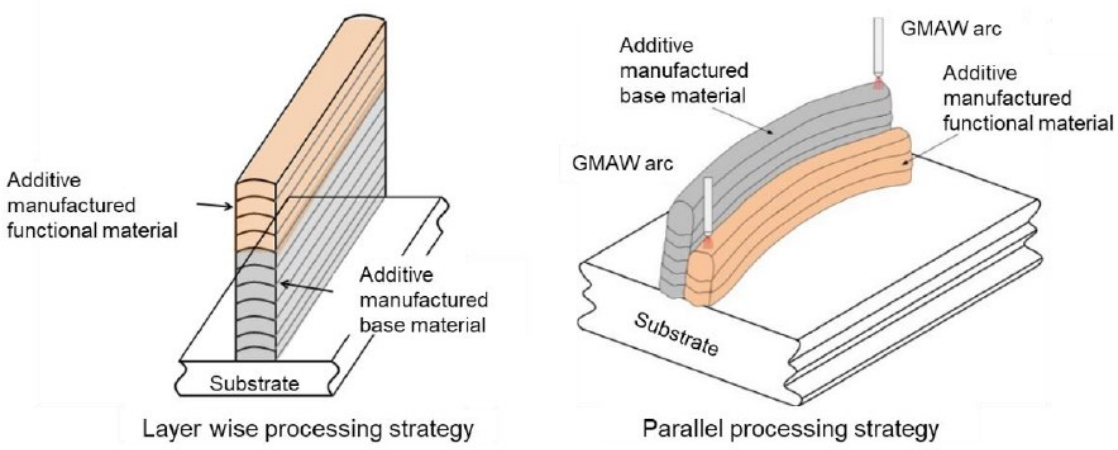


Figure 56: Dissimilar material structures made by WAAM (HENCKELL, 2018).

The present work, as formerly exposed, will deal with the ground base of that manufacturing concept. In this initial research only one alloy was used, and the pipe will not present steep walls. Future works are intended to fulfill the aim of building the pipe fitting concept with graded deposited dissimilar materials.

#### *4.7.1.1 Validation Part Geometry*

The geometry of the validation part consists of a thick-walled pipe-like structure. The pipe's walls are 15 mm thick, similar to the first stages' sample. The outer radius of the pipe 115 mm. The inner radius is 100 mm. The height of the pipe has been set at 50 mm. The Figure 57 presents a perspective view of the designed geometry, while the Figure 58 brings it's geometry according to a top view.

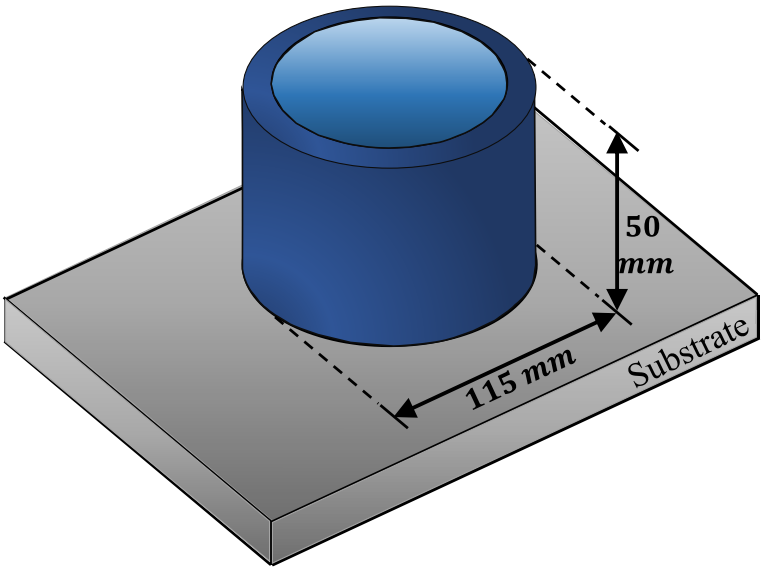


Figure 57: Pipe-like sample geometry. Perspective view.

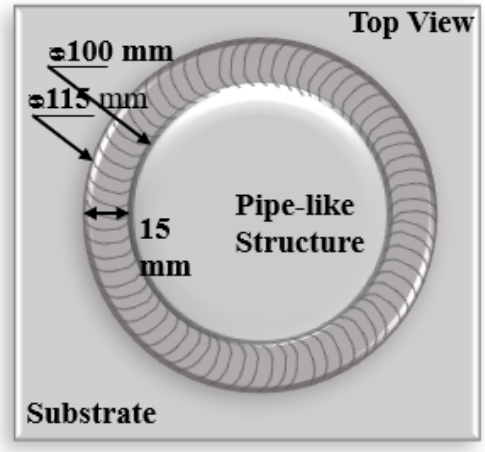


Figure 58: Sample Top view.

### *4.7.1.2 Validation Part Deposition Strategy*

The deposition strategy used was defined as alternating layers with idle time between each layer. This strategy demands the electric arc to extinguish as reaching the end point of each layer. Subsequently, the part was cooled down to the defined interpass temperature, then the next layers started being successively deposited. It is important to notice that the deposition started always in the same direction, towards the colder side of the part, weakening even more overheating issues.

Differing to helicoidal strategy, where the arc does not extinguish, this deposition strategy requires an overlap deposition to join the structure and form a circumference. The overlap used had an offset of 1.5 period (full oscillations) in both modes. In this specific

strategy, no parameters ramp was use. At the end of the deposition a crater filling time of 0.5 s was applied right after stopping the torch displacement.

To achieve the desired layer width, two different deposition strategies were tested. Both of them consisted in the weaving technique but differing in how the tool was programed to oscillate. Both weaving had a triangular pattern with same amplitude of 14.5 mm. The Table 17 presents a summary of both strategies.

Table 17: Deposition strategy comparison.

| Part | Structure type | Layer height average (mm) | Path Planning | Tranversal Material Spreading |
|---|---|---|---|---|
| A | Multi-layer | 2.5 | Unidirectional | Weaving - Triangular Pattern |
| | Total height (mm) | Layers to reach part height | Fixed Arc Start/Stop Point | "X" and "Y" axes movement following points |
| | 50 | 20 | PA (flat position) | A= 14.5 mm<br>f = 1 Hz |
| **Part** | **Structure type** | **Layer height average (mm)** | **Path Planning** | **Tranversal Material Spreading** |
| B | Multi-layer | 2.5 | Unidirectional | Weaving - Triangular Pattern |
| | Total height (mm) | Layers to reach part height | Fixed Arc Start/Stop Point | Turn Table + Torch Oscillation |
| | 50 | 20 | PA (flat position) | A= 14.5 mm<br>f = 1 Hz |

The part “A” was built with the first weaving technique. It consisted in the tool following a trajectory of multiple points previously programmed to satisfy an input frequency, amplitude, and TS. In this case the axes “x” and “y” are constantly changing its direction and speed to reach the points as programed. The Figure 59 present the tool trajectory by its points dispersion. Still in the Figure 59 a zoom shows the Start Point (green) and End Point (red), with the overlapping path highlighted with a blue line.

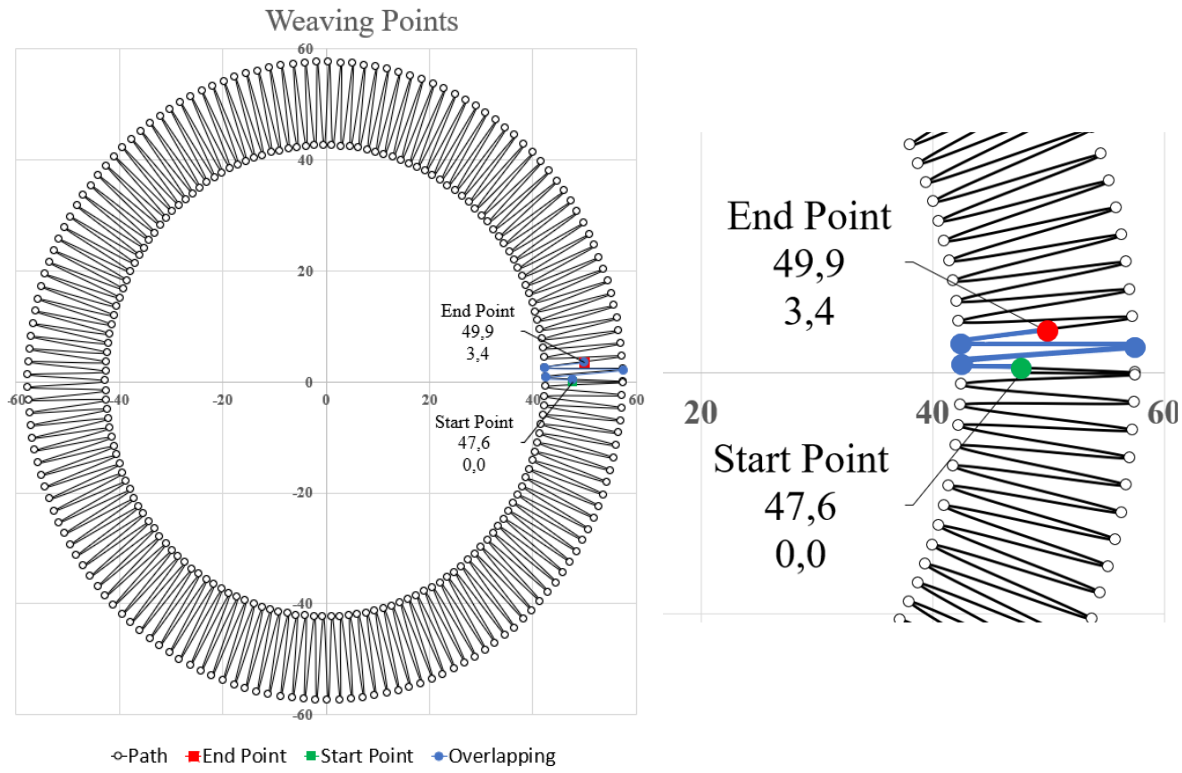


Figure 59: Deposition strategy by multiple points.

The Figure 60 shows the overview of the equipment setup used to build the part “A”. The CNC table used had a wide working envelop (3.0 x 1.5 x 0.5 m³), however, the substrate was positioned near to the front of the table for easiness of access.

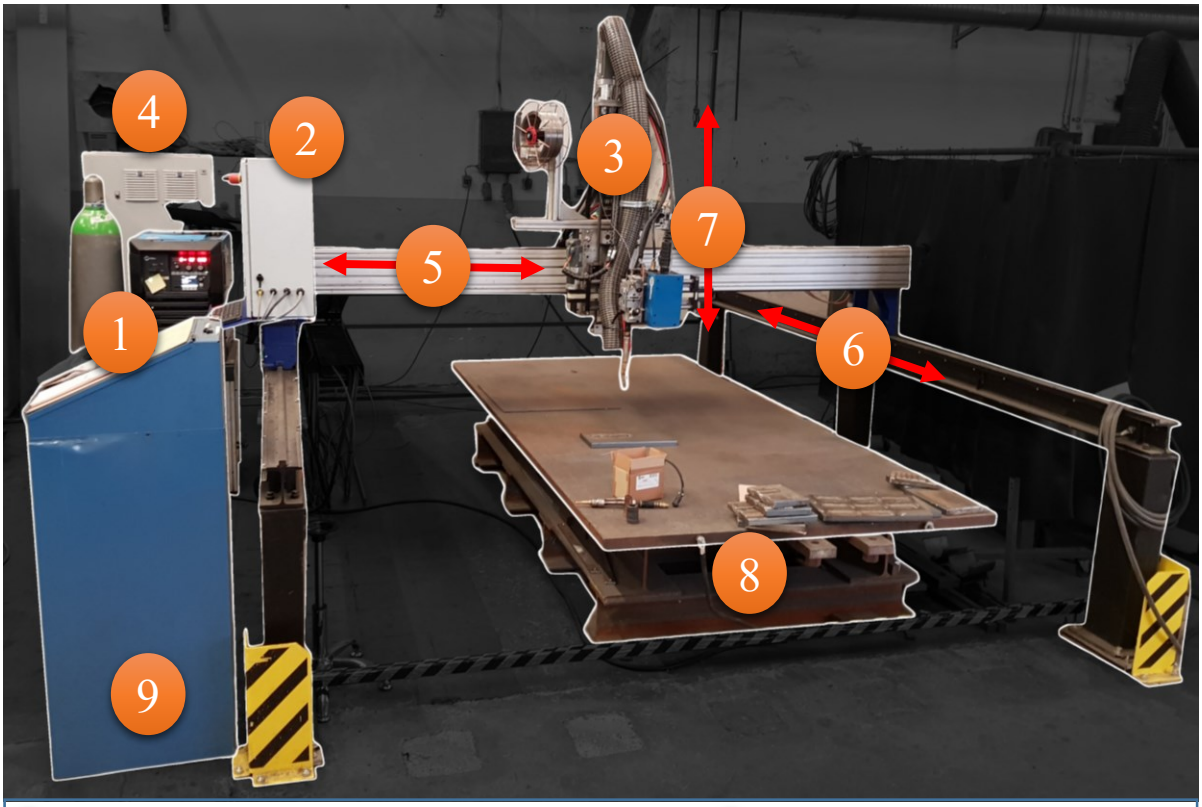


1. Miller Auto-Continuum power source + Gas Flask;
2. CNC HMI;
3. Wire Feeder/Torch head;
4. CNC controller box;
5. “y” axis;
6. “x” axis;
7. “z” axis;
8. Table;
9. Support desk.

Figure 60: Working bench of validation stage.

The wire feeder used was compact and had a direct connection between the wire feed head with the torch, without any extension cable to guide the wire to the torch. Cooling and gas hoses were directed connected to the torch. The whole structure was attached to both “y” and “z” axes. A fourth axis, called “A1” was present to make a lateral oscillation. However, its amplitude/frequency ratio was limited and, thus, not used in this work. The Figure 61 shows the apparatus in detail.

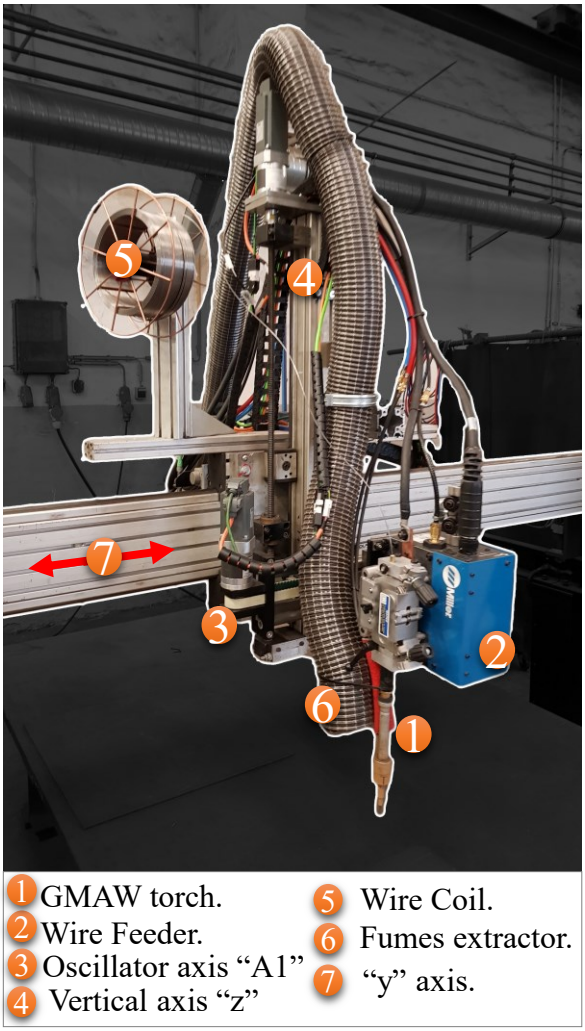


Figure 61: Wire feeder head.

The part "B" was built with the second technique. It consisted in fixing the substrate on a turn table that turned in a programed speed while the torch oscillated horizontally with the need of only one axis ("y") to do so. The Figure 62 presents the turn table setup.

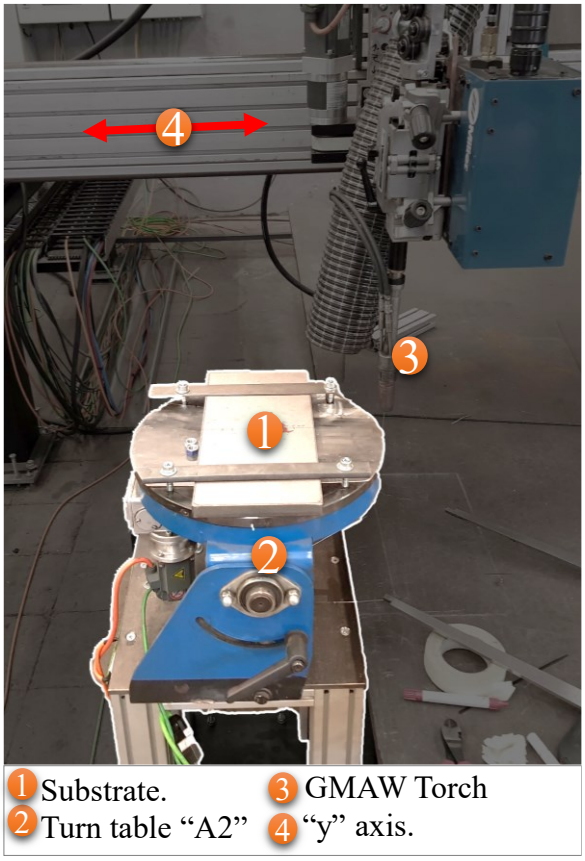


Figure 62: Turn table used in validation stage.

The number of layers to achieve this height were estimated as 20 layers of around 2.5 mm height, the same estimated for the manufacture of the wall-like structures, in the early stages of the research. The first task of the program when starting a new layer was to give a vertical increment (“z” axis) to deposit the new layer over the former one. This value was kept constant, following the layer height estimation of 2.5 mm.

A cooling strategy was used in both cases. It consisted in depositing a certain number of layers (10 layers in part “A” and 4 layers in the part “B), until enough height was reached to fill the inner space with water without interfering directly in the metal deposition. The water level was kept at least three layers below the deposition surface area (approximately 7.5 mm).

#### *4.7.1.3 Validation Sample Manufacturing*

Two samples were built following the geometry and deposition strategy exposed in the methodology. Each sample was built in a different equipment setup, requiring two different deposition strategies.

The Part “A” was built using a deposition path with multiple points that formed a triangular weaving pattern, as explained in the stage 4 of the methodology. This first strategy of using simultaneously both the “x” and “y” axes to change the tool center point orientation was not beneficial to the achievement of a steady material deposition. As the Figure 61 shows, the wire feeding header was assembled on the “y” axis, with the torch assembled directly to it. This compact concept is beneficial to avoid problems with wire feeding anomalies, but it turned the feeding head too heavy, impacting in the stiffness of the mechanism. As the “y” and “x” axes changed its orientation, the torch recoiled. While it may not had been a problem for hardfacing application with high depositions rates, in which the superficial aspects of the deposits are not of vital importance, for WAAM practice it can cause inconvenient disarrangements in the layer geometry. Even small discrepancies from the desired layer geometry may have its effect multiplied by the posterior deposits. Using lower TS may decrease the problem, however, loss in productivity is expected. For the additively manufacturing of parts with simple geometry, like the one proposed in this work, it might be not a critical issue, but, on one occasion of superior deposition path challenge, like depositing sloped sections, a very rigid tool center point is required. The Figure 63 shows the Part “A” as welded.

Figure 63: Part "A" as welded.

The Part “B” was built with the second deposition strategy that consisted in a turn table with continuous rotative movement while only the “y” axis oscillates between two fixed points. This setup showed better stability in the tool center point movement. Even though the torch was still not completely steady, using only the “y” axis decreased the mechanical hysteresis, or, at least, imposed a repetitive movement pattern during all the oscillation. Thus, resulted in less variance in the layer geometry, especially in width. It was also easier to program the trajectory once the travel speed was controlled by the turn table only and the oscillation parameter (frequency and amplitude) only by the “y” axis. The Figure 64 shows the Part “B” as welded.

Figure 64: Part "B" as welded.

An advantage of the equipment setup used for the Part “A” manufacturing was the large working envelop, which is of great interest for the WAAM, although the vertical axis could be extended and worked for somehow provide better rigidity to the torch. The wide working envelop can be used to produce small batches of similar parts simultaneously, using the idle time between layer as strategy to cool down one part while depositing a new layer in another region of the table that was already cooled to the required interlayer temperature. On the other hand, the use of the second technique (turn table) provides a better solution for a

research apparatus with a mindset of rapid prototyping with easy deposition path programming rather than flexible mid-size bath production.

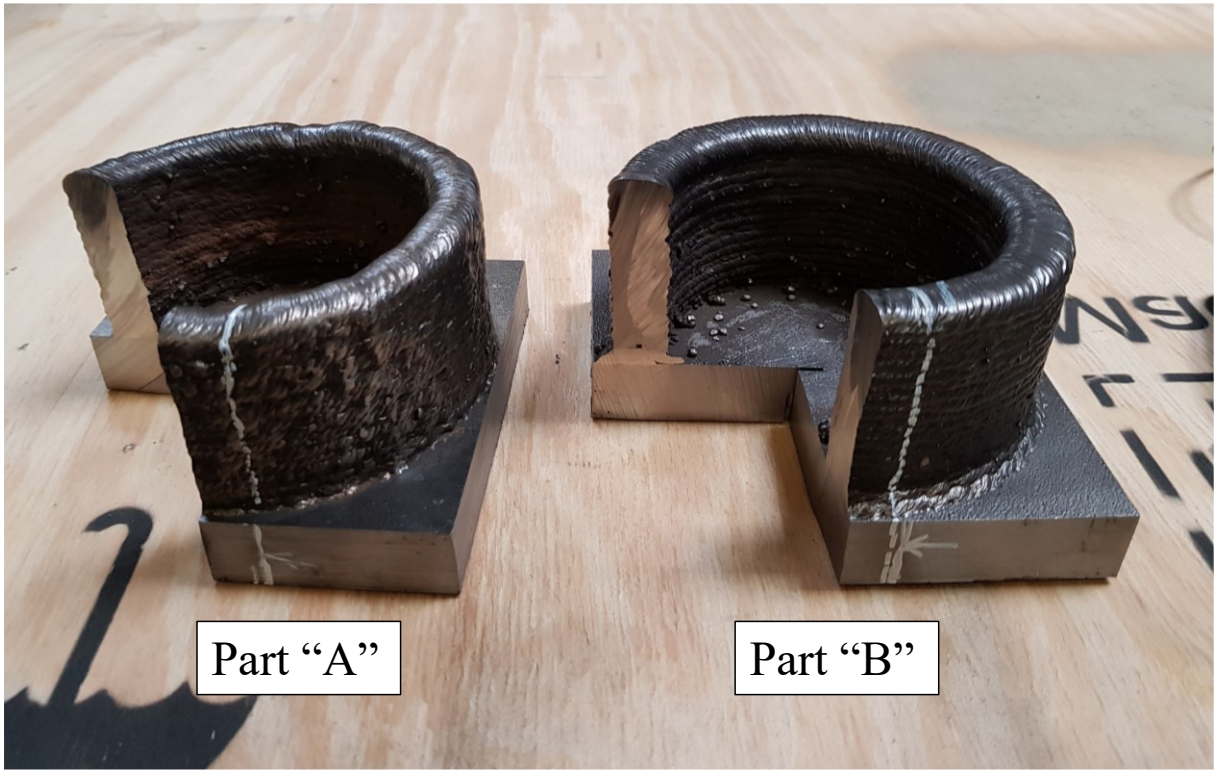


Figure 65: Part "A" and Part "B" after cleaning and sectioning.

The outlook of the layers looked regular in both width (16 mm) and height (3,2 mm). The width over 15 mm was a requisite for the first two layer to make a structure buffer between the actual part and the substrate. This also avoid over dilution with the substrate alloy. The volume of the substrate (400 x 180 x 24.5 mm3) and room temperature of 18 ˚C was not correctly taken in account during the pre-parametrization resulting in poor bonding in the beginning of the first layer. As the substrate was getting warmer both adding material and substrate started diluting.

Table 18: Electric and welding parameters.

| Process | Voltage (V) | Current (A) | Power (W) | Wire Feed Rate (cm/min) | Travel Speed (cm/min) | Frequency (Hz) | Amplitude (mm) |
|---|---|---|---|---|---|---|---|
| GMAW | 22 | 99 | 2178 | 3,2 | 6 | 1 | 15 |
| RMD | 16,3 | 86 | 1402 | 3 | 6 | 1 | 15 |

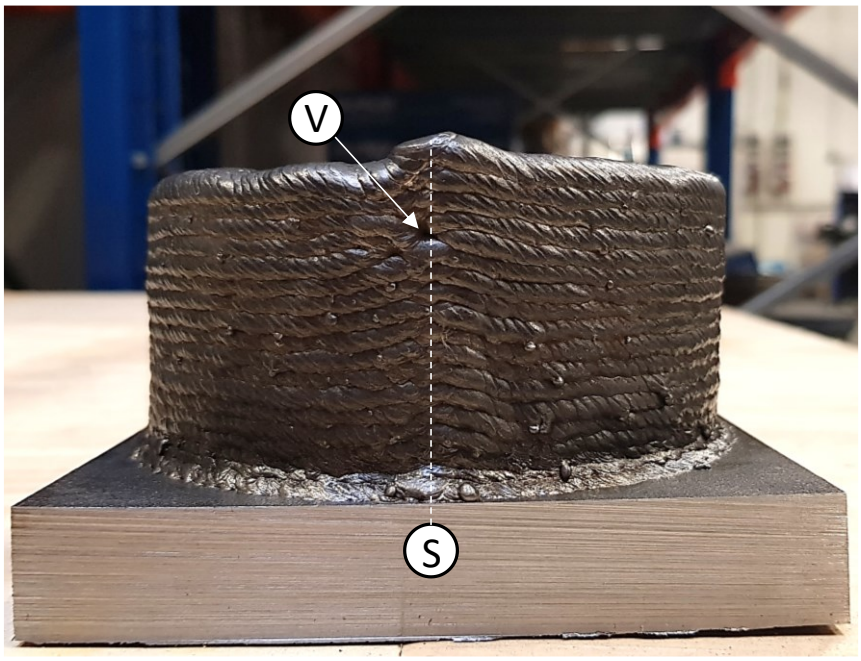


Figure 66: Side view of the part. Overlapping with excessive offset.
S: Starting Point
V: Void.

The Figure 67 shows the macro picture of the Start Point transversal sections cut. There was lack of bonding with the substrate. Voids resulted from lack of fusion between the first layers. Even though the first two layers were made with higher welding power, it was not enough to guarantee dilution, especially under the bead extreme points, also known as “Weld Bead Toe”. The first layer needs to be even warmer. The improved version of this program has increased tension (from 22V to 26V) and use waiting time in both sides. After the process was changed to RMD, in the third layer, the welding power decreased to avoid heat accumulation.

Figure 67: Macro picture of the start point.

The first walls made during the first part of this project were deposited with the same parameters of the other layers. That caused lack of bounding in almost all the walls. The first two layers this time were set with extra power. Although, according to the preliminary macro analysis it was not enough. Lack of bonding were evident in the beginning of the path. In the hottest part of the path, the end, the dilution was about 15-20%.

#### *4.7.1.4 Thermal Behavior*

To monitor the IT, the temperature was measured by means of a manual thermocouple after every deposition in the same spot. The measurements started immediately after the arc extinction, while the torch was returning to the origin, waiting to start the next deposition. Then, the measurements were repeated with a 30 s period for at least 120 s or until reaching the IT, when it took longer time to cool down. The temperature measurement point was set at the starting point once the next layer would start being deposited over this region.

The Figure 68 shows the temperature measurements over time during the part “A” manufacturing. In the Figure 68, the maximal temperature is presented. A striped red line helps the visualization of the maximal temperature during the part manufacturing. The deposition of one layer last 5,55 min with the settled parameters exposed in the Table 18. Another 4,5 min were used for the temperature, and wall height measurement.

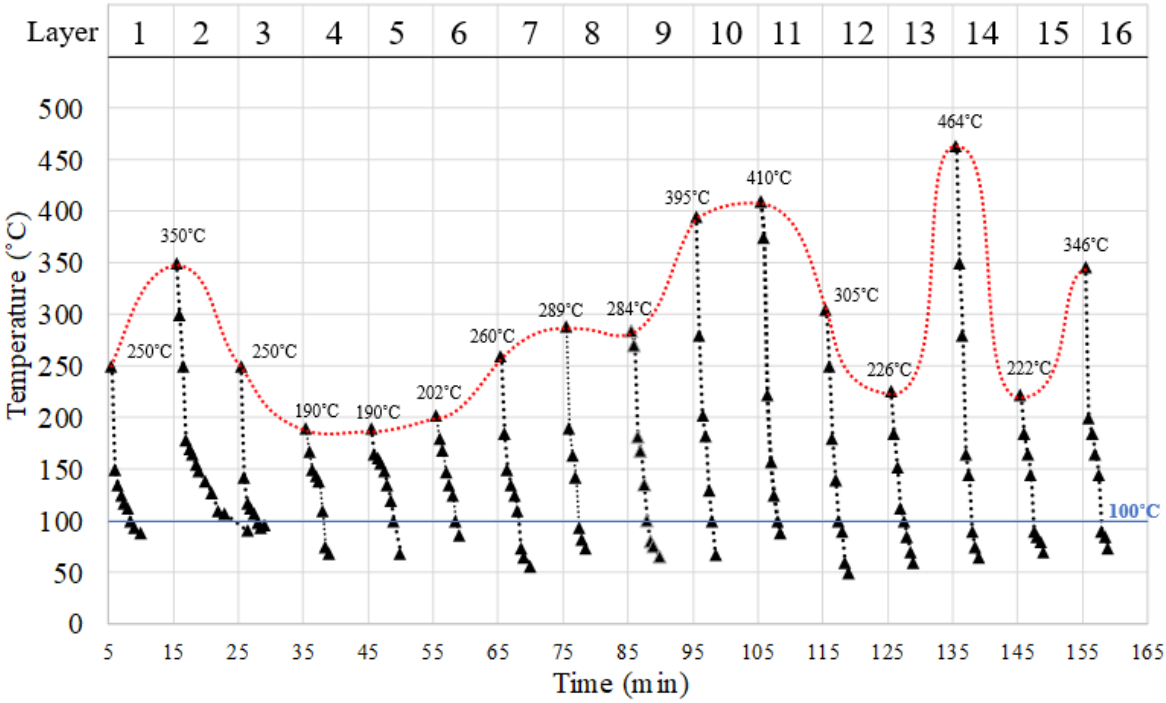


Figure 68: Temperature behavior of Part "A".

A manual water-cooling strategy was set to reduce the manufacturing time. It was set an interval of 10 minutes between the start of every new layer being 5,5 of depositing time and 4,5 for the measurements and cooling down the part.

The temperature results can be correlated with noted events of the manufacturing process (changing power, forced cooling), although the measurements errors might have a significant influence on the results. Per example, the hysteresis between making contact with the thermocouple on the layer surface and getting a result on the display were high. It happens due to the weak bond between the thermocouple tip and the surface. The formation of an oxide layer over the metal layer also showed to interfere the results as well. The user error on the results might be elevated due to these difficulties. Even though, this chart must be analyzed with a qualification view, comparing the temperature between the layers and not comparing with other studies.

First layer ends being deposit after 5,55 min. T0,5=250˚C. The first two layers are the structure base. It must have a safe bounding with the substrate plate. The process chosen for the first two layers was the conventional GMAW with the parameters showed in Table 18. The GMAW power (21780 W) was 776,2 W higher than the RMD (1401,8 W). The welding parameters tension and current were taken from the power source display after the end of a layer, without auxiliary acquisition of the welding electric signals.

The Part "B" showed similar results as Part "A".

*4.7.1.5Microhardness Profile*

The Figure 69 shows the microhardness profile with the results of both the two parts A and B. The Part “A” presented a mean hardness of 269 HV. The Part “B” presented a mean hardness of 268 HV. A pattern can be seen in the hardness profile due to the different stages of cooling.

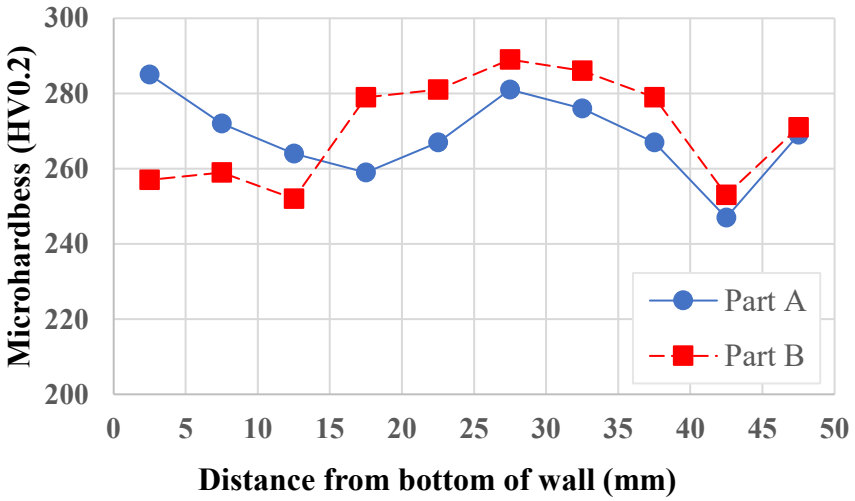


Figure 69: Microhardness profile. Part “A” and Part “B” comparison.

*4.7.1.6 Chemical Composition*

The Figure 70 brings a series of charts comparing the chemical composition of the part “A” and part “B” in three regions of the sample: bottom, middle and top region. The elements analyzed were carbon, manganese, iron, and chromium. The chemical composition of the deposits as welded showed only little deviation compared to the data sheet information, especially for the carbon content.

The effect of dilution with the substrate is observed with the decrease of iron content and increase of alloying elements as the measurement goes to the top of the deposit. A higher dilution with the substrate was noted in the base of the Part B, showing more iron content in detriment of manganese and carbon, though the chromium content remained constant. This higher dilution can be explained by the deposition strategy that programed a first layer with higher heat input to provide a wider base with safe bonding with the substrate. The chemical

content results showed the negative side of this strategy: the first layers of the deposit usually present higher dilution with the substrate if the substrate is made of a different material. In this case the bottom of the deposit needs to be sacrificed to comply with the part requirements.

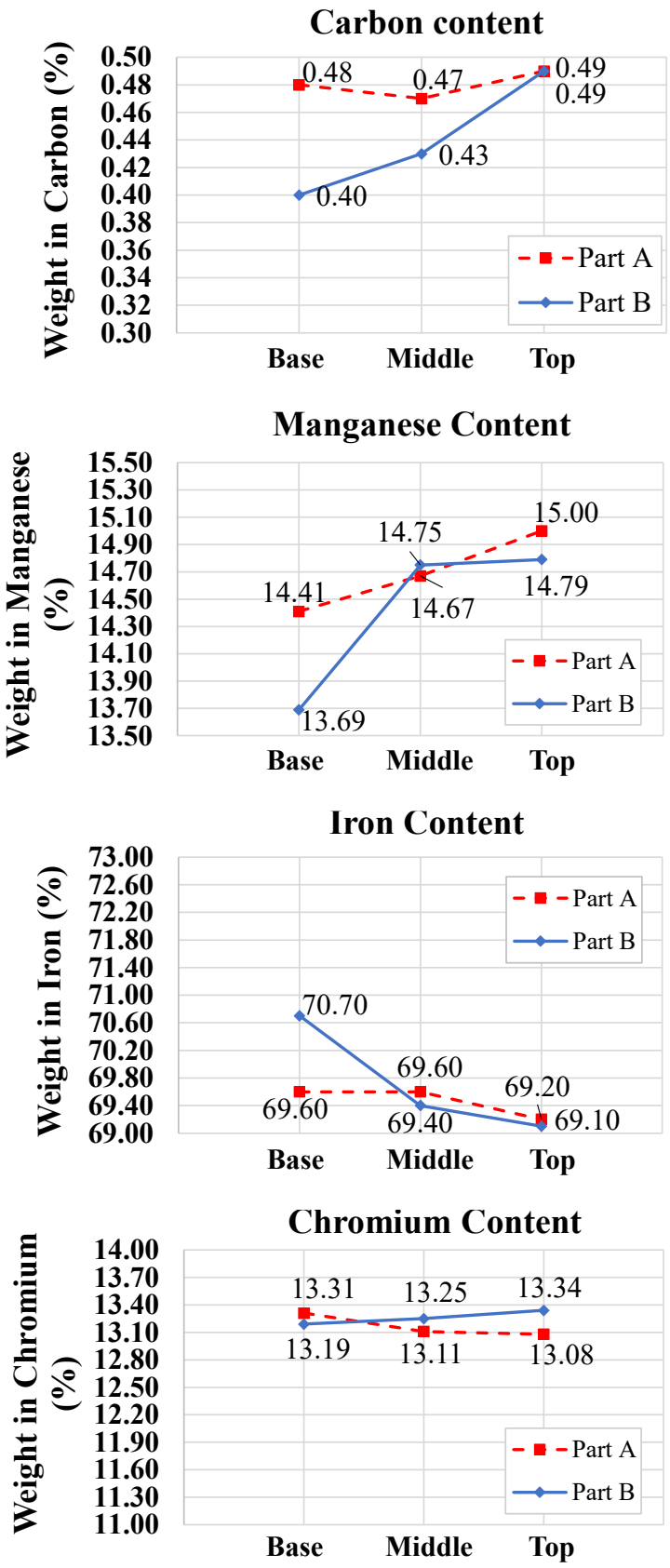


Figure 70: Chemical composition analysis comparing Part “A” and Part “B”.

# 5 CONCLUSIONS

Following this work's objectives, the use of metal cored wires as a feedstock option to additively manufacture wall like samples with thick width was analyzed in the LABSOLDA followed by the development of deposition strategy and manufacturing of a validation part in the industrial environment inside the German company DURUM Verschleiss-Schutz. The following topics highlight the most important conclusions of this work.

- The metal-cored wires presented excellent weldability within the WAMM conditions of depositing thick layers structures in the laboratory and industrial environment disregard of the GMAW variant used (CMT, CMT Pulse and RMD). This result highlights the possibility of prospecting the use of WAAM for the manufacturing of parts with wear resistance requirements that relies in the use of ceramic-metallic composites cored wires.

- The material transfer during the CMT Pulse variant occurred mainly by short-circuit mode instead of free fly and short circuit, as expected. The current pulse was not high enough to reach the transition current. The mass transfer happened preferentially by a high-volume droplet formed during 7 pulses in every short-circuit period. During the pulse period a continuous ejection of small solid particles and tiny droplets from the metal core could be seem. This different material transfer occurred due to the intrinsic current flow behavior of the metal core wire in which the current flows preferentially through the external metallic band rather than the powder core.

- According to high-speed filming analysis, the wire`s core still in its solid form dives into the welding pool in both process variants. It can be understood that when entering the welding pool, the solid core in the form of aggregated powder influences the thermal dynamics of the welding pool, in fact, cooling it. This behavior acts as another artifice to remove heat from the deposition process, which is commonly desired in WAAM. However, no specific studies have been made yet to evaluate the effect relevance over the solidification.

- The CMT Pulse variant resulted in a 23% more heat input than the CMT variant for the same travel speed (10 cm/min) and wire feed speed (3.5 m/min). This heat input difference leads to a mean temperature difference of 50˚C between the two process variants.

- The mean temperature analysis during deposition showed that at approximately 960s, or 8 layers, the samples entered in a quasi-steady state of heat flow with its surrounds. Until the end of the deposition the samples mean temperature increased at a slow rate compared to the initial transient regimen disregard of the process variant, almost reaching a constant temperature plateau.

**Regarding the validation sample made in Germany at DURUM Verschleiss-Schutz**

- The proposed validation sample was successfully manufactured at the DURUM`s workshop with conventional hardfacing equipment with two different building strategies. The first strategy, with multiple path points, has provided a large working envelop, but with less robustness and easiness of programming than the second strategy. The wide working range enabled the production of small batches of similar parts simultaneously, using the idle time between layer as strategy to cool down one part while depositing a new layer in another region of the table that was already cooled to the required interlayer temperature. On the other hand, the use of the second technique, the turn table strategy, provided a better solution for a research apparatus with a mindset of rapid prototyping with easy deposition path programming rather than flexible mid-size bath production.

## 6 SUGGESTIONS FOR FUTURE WORKS

- In future works the manufacturing of pipe like structure with superior dimensional complexity needs to be explored. Building sloped thick layers and non-regular sections is one of the next steps of this research until being able to manufacture of nonlinear pipe fittings.

- The study of manufacturing thick structures with dissimilar material composition is another step to fully reach the goal of additively manufacturing a part with functionally graded material composition that would increase the WAAM use appeal.

- A broader study of the melting behavior and material transfer of the metal cored wires by high-speed filming made with wider welding condition. The comparison of different metal cored wire alloys, wire diameter, power input, between other variables will increase the phenomena understanding.

- With a better understanding of the intrinsic metal-cored wire deposition behavior the creation of dedicated synergic programs would benefit the deposition control in terms of heat input, material waste, surface roughness, and, consequently, productivity of the process.

# 7 REFERENCES


ALBERTI, E. et al. Manufatura aditiva: o papel da soldagem nesta janela de oportunidade. v. 19, n. 2, p. 190-198, 2014.

ASTM. F3187 - 16 - Standard Guide for Directed Energy Deposition of Metals. p. 1-22, 2016.

ASTM, A. Standard terminology for additive manufacturing technologies F-12a. **American Society for Testing and Materials**, 2012.

ASTM, B. 52900 Additive Manufacturing—General Principles—Terminology. **American Society for Testing and Materials**, 2018.

AWS. **American Welding Society Handbook Vol. 2**. Miami: 2004.

BAI, X.; ZHANG, H.; WANG, G. J. T. I. J. O. A. M. T. Improving prediction accuracy of thermal analysis for weld-based additive manufacturing by calibrating input parameters using IR imaging. v. 69, n. 5-8, p. 1087-1095, 2013.

BHARDWAJ, A. Fundamentals of Corrosion and Corrosion Control in Oil and Gas Sectors. p. 41-76, 2020.

BOBBIO, L. D. et al. Additive manufacturing of a functionally graded material from Ti-6Al-4V to Invar: Experimental characterization and thermodynamic calculations. v. 127, p. 133-142, 2017.

BRITO, U. H. D. O. **Investigações em Processo e Automação como Contribuição para a Soldagem MIG/MAG Orbital no LABSOLDA - UFSC**. 2019. 139 Masters Thesis (Mechanical Engineering Masters Degree). Programa de Pós-Graduação em Engenharia Mecânica, Universidade Federal de Santa Catarina

BRUCKNER, J. Cold Metal Transfer (CMT)–Ein neuer Prozess in der Fügetechnik. 2005.

CARLYLE, T. SARTOR RESARTUS. 2001.

CARY, H. B. **Modern Welding Technology Second Edition**. Prentice-Hall, Inc., 1988.

CHEEPU, M.; LEE, C. I.; CHO, S. M. J. T. O. T. I. I. O. M. Microstructural characteristics of wire arc additive manufacturing with Inconel 625 by super-TIG welding. p. 1-5, 2020.

COLEGROVE, P. A. et al. Microstructure and residual stress improvement in wire and arc additively manufactured parts through high-pressure rolling. v. 213, n. 10, p. 1782-1791, 2013.

CUNNINGHAM, C. et al. Invited review article: Strategies and processes for high quality wire arc additive manufacturing. v. 22, p. 672-686, 2018.

D'ARCY, A. **How metal-cored wires reduce hidden welding costs**. 2012. Disponível em: < https://www.thefabricator.com/thefabricator/article/arcwelding/how-metal-cored-wires-reduce-hidden-welding-costs-- >. Acesso em: 22/04/2020.

DA SILVA, L. J. et al. Concept and validation of an active cooling technique to mitigate heat accumulation in WAAM. p. 1-11, 2020.

DAHAT, S. et al. A Methodology to Parameterize Wire+ Arc Additive Manufacturing: A Case Study for Wall Quality Analysis. v. 4, n. 1, p. 14, 2020.

DAS, S.; VORA, J. J.; PATEL, V. J. A. I. W. T. F. P. D. Regulated Metal Deposition (RMD™) technique for welding applications: an advanced gas metal arc welding process. p. 23-32, 2019.

DEBROY, T. et al. Additive manufacturing of metallic components–process, structure and properties. v. 92, p. 112-224, 2018.

DING, D. et al. A practical path planning methodology for wire and arc additive manufacturing of thin-walled structures. v. 34, p. 8-19, 2015.

DING, D. et al. Wire-feed additive manufacturing of metal components: technologies, developments and future interests. **The International Journal of Advanced Manufacturing Technology,** v. 81, n. 1-4, p. 465-481, 2015.

ERLANDSON, J. M.; BRAJE, T. J. J. A. Archeology and the Anthropocene. v. 4, p. 1-7, 2013.

FINDIK, F. J. M.; DESIGN. Recent developments in explosive welding. v. 32, n. 3, p. 1081-1093, 2011.

FORD, S.; DESPEISSE, M. J. J. O. C. P. Additive manufacturing and sustainability: an exploratory study of the advantages and challenges. v. 137, p. 1573-1587, 2016.

FÖRSTER, R.; FÖRSTER, A. Einteilung der Fertigungsverfahren nach DIN 8580. In: (Ed.). **Einführung in die Fertigungstechnik**: Springer, 2018. p.23-136.

FORTES, C.; ARAÚJO, W. J. L. E. B., CONTAGEM. Arames Tubulares. 2004.

FRAZIER, W. Metal additive manufacturing: a review. **Journal of Materials Engineering Performance,** v. 23, n. 6, p. 1917-1928, 2014.

FUNDERBURK, R. S. J. W. I. The importance of interpass temperature. v. 15, n. 1, p. 31-32, 1998.

GEBHARDT, A.; HÖTTER, J.-S. **Additive manufacturing: 3D printing for prototyping and manufacturing**. Carl Hanser Verlag GmbH Co KG, 2016.

GOHR, R. **Novos métodos de controle da soldagem MIG/MAG**. 2002. (Doutorado). POSMEC, UFSC

GONÇALVES E SILVA, R. H. et al. Double-Sided Welding as an Alternative for Joining Internally Clad Pipes. v. 11, n. 2, p. 04020012, 2020.

HENCKELL, P. A., YAROP; BERGMAN, JEAN PIERRE. Additive Fertigung Verschleßbeständiger Verbundstrukturen mittels Metall-Schutzgasschweißprozess. **Schweissen un Schneiden,** v. Heft 7, p. 4, 2019.

HENCKELL, P. A., YAROP; SCHRICKER, KLAUS; BERGMAN, JEAN PIERRE. **Wire Arc Additive Manufacturing Of Wear Resistant Compound Structures By Gas Metal Arc Welding**. Hybrid Material and Structures. Bremen, Germany 2018.

HU, Z. et al. Understanding and overcoming of abnormity at start and end of the weld bead in additive manufacturing with GMAW. v. 95, n. 5-8, p. 2357-2368, 2018.

HUANG, R.-S. et al. Infrared temperature measurement and interference analysis of magnesium alloys in hybrid laser-TIG welding process. v. 447, n. 1-2, p. 239-243, 2007.

KAH, P.; SUORANTA, R.; MARTIKAINEN, J. J. T. I. J. O. A. M. T. Advanced gas metal arc welding processes. v. 67, n. 1-4, p. 655-674, 2013.

KIM, I.; KWON, W.; PARK, C. J. J. O. K. The effects of welding process parameters on weld bead width in GMAW processes. v. 14, n. 4, 1996.

KVASOV, F. J. W. I. Special features of mechanised welding with controlled electrode metal transfer. v. 14, n. 2, p. 158-161, 2000.

LAMPKE, T. et al. Development of particle-reinforced nanostructured iron-based composite alloys for thermal spraying. v. 205, n. 12, p. 3671-3676, 2011.

LEVY, G. N.; SCHINDEL, R.; KRUTH, J.-P. J. C. A. Rapid manufacturing and rapid tooling with layer manufacturing (LM) technologies, state of the art and future perspectives. v. 52, n. 2, p. 589-609, 2003.

LIN, Z. et al. Microstructure and mechanical properties of medium carbon steel deposits obtained via wire and arc additive manufacturing using metal-cored wire. v. 9, n. 6, p. 673, 2019.

MARQUES, C. Prospecções da natureza física da soldagem MIG automática de ligas de alumínuio. 2013.

MARQUES, C. Análise de técnicas e efeitos físicos da alimentação dinâmica do arame no processo de soldagem MIG/MAG com vistas ao desenvolvimento de um sistema flexível nacional. 2017.

MODENESI, P.; MARQUES, P.; SANTOS, D. J. B. H. D. D. E. M. E. D. M. U. Fontes de energia para a Soldagem a Arco. 2005.

MYERS, D. J. W. J. Metal cored wires: Advantages disadvantages. v. 81, n. 9, p. 39-42, 2002.

NORRISH, J. **Advanced welding processes**. Elsevier, 2006.

OJO, O. O.; TABAN, E. J. M. T. Microstructure, Mechanical and Corrosion Behavior of Additively Manufactured Steel: A Review (Part 1). v. 62, n. 5, p. 503-516, 2020.

POSCH, G. et al. Manufacturing of nickelbase-overlays: Comparison of various welding technologies under consideration of clad properties. **IIW International Congress IC 2014**, 2014.

PRINCE, J. D. J. J. O. E. R. I. M. L. 3D printing: an industrial revolution. v. 11, n. 1, p. 39-45, 2014.

RADI, H. A.; RASMUSSEN, J. O. **Principles of physics: for scientists and engineers**. Springer Science & Business Media, 2012.

REINMANN, J. **3D-gedruckte Knotenpunkte aus Stahl für bionische Tragstrukturen mittels WAAM**. Disponível em: < https://baukultur-thueringen.de/thueringerawards/ibp/?id=73 >. Acesso em: 27/03/2020.

RIFFEL, K. C. **AVANÇOS TECNOLÓGICOS DO PROCESSO TIG: TÉCNICAS INOVADORAS DE ALIMENTAÇÃO DE ARAME E PROCEDIMENTOS AUTOMATIZADOS COMO CONTRIBUIÇÃO PARA A UNIÃO DE TUBOS INTERNAMENTE CLADEADOS. 2018. 172 f**. 2018. Dissertação (Mestrado)-Curso de Programa de Pós-graduação em Engenharia …

ROCHA, P. C. J. **A New Solution for Wear and Corrosion Protection: Alternating Current MIG Welding Process With Nickel, Cobalt and Iron Basis Flux-Cored Hardfacing Wires**. 2017. 60 Bachelor thesis (Undergraduate). Mechanical Engineering Department, Universidade Federal de Santa Catarina, Brazil

ROCHA, P. C. J. et al. Analysis of Interlayer Idle Time as a Temperature Control Technique in Additive Manufacturing of Thick Walls by Means of CMT and CMT Pulse Welding Processes. v. 25, 2020.

RODRIGUES, A. G. Controle e Atuação do Sistema de Movimentação Dinâmica de Arame em Processos de Soldagem a Arco. 2016.

RODRIGUES, T. A. et al. Wire and arc additive manufacturing of HSLA steel: Effect of thermal cycles on microstructure and mechanical properties. v. 27, p. 440-450, 2019.

SCHÖRGHUBER, M. **Cold-metal-transfer welding process and welding installation**: Google Patents 2015.

SCHREIBER, F. J. F., VERSCHLEIßSCHUTZ VON BAUTEILEN DURCH AUFTRAGSCHWEIßEN. Wolfram Schmelzkarbid im Verschleißschutz: Besonderheiten bei der schweißtechnischen Verarbeitung und Qualitätssicherung. 2000.

SCOTTI, A.; PONOMAREV, V. **Soldagem MIG/MAG: melhor entendimento, melhor desempenho**. Artliber, 2008.

SHIN, D. Y. C. **Micro Walls machined using a 100 micron endmill.**, Disponível em: < https://engineering.purdue.edu/ManLab/micromachine.html >. Acesso em: 04/08/2020.

SILVA, F. C. Desenvolvimento de algorítmos para geração de trajetórias de revestimento por soldagem automatizada aplicados em caldeiras de usinas termoelétricas. 2012.

TSURUMAKI, T. et al. Precise additive fabrication of wall structure on thin plate end with interlayer temperature monitoring. v. 13, n. 2, p. JAMDSM0028-JAMDSM0028, 2019.

VEVERS, A. et al. Additive Manufacturing and Casting Technology Comparison: Mechanical Properties, Productivity and Cost Benchmark. v. 55, n. 2, p. 56-63, 2018.

VILARINHO, H. D. H. A. L. O. Development and assessment of calorimeters using liquid nitrogen and continuous flow (water) for heat input measurement. **Soldagem & Inspeção,** v. 17, p. 15, 2012.

VILARINHO, L. **Mecânica da UFU fabrica primeira peça 3D para indústria de óleo e gás**. 2020. Disponível em: < http://www.comunica.ufu.br/noticia/2020/01/mecanica-da-ufu-fabrica-primeira-peca-3d-para-industria-de-oleo-e-gas >. Acesso em: 27/03/2020.

WEBSTER, M. **"Manufacture. Etymology"**. Merriam-Webster 2020.

WIDGERY, D. **Tubular wire welding**. Elsevier, 1994.

WILDEN, J. et al. Lichtbogenspritzen verstärkter selbstfließender Legierungen zum kombinierten Korrosions-und Erosionsschutz. 1999.

WOOD, J. J. I. J. O. P. V.; PIPING. A review of literature for the structural assessment of mitred bends. v. 85, n. 5, p. 275-294, 2008.

XU, X. et al. Preliminary investigation of building strategies of maraging steel bulk material using wire+ arc additive manufacture. v. 28, n. 2, p. 594-600, 2019.

YANG, D.; WANG, G.; ZHANG, G. Thermal analysis for single-pass multi-layer GMAW based additive manufacturing using infrared thermography. **Materials Processing Technology,** v. 244, p. 215-224, 2017.

YEHOROV, Y. et al. Balancing WAAM Production Costs and Wall Surface Quality through Parameter Selection: A Case Study of an Al-Mg5 Alloy Multilayer-Non-Oscillated Single Pass Wall. v. 3, n. 2, p. 32, 2019.

YUAN, L. et al. Fabrication of metallic parts with overhanging structures using the robotic wire arc additive manufacturing. 2020.

ZHAO, Y. et al. Process planning strategy for wire-arc additive manufacturing: Thermal behavior considerations. v. 32, p. 100935, 2020.